ROMA
TRE
UNIVERSITÀ DEGLI STUDI

Dynamics and Thermodynamics in Supercooled Bulk and Confined Water

A Molecular Dynamics Simulation Study

PhD Thesis in Physics

MARGHERITA DE MARZIO

Supervisors: Paola Gallo and Mauro Rovere

Department of Mathematics and Physics
UNIVERSITÀ DEGLI STUDI ROMA TRE
Rome, Italy 2016

PhD's thesis 2016

Dynamics and Thermodynamics in Supercooled Bulk and Confined Water

A Molecular Dynamics Simulation Study

MARGHERITA DE MARZIO

Supervisors: Paola Gallo and Mauro Rovere

Department of Mathematics and Physics
Università degli Studi Roma Tre
Rome, Italy 2016

Dynamics and Thermodynamics in Supercooled Bulk and Confined Water
A Molecular Dynamics Simulation Study
MARGHERITA DE MARZIO

Supervisors: Paola Gallo and Mauro Rovere, Department of Mathematics and Physics, Università degli Studi Roma Tre
Examiners: Giorgio Pastore, Department of Physics, Università degli Studi di Trieste; Renato Torre, Department of Physics and Astronomy, Università degli Studi di Firenze.

PhD's Thesis 2016
Department of Mathematics and Physics
Università degli Studi Roma Tre
Via della Vasca Navale 84, Rome, Italy

Typeset in LaTeX

Acknowledgements

This PhD would not have been possible without the help of Prof. Paola Gallo and Prof. Mauro Rovere. Their advices and support in both work and life have allowed me to complete this 3 years path with a greater scientific and professional knowledge, also thanks to their comprehension and patience in difficult moments. I am also grateful to Gaia, my adventuring companion. Finally, I always thank Enrico, for his love, patience and support during this PhD.

Contents

1

Introduction

Water is one of the most abundant and at the same time anomalous liquid in the world. The interest in studying the thermodynamic and dynamical properties of water derives from its relevant role in numerous aspects of life. In particular, water has a great utility and a large range of application in various chemical and technological processes [1, 2]. This liquid has a primary role in biological field, for example in cryopreservation [3] and in the protein folding mechanism [4], where the hydrophobic interactions between water molecules with hydration water seem to be one of the main contribution to the folding process. Finally water exhibits more than 60 thermodynamic and dynamical anomalies [2, 5–7]. Differently from simple liquids, in fact, at sufficiently low temperatures water expands its volume by cooling, presenting a Temperature of Maximum Density Line (TMD) in the phase diagram. Also the thermodynamic response functions, that represent a measure of the density and entropy self and cross-correlations of the system, anomalously increase below a certain temperature, deviating from the monotonic behaviour of normal liquids. All these anomalies originate probably from the unique capability of water molecules of interacting through a strong directional attractive bond, the so called *hydrogen bond* [8].

A huge amount of theoretical, computational and experimental works [5, 7, 9] have been carried out to understand the phase diagram and the peculiar properties of water but nowadays there is a lack of a complete understanding of the thermodynamic, dynamical and structural features of this anomalous liquid.

A possible way to investigate the thermodynamics and dynamics of water is through supercooling, since in the supercooled regime many water anomalies appear to be especially pronounced [5, 7, 9, 10]. Water is said supercooled when it remains at the liquid state also below the melting temperature. A supercooled state is a meta-equilibrium state with a finite lifetime, called *metastable state*, where the system is trapped in a relative minimum of the appropriate thermodynamic potential. In order to be able to investigate water in its supercooled metastable state, its lifetime must be longer than the observation time necessary to perform measurements on the sample but, on the contrary, the time necessary to the system for rearrange and equilibrate itself has to be much shorter of the minimum duration of the experiments [7].

The maintenance of water in the supercooled regime depends on various factors, such as the extreme purity of the sample and the absence of external mechanical and thermal perturbations. However at certain thermodynamic conditions water cannot be kept supercooled anymore and two possible outcomes of the supercooling can occur: ice crystallization or glass transition. In the first case, a first order phase transition from liquid to solid takes place and nucleation drives the liquid in the stable ice phase, the correspondent stable state at the specific thermodynamic conditions. In the second case, through a rapid quenching of the liquid down to sufficiently low temperature in order to prevent ice nucleation, the supercooled liquid reaches a state where the molecules are structurally arrested: the liquid has become a glass.

The range of metastability of supercooled water is therefore determined by the nucleation temperature line T_H,that is a kinetic constraint function of the cooling rate and of the observation time. On the other hand by heating glassy water just above the glass transition temperature T_G water crystallizes to the cubic ice at a temperature T_x. T_G is around 136 K while $T_X = 150$ K.

The range of temperatures and pressures below T_H, where experiments are impossible to perform due to the fast crystallization of the sample, and above T_X is called the "no man's land" [11] and defines the thermodynamical region where measurements on supercooled water are really difficult to execute.

Experimental and computational efforts in studying supercooled water have shown interesting thermodynamic and dynamical features of this metastable regime. From the thermodynamic point of view, the anomalous increase of the thermodynamic response functions seem to diverge asymptotically in the deep supercooled region. Moreover, in the glassy phase, vitreous water exhibit two distinct amorphous structures: High Density Amorphous Ice and Low Density Amorphous Ice. Experiments of Mishima and Stanley [11, 12] have shown the existence of a first order phase transition between HDA and LDA. These two amorphous phases show different local structures: LDA has a short range order similar to ice Ih, while HDA has a local structure similar to liquid water

Several theoretical studies have been developed to explain glassy water polyamorphism and its connection with the anomalies of supercooled water, in particular the apparent divergence of the thermodynamic response functions. Various scenarios have been proposed. Among these hypothesis, the one that has received by far the greatest attention is the Liquid Liquid Critical Point Scenario (LLCP) [13]. This scenario gives the better connection between the first order transition in the glassy state and the thermodynamics of the supercooled liquid. According to this model, the HDA-LDA transition would be the prosecution at lower temperatures and higher pressure of a first order phase transition occurring between two different supercooled liquid states, the High Density Liquid water and the Low Density Liquid water. This HDL-LDL transition would terminate at a second order liquid liquid critical point located in the no man's land. The eventual presence of LLCP would explain both the divergence of the thermodynamic anomalies, that diverge upon approaching a critical point, and the existence of the phenomenology in the glassy phase of water.

From the dynamical point of view, less attention has been devoted to the analysis of this aspect in supercooled water.

The first important achievement was obtained in computer simulation of SPC/E water [14, 15]. It was found that the relaxation dynamics upon supercooling can be described in terms of the Mode Coupling Theory of the glassy dynamics [16]. It was demonstrated that water can be considered as a glass-forming liquid. More recently experiments confirmed those results [17, 18]. Computer simulations on different water models showed the same behaviour but it was found that lowering the temperature in a region of deep supercooling deviations from the MCT predictions are observed.

The appearance of activated processes not taken into account by MCT, in fact, introduces changes in the structural relaxation mechanism. By lowering temperature water shows a crossover from an high temperature phase where dynamics follows MCT predictions, called fragile phase, towards a low temperature state where the relaxation process is dominated by activated phenomena, called strong state. The crossover from one state to the other is called Fragile to Strong Crossover (FSC). Due to the difficulties of performing experiments on bulk supercooled water, the FSC has been evidenced in water confined in MCM-41 [19]. MCM-41 is a mesoporous structure composed of multiple hexagonal channels obtained from assemblies of organic molecules and has a wide range of application in many technological processes. These experimental results were supported by computer simulation [20]. The analysis of water in confined geometries is extremely important since the effect of confinement on supercooled water is to prevent crystallization at temperature and pressure not accessible in the bulk. Moreover the role and properties of interfacial water in contact with hydrophilic or hydrophobic surfaces is central in many biological systems.

In spite of the large amount of information recorded on the thermodynamical and dynamical behaviour of supercooled water, several aspects of this liquid in the stable and metastable state are not totally clear, in particular if there exists a connection between the thermodynamical curves of its phase diagram and its dynamics.

In this PhD Thesis dynamical studies on bulk water are conducted through the use of Molecular Dynamics Simulations, in order to provide new insights on the dynamical properties of supercooled water and how they are related to the thermodynamical anomalies observed.

For what concerns the bulk water, its behaviour in the mild and deep supercooled regime is investigated using the TIP4P/2005 water potential [21]. TIP4P/2005 water potential is currently one of the most popular water model potentials. It reproduces with very high quality the TMD curve [22] and low temperatures properties of stable water, like ice polymorphism [21], much better than TIP5P and SPC/E. It also shows the anomalous increase of thermodynamic response functions and the existence of a second order liquid liquid critical point LLCP [23]. Moreover TIP4P/2005 values of the diffusion coefficients are close to the experimental values [24].

The results of the Molecular Dynamics Simulations performed in this work on TIP4P/2005 supercooled bulk water are analysed focusing on the dynamical properties of the system. The validity of the Mode Coupling Theory is tested on the dynamics of the simulated box, studied through the calculation of the Self Intermediate Scattering Functions (SISF) in the mild and deep supercooled regime. The temperature dependence of the structural relaxation time is investigated, concentrating on the search of a possible connection between the relaxation mechanism through which water molecules rearrange and the thermodynamic conditions of the liquid. The analysis of this relation is carried out within the Liquid Liquid Critical Point Scenario and shows a clear agreement with the MCT predictions.

In light of the results obtained Van Hove Self Correlation Functions are calculated in order to better understand the dynamical behaviour of the system at the lowest temperature simulated in the deep supercooled regime. This kind of study is important to evidence the occurrence upon supercooling of activated processes, called hopping processes, neglected by MCT in its ideal formulation and responsible of modification in the relaxation mechanism at low temperature. Moreover the appearance of hopping phenomena emerged from this analysis is then explained in terms of changes in the structural and thermodynamical state of the system.

Overall, calculations performed on TIP4P/2005 in this first part of the PhD project will provide an extensive panoramic on the dynamics of supercooled bulk water and will show the existence of a strong interplay between the thermodynamic and dynamical phenomena occuring in the supercooled regime.

Besides bulk water, the structural properties of confined water have been studied to make connection with previous results obtained from Molecular Dynamics Simulations on confined water in MCM-41 in the works of Gallo et al. [20, 25].

Using the SPC/E potential, water confined in a cylindrical hydrophilic pore, MCM-41, is simulated at different temperatures in order to study the structural properties of the liquid upon lowering temperature. Behaviour of water in such a confining substrate has been largely investigated computationally and experimentally. SPC/E is one of the most used water potential both for the study of bulk water and water near extended surfaces[26].

In this second part of the PhD thesis, simulations are performed on water confined in MCM-41 with the scope of understanding the effect of confinement on the structural properties of the liquid. Specifically the radial distribution functions are determined both for SPC/E bulk and confined water and a detailed comparison between the two systems allow to explain to what extent water in geometrical confinement present a bulk-like character. The existence of a possible relation between the local order of the liquid and its thermodynamical state is examined.

The abstracts of the papers published on all the sets of simulations performed in this PhD Thesis can be found in the section Publications and Presentations.

The Thesis is organized as follows: Chapter 1 is devoted to a general introduction to the properties of liquid water and the anomalies of water of interest for the present study. The supercooled metastable state of water is introduced and the conditions that makes possible its experimental studies in presence of the competition between ice nucleation and the glass transition. These topics are discussed more in details in Chapter 3 where a short review of the phenomenology of supercooled water and glassy water is presented. Theoretical scenarios aimed to explain the anomalies are also introduced with particular emphasis on the hypothesis of the liquid liquid critical point (LLCP). In this framework the Widom line is defined as an important signature of the presence of the LLCP. In this Chapter it is particularly important the discussion of the relaxation dynamics of supercooled water and its interpretation in terms of MCT. A short introduction to this theory is also presented together with the results obtained by computer simulations on SPC/E water mentioned above. Chapter 4 contains an introduction to the Molecular Dynamics methods used in our work with the description of several algorithms and numerical procedures. In Chapter 5 the results obtained from our computer simulation study of supercooled water with the TIP4P/2005 potential are presented. After a description of the model and some technical details the behaviour of the self intermediate scattering functions is shown upon supercooling. The range of validity of the MCT is tested together with the possible transition from a fragile to a strong regime in the structural relaxation. It will be shown the relevance of the hopping phenomena that are evidenced by a deep study of the Van Hove self correlation functions. The connections between our results and the presence of a LLCP in TIP4P/2005 water are discussed, in particular it is underlined how the Widom line signs the onset of the hopping regime. Chapter 6 is focused on the computer simulation of SPC/E water confined in MCM-41. By following previous studies on the dynamics of this system upon supercooling, structural properties are considered and the connection between thermodynamics and relaxation dynamics in confined water is shown. Some preliminaries results are also added on TIP4P/2005 confined in MCM-41. Chapter 7 is devoted to the conclusions.

2

Water: a common but strange liquid

2.1 The water molecule

The water molecule is a planar v-shaped molecule composed of two hydrogen atoms at the external vertices and one oxygen atom at the central vertex. The atoms are arranged in such a way that the HOH angle is 104.5° and the intramolecular distance OH is 0.957 Å in the gas phases [27, 28]. A schematic picture of the water molecule is shown in Fig. 2.1. Due to the large electronegativity difference $\Delta\chi = 1.24$ between the oxygen and the hydrogens, the total electronic molecular distribution is strongly condensed towards the oxygen atom. It follows that water molecule presents partial charges $\delta q \simeq -0.7e$ and $\delta q \simeq +0.35e$ for the oxygen and hydrogen respectively [29]. The partial charges and the mutual geometrical arrangement of the atoms make water a polar molecule with a dipole moment of 1.84 D in the vapour phase [30]. The dipole moment for a completely ionic O-H bond would be 5.61 D and therefore each O-H bond is approximately 1/3 ionic and 2/3 covalent [8]. The valence electrons of the oxygen atom form two lone pairs that dispose together with the hydrogens in a tetrahedral structure (see Fig. 2.1). One of the most important features of water molecules is the ability to interact each other through a strong directional attractive force responsible of the formation of the so-called *hydrogen bonds* [31]. An hydrogen bond occurs between the oxygen atom and the hydrogen atom of two different water molecules when a partially positive hydrogen lies between two oxygens with partial negative charge.

The water molecules capability of construct multiple hydrogen bonds makes water one of the most anomalous liquid in the world.

The best example of hydrogen bond network is represented by the structure of ordinary ice I_h, the stable form of ice at $T = 273$ K and ambient pressure. Each molecule has four first-neighbors located at the four vertices of a tetrahedron centered around the oxygen atom and it behaves as a donor

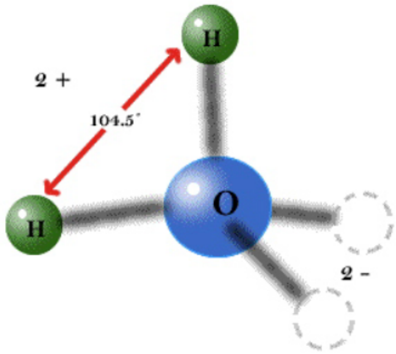

Figure 2.1: Schematic picture of water molecule. The experimental HOH angle is 104.5° and the intramolecular distance OH is 0.957 Å. The lone pair of oxygen electrons arranges together with the two hydrogen atoms into a tetrahedral structure.

of hydrogen for two of them and as an acceptor of hydrogen for the others. The result is a space-filling network with long range order. The strong directionality of the hydrogen bond causes the ice I_h to have many voids in its structure. It is this *open* character of the hydrogen bond network to induce melted ice to have a short range tetrahedral order but a closer packing of water molecules.

The energy associated with the hydrogen bond is circa 20 kJ/mol that is a value much bigger than the energy of dipole-dipole interactions (circa 1kJ/mol) and much weaker than the energy of a covalent bond, circa 400 kJ/mol. Since the latent heat of fusion is low with respect to the latent heat of sublimation, in liquid state most hydrogen bonds are preserved but the long range order typical of crystal phase reduces to a short transient range order.

The peculiar property of water molecules of creating open networks held together by multiple hydrogen bonds is probably one of the main reason of the several water anomalies [8]. In order to understand why water is considered a unique liquid, a brief summary on its anomalies both from the thermodynamic and dynamical point of view has to be discussed.

2.2 Anomalies and peculiarities of water

Even if water is one of the most common compound on earth, it exhibits more than 60 thermodynamic and dynamical anomalies [2, 5–7]. A brief review on these anomalies is therefore necessary in order to comprehend the

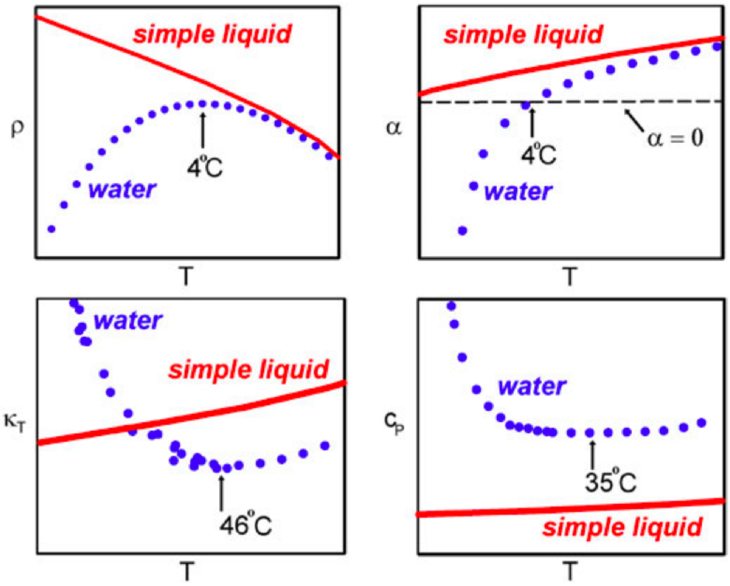

Figure 2.2: Schematic comparison of the isobaric temperature dependence of the density ρ, thermal expansion coefficient α_P, isothermal compressibility k_T and isobaric heat capacity c_P for water and a simple liquid. Figure from Ref. [5].

importance of such a peculiar liquid. Fig. 2.2 displays a sketch of three of the main thermodynamic water anomalies in comparison with the behaviour of simple liquids. Each panel shows the temperature dependence at ambient pressure of the density ρ, the isothermal compressibility k_T, the coefficient of thermal expansion α_P and the isobaric specific heat c_P respectively. The most known and visible water anomaly is the density anomaly, depicted in the upper left panel of Fig. 2.2. As it is clear from the figure, in simple liquid density increases upon decreasing temperature. At ambient pressure and in the high temperature range water density behaves as in normal liquids, increasing by cooling the system. Nevertheless, at $T = 4\ °C$ this trend drastically changes and density reaches a maximum below which begins to decrease. The temperature at which density exhibits a maximum is called *temperature of maximum density* (TMD) and for each value of the pressure water presents a maximum that moves towards lower temperatures upon increasing pressure. The loci of these maxima in the $P-T$ plane constitute the so-called TMD line, an important thermodynamic curve of water phase diagram. The TMD line marks the border between the region where water behaves as simple liquids and the region where the liquid anomalously expands on cooling. In Fig. 2.3 the experimental TMD line is shown for

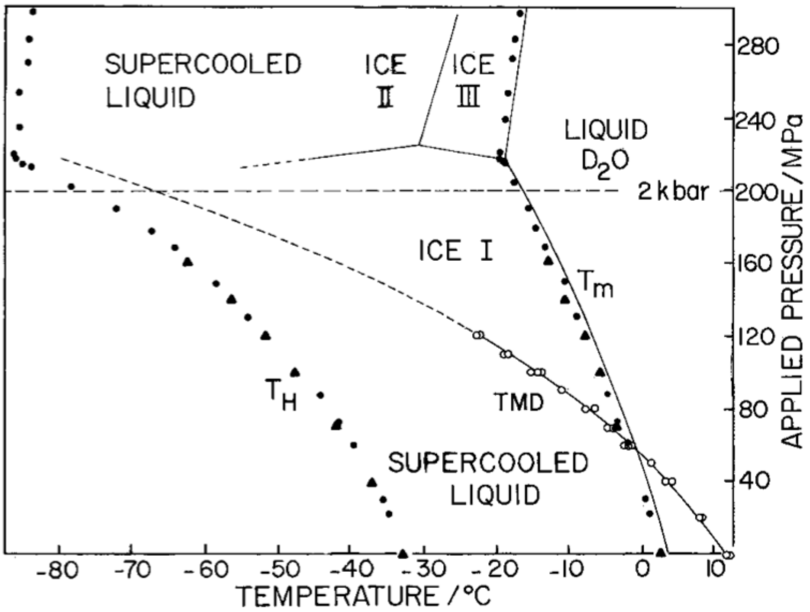

Figure 2.3: TMD line for D_2O in the $P-T$ plane. Circles are from experiments and the line is an extrapolation from Ref. [33]. T_M represents the melting line and T_H the locus of homogeneous nucleation. Figure from Ref. [32].

D_2O [32], together with the melting line T_M and the locus of homogeneous nucleation T_H (see the next Section).

Also the thermodynamic response functions show an anomalous behaviour as a function of temperature in water.

The existence of the TMD line implies that the thermal expansion coefficient $\alpha_P = 1/v(\partial v/\partial T)_P$ for a fixed pressure P vanishes at the temperature of maximum density and becomes negative below it. Moreover, provided the negative slope of the TMD, the values of temperatures at which α_P changes sign is automatically lower upon compression of the system, as shown in Fig. 2.4.

As in case of density, the temperature dependence of the isothermal compressibility k_T follows the same trend of simple liquids in the high temperature range, slightly decreasing with cooling. Nevertheless, at $T = 46\ °C$ an abrupt and rapid increase of k_T upon decreasing temperature occurs and the behaviour of the isothermal compressibility deviates immediately from the monotonic decrease of simple liquids. For each pressure, therefore, a clear k_T minimum appears at temperatures higher and higher by decreasing pressure indicating that the effect of compression on the system is to move

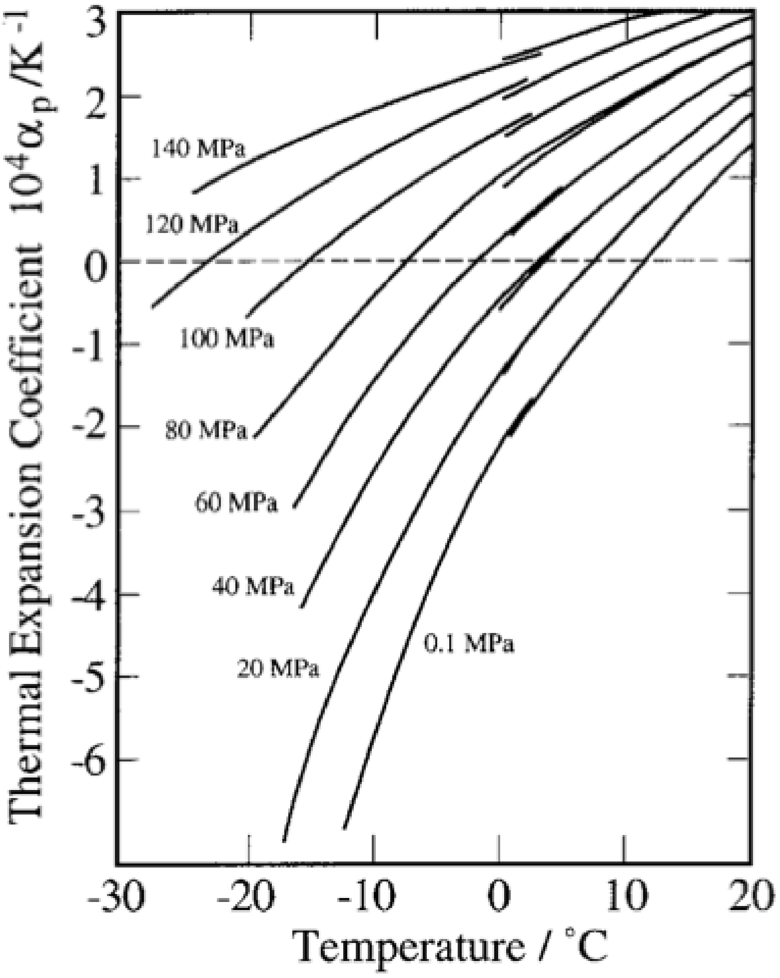

Figure 2.4: Experimental coefficient of thermal expansion for several pressures for D_2O. Data from Ref. [34] and Figure from Ref. [7].

the dramatic increase of the isothermal compressibility towards lower temperatures as evident in Fig. 2.5, where the experimental behaviour of the k_T at several pressures is shown [35]. It should be notice that the manifestation of k_T minima in the phase diagram of water is a direct consequence of the presence of the TMD line. The following thermodynamic identity connects the inclination of the TMD to the temperature dependence of k_T:

$$\left(\frac{\partial k_T}{\partial T}\right)_{P,\ at\ TMD} = \frac{v^{-1}\left(\partial^2 v/\partial T^2\right)_{P,\ at\ TMD}}{(dP/dT)_{TMD}} \tag{2.1}$$

where v is the molar volume, the subscript 'at TMD' signifies that the partial derivative is evaluated at a point on the TMD locus, and the subscript TMD signifies that the derivative is evaluated along the TMD locus, at the state point of interest. Since the numerator at the right hand side of Eq. 2.1 is positive at TMD [36] and the slope of the TMD is negative in the $P-T$ plane the overall trend of the isothermal compressibility at TMD is to increase upon isobarically decreasing temperature. On the contrary the presence of the liquid-vapour critical point in the high temperature range causes an asymptotic increase of the thermodynamic response functions. This means that the occurrence of k_T minima is connected both to the TMD and the liquid gas second order critical point.
Similarly to k_T, for each pressure the isobaric specific heat presents a slow varying temperature dependence in the high temperature range and, after a certain T ($T = 35\ °C$ at ambient pressure), a sharp increase with the progressive cooling of the system, as shown in the lower right panel of Fig. 2.2 and in the experimental results exhibited in Fig. 2.6.
The anomalous behaviour of water thermodynamic response functions can be considered also in terms of the fluctuations of the liquid. In fact, the following relations hold:

$$k_T = -\frac{1}{V}\left(\frac{\partial V}{\partial P}\right)_T = \frac{\langle(\delta V)^2\rangle}{V k_B T} \tag{2.2}$$

$$c_P = \frac{T}{N}\left(\frac{\partial S}{\partial T}\right)_P = \frac{\langle(\delta S)^2\rangle}{N k_B} \tag{2.3}$$

$$\alpha_P = \frac{1}{V}\left(\frac{\partial V}{\partial T}\right)_P = \frac{\langle\delta V \cdot \delta S\rangle}{V k_B T} \tag{2.4}$$

These equations connect the isothermal compressibility and isobaric heat capacity coefficient to the volume and entropy fluctuations of the system. The anomalous increase of these functions corresponds, therefore, to an increase in the self correlations of the liquid upon decreasing temperature, contrary

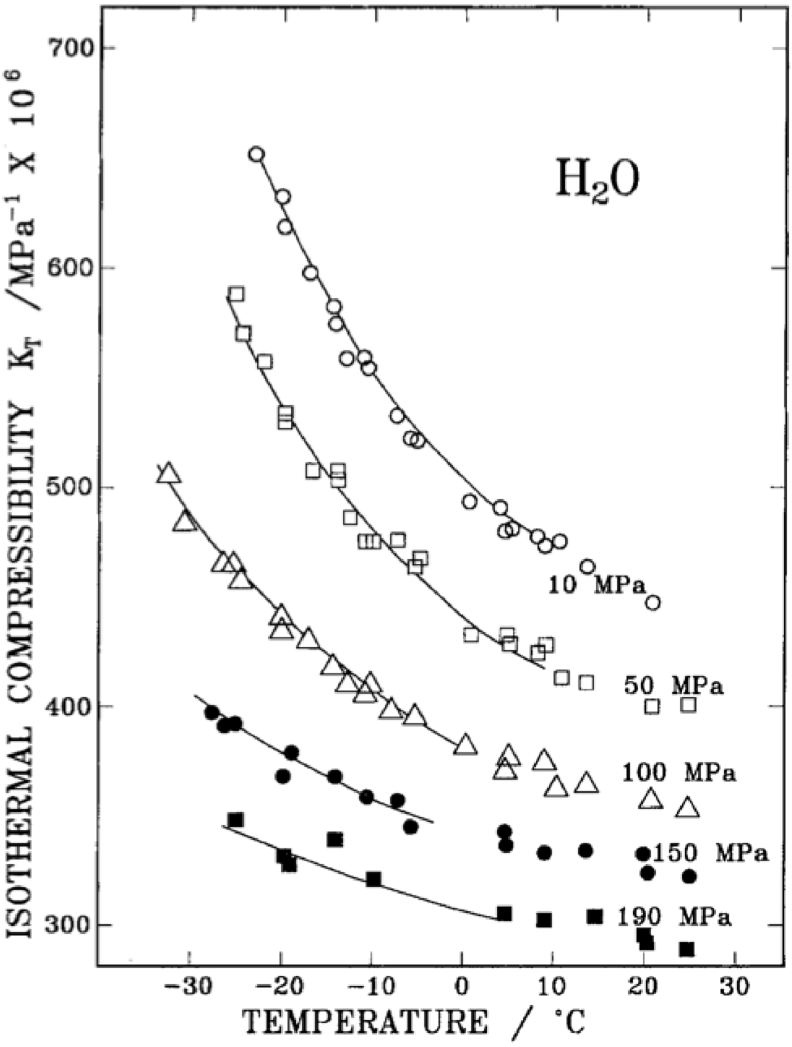

Figure 2.5: Experimental isothermal compressibility for several pressures. Curves are fit of experimental data with power law relations. Data from Ref. [35] and Figure from Ref. [7].

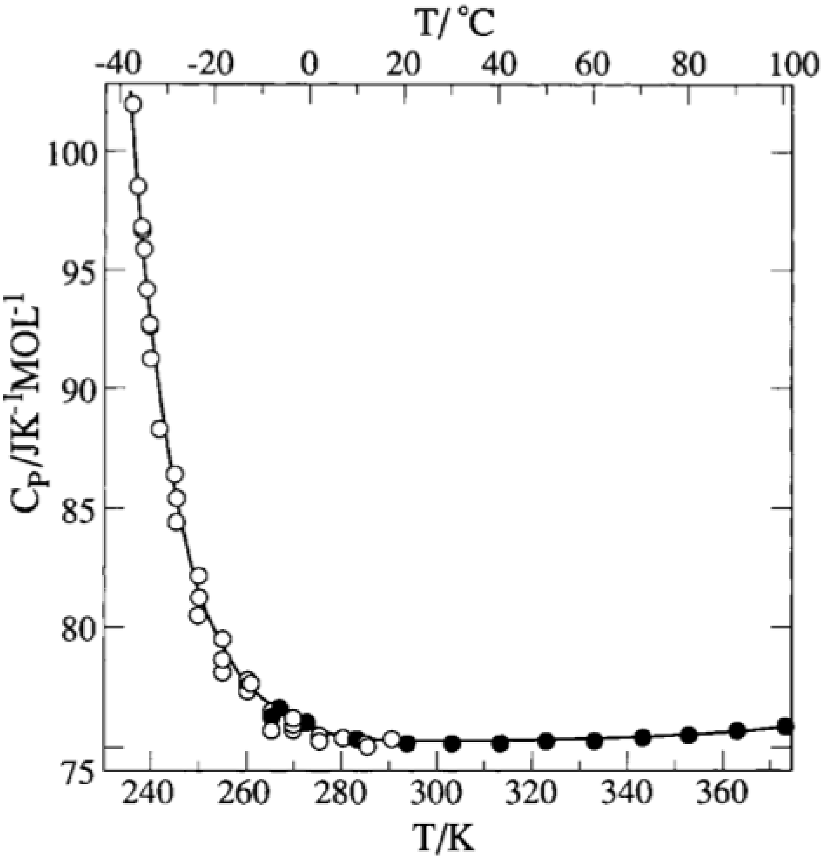

Figure 2.6: Experimental isobaric specific heat c_P at ambient pressure. Data from Ref. [37] and Figure from [7].

to normal liquids where lower temperatures are associated to smaller fluctuations. Moreover last equation on α_P expresses the thermal expansion coefficient as a measure of the cross-correlations between volume and entropy. It follows that the transition from positive to negative values of α_P imposes a loss of entropy by increasing volume, differently to what happens in simple liquids. The anti-correlation between entropy and volume is a direct consequence of the formation of hydrogen bonds, for which a decrease in orientational entropy is accompanied by an increase in volume.
The analysis of the thermodynamic response functions in the supercooled regime, a metastable state where water is at the liquid state also below its melting temperature T_M (see next Section), evidences a continuation of the anomalous increase of stable water also below T_M. In particular, an apparent asymptotically divergence seems to emerge by further cooling. The singular trend of these quantities has been sometimes represented as a power law:

$$X = A\left(\frac{T - T_S}{T_S}\right)^{\lambda_X} \tag{2.5}$$

where X is a generic response function, T_S is the singular temperature at which the divergence should occur and λ_X is the relative exponent. A value for T_S based on experimental measurements has been proposed by Speedy and Angell [38] at 228 K. In the next Chapter it will be discussed the various theoretical scenarios developed in order to explain these and other water anomalies.
It should be notice that water is an anomalous liquid also from the dynamical point of view. One of the main water dynamical anomaly concerns the self diffusion coefficient D defined through the mean square displacement (MSD) as:

$$D = \lim_{t\to\infty} \frac{\langle |\mathbf{r}_j(t'+t) - \mathbf{r}_j(t')|^2 \rangle}{6t} \tag{2.6}$$

and related to the liquid viscosity through the Stokes-Einstein relations:

$$D = \mu k_B T \tag{2.7}$$

with μ the mobility coefficient. For spherical particles in a liquid $\mu = 1/(6\pi\eta r)$, where η is the viscosity and r is the radius of the particles. In simple liquids, the coefficient D should decrease upon increasing pressure, since compression is usually correlated to a loss of fluidity. Also for this quantity, water deviates from the ordinary behaviour. Fig. 2.7 shows, in fact, that in the high pressure range the self-diffusion decreases with compression but at sufficiently low temperatures a change occurs and D begins to increase with increasing pressure. This anomaly is called *diffusivity*

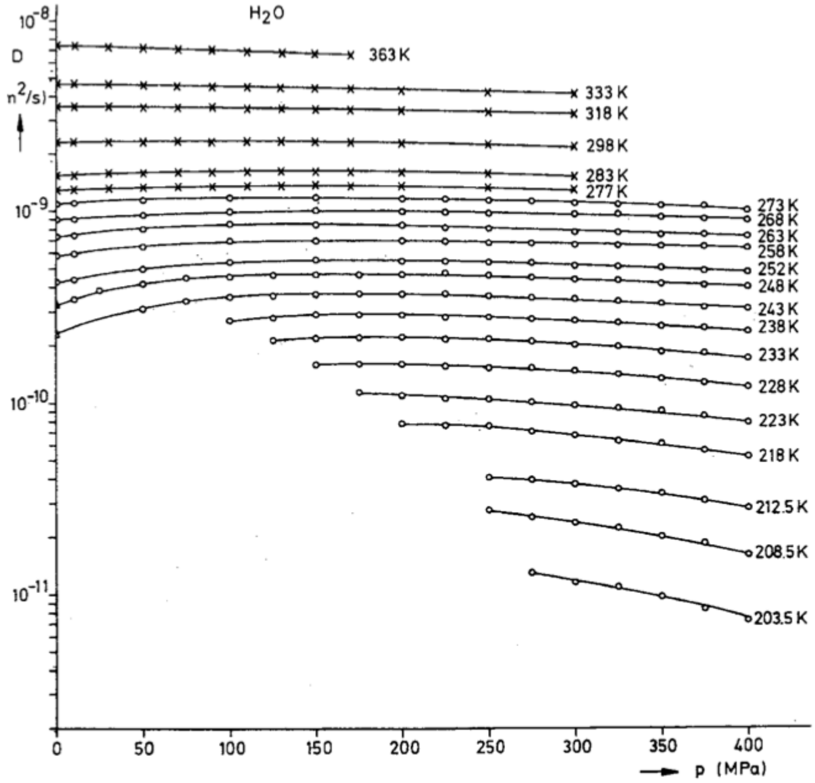

Figure 2.7: Experimental self diffusion coefficient D of water, at constant temperature, as a function of pressure. Figure from Ref. [5].

anomaly and it has been observed in several water potentials [22, 39–41] and experiments [42, 43].

Once again the explanation of such a phenomenon lies in the hydrogen bond network forming at low temperatures. In water, higher pressures correspond to a larger number of broken hydrogen bonds and so to an overall greater mobility of particles within the liquid.

The thermodynamic and dynamical anomalies of water discussed in this Section have clearly shown the importance of investigate its phase diagram. In particular, all the anomalies seem to persist with continuity also below the melting temperature, in the so called supercooled regime. It follows that experimental and theoretical efforts have to be done not only in the stable liquid state of water but also in its metastable supercooled phase. Before discussing the huge amount of works carried out on supercooled water, it is important to mention briefly the definition of supercooled liquid and the reasons that make possible the existence of such a state.

2.3 Supercooled water: possible answers to open problems

As already mentioned in the previous Section, water in the supercooled state is water at the liquid state below the freezing temperature. The physical conditions at which the system can be kept in this metastable state are related both to thermodynamic equations and to the presence of impurities or perturbations in the liquid.

2.3.1 The supercooled metastable state

Thermodynamics is by definition the study of equilibrium states that possess an indefinite lifetime. However, there exist (meta-)equilibrium states with a finite lifetime, for which the system is trapped in a relative minimum of the appropriate thermodynamic potential. These states are defined metastable states. Small thermal fluctuations, the presence of impurities or even roughness of the container (for liquids and gases) are in general sufficient to induce the transition from metastable states to the energetically favored corresponding equilibrium states. In order to be able to investigate a metastable state, its lifetime must be longer than the observation time. In turn this needs to be much longer than the structural relaxation time, defined as the time that the system takes for structurally rearrange and equilibrate, so that

$$\tau_{rel} << \tau_{obs} < \tau_{life} \tag{2.8}$$

The theory of metastability [7] will be not discussed here in details but some concepts useful will be recalled. Starting from the second principle of thermodynamics, the conditions of thermal and mechanical equilibrium can be derived [7]. In order to have mechanical stability the isothermal compressibility and the adiabatic compressibility must be positive. In order to have thermal equilibrium the isobaric specific heat and the isochoric specific heat must be also positive. A good example is represented by the van der Waals theory of a phase transition. In Fig. 2.8 generic isotherms in the P-V plane are reported. The Maxwell construction is used to draw the coexistence line AKD. However doing so, all the points between the left intersection of the isotherms with the coexistence line and the minimum and the ones between the maximum and the right intersection of the isotherms with the coexistence line are excluded. These points are not thermally stable but are still mechanically stable. In fact for these points k_T and k_S are larger than zero. The compressibility diverges at the extrema of the isotherms and it is negative in the region between the minimum and the

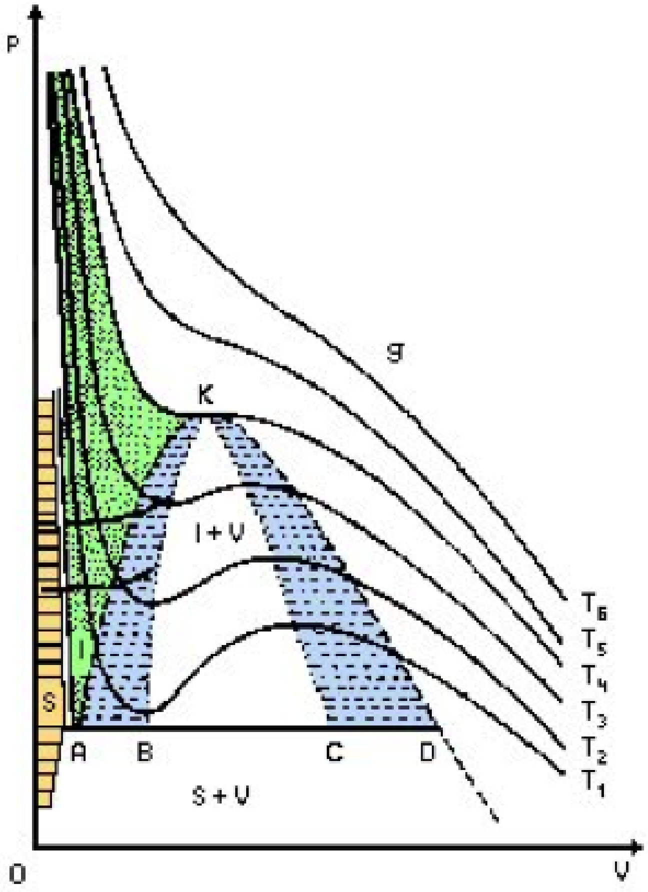

Figure 2.8: Isotherms of a generic system near a phase transition in the van der Waals theory. The Maxwell construction is used to draw the coexistence line AKD. The limit of mechanical stability (LMS) line BKC is also shown.

maximum. Joining the minima of the isotherms on the left side and the maxima on the right side the limit of mechanical stability (LMS) line BKC can be drawn. Thus the region of metastability can be defined as the region enclosed between the coexistence line and the LMS line. The only point in common between the coexistence line and the LMS line is the critical point K, that is also the only stable point belonging to the LMS line. In the metastability region, nucleation phenomena of the stable phase can occur and special techniques must be used in experiments in order to avoid the transition to the stable phase.

2.3.2 Ice nucleation and glass transition

Under special conditions, such as the extreme purity of the sample, the absence of external mechanical and thermal perturbations, the high degree of smoothness of the walls of the container, the range of existence of liquid water can be significantly extended. Nevertheless at certain condition the metastable supercooled state cannot more maintained and two possible outcomes of the liquid can occur: the ice crystallization of the system at the correspondent stable phase or a continuous dynamical transition into an amorphous solid, a glass. The central concept at the basis of these two phenomena concerns the two times that characterize a supercooled liquid: the nucleation time τ_1, defined as the time required for a given volume fraction of a sample to crystallize, and the structural relaxation time τ_2. It is the competition between these two characteristic times to be responsible of the sudden phase transition to ice or the smooth glass transition [7]. Fig. 2.9 shows the qualitative behaviour of τ_1 and τ_2 as a function of temperature. The Figure displays that the nucleation time τ_1, which is the time required to crystalize a given volume fraction of liquid following an instantaneous quench to the desired temperature, first decreases, reaches a minimum and then increases with the extent of supercooling. This nonmonotonic trend of τ is the result of the competition between the thermodynamic driving force for nucleation, i.e. the tendency of the liquid to crystallize by cooling the system and the increasing viscosity of the liquid, that slows down and obstructs the growth of the ice nuclei.

The second characteristic time of relevance to the fate of a supercooled liquid is τ_2, the internal molecular relaxation time. As the temperature is lowered below the freezing point, τ_2 increases very sharply from a high temperature limiting value of circa 10^{-13} sec to a point where it becomes comparable to the duration of a macroscopic experiment, circa 10^2 sec. Thus, if a liquid can be prevented from crystallization through a rapid quench down to a temperature at which the characteristic time for molecular rearrangement

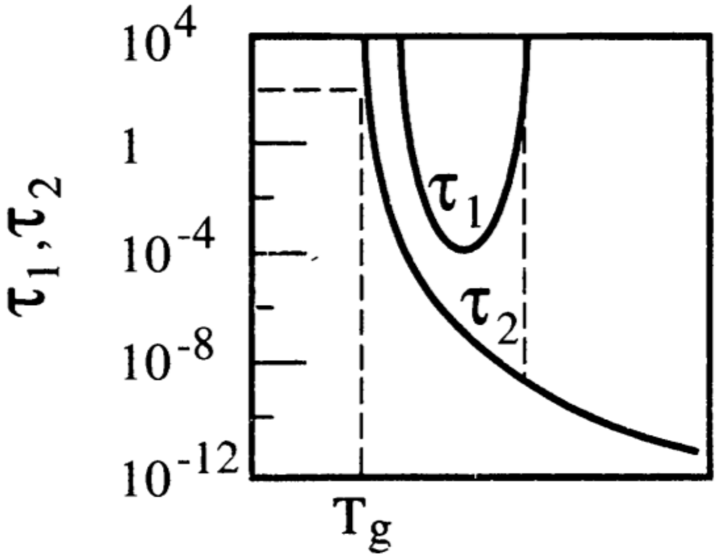

Figure 2.9: Schematic representation of the characteristic nucleation time τ_1 and the internal relaxation time τ_2 as a function of temperature. T_G is the glass transition temperature, defined as the temperature at which $\tau_2 \sim 10^2$ sec. Figure from Ref. [7].

becomes comparable to the experimental time scale, it appears structurally arrested on that time scale. The liquid is then said to have vitrified.
Previous Section has demonstrated the importance of investigate supercooled and glassy water both thermodynamically and dynamically. Next Section will be devoted to a summarized description of the experimental and theoretical results nowadays reached in this regime.

3

Supercooled Water: Theory and Experiments

Chapter 2 has been devoted to a brief description of the thermodynamic and dynamical anomalies that make water one of the most anomalous liquid in the world. As already mentioned, although the great amount of theoretical and experimental works, a real comprehension and interpretation of water phase diagram is still missing. A primary role in this research is given by the study of its supercooled metastable regime, that could represent a possible way to investigate the deep origins of water anomalies. For this reason, in this Chapter the main aspects of thermodynamics and dynamics of supercooled water together with the theoretical interpretations developed will be discussed in detail.

3.1 Supercooled Water Thermodynamics

It has been anticipated in previous Chapter that the thermodynamic anomalies appearing in the stable liquid state of water seem to proceed continuously also in the supercooled regime. Consequently, a complete vision of the thermodynamic phenomenology of water in the mild and deep supercooled region is extremely important to understand the causes of its peculiar behaviour.

3.1.1 Phenomenology

A huge amount of theoretical, computational and experimental research has been developed in the last years in order to build a picture as much as possible complete of the phenomenological behaviour of supercooled water thermodynamics [9]. Even if several aspects of this unique supercooled liquid are not still totally clear and understood today and have to be further investigate, relevant steps forward have been taken by the scientific community. It was exactly from these efforts that it has been possible to determine clearly the starting point from which developing theoretical scenarios and models to explain water peculiar properties. Nowadays, the overall knowledge of the metastable water phase diagram in the supercooled and vitreous regime can be schematically summarized with the picture in Fig. 3.1. Water can be supercooled, i.e. it can be kept in the liquid state under its crystallization temperature for a macroscopic time interval comparable to the duration of the experimental measurements, in the thermodynamic region marked by the melting curve T_M in the upper high temperature border confining with the stable liquid phase and by the homogenous nucleation temperature curve T_H in the low temperature border. In this interval, the rapid quenching of the system prevents the formation and the growth of ice nuclei and the liquid rearranges molecularly with a characteristic time smaller than the nucleation rate. Several experimental works have been carried out by purifying the sample from the presence of nucleation-inducing impurities and separating it in small droplets in order to lower the nucleation temperature. The results obtained from the totality of these experiments had established $T \sim 232$ K as the lowest temperature at ambient pressure below which the crystallization of the liquid was unavoidable. Only very recently, new experimental techniques using nanodroplets, nanoconfinement and association with biomolecules have successfully shifted the limit of 232

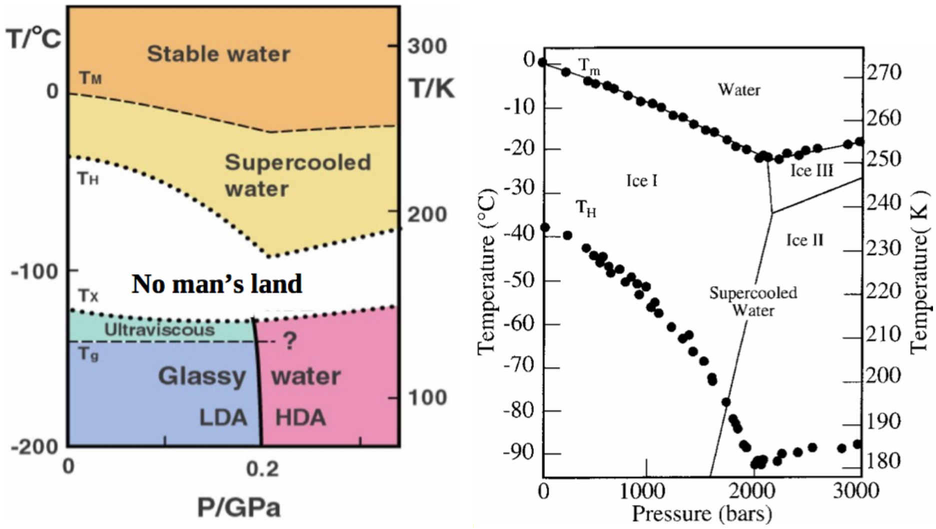

Figure 3.1: Left Panel: Schematic representation in the $P - T$ of the metastable phase diagram of supercooled and glassy water (Picture adapted from Ref. [10]). Right panel: significant thermodynamic curves of water drawn experimentally in the supercooled state and correspondent stable ice phases in the same range of pressure and temperature (Figure from Ref. [7]).

K down to 227 K [44].

Even if it is not possible experimentally to overcome the nucleation temperature line, upon cooling the system very rapidly down to the glass transition temperature T_G in order to inhibit the sudden transition of the liquid towards the ice stable state, the system transforms into glassy water, becoming an amorphous disordered solid. In this state, the relaxation time of the system is similar to the macroscopic time scale of the experiment and the liquid is structurally arrested. The experimental value of T_G is controversial: the general consensus is that water vitrifies around 136 K [45, 46] but latest measurements would relocate T_G at 165 K [47, 48].

A large number of experiments [49–52] realized in the past years on the amorphous phase of water have definitely confirmed the existence of two distinct forms of glassy water: the high density amorphous ice (HDA) and the low density amorphous ice (LDA).

The first observation of the HDA state was done by Mishima and co-workers in 1984 [53] when, through the compression at low temperature of a sample of ice Ih, they found a dense disordered vitreous solid with local structure similar to the local arrangement of liquid water. This high density amorphous state of water can be achieve in the deep supercooled region at high values of pressure, as shown in Fig. 3.1.

Low density amorphous ice, on the contrary, occurs penetrating the thermodynamic region below the glass transition temperature from the low pressure side. Similarly to HDA, LDA local structure presents strong analogies with molecular distribution of ice Ih.

Fig. 3.2 displays the oxygen-oxygen, oxygen-hydrogen and hydrogen-hydrogen radial distribution functions (RDF) in HDA and LDA at T=268 K [54].

The separation between HDA and LDA in the glassy phase of water originates from the existence of a first order phase transition discovered in 1985 by Mishima and co-workers [49]. By pressurizing a sample of LDA, measurements on the volume and other thermodynamic properties of the system evidenced, at approximately 6 $Kbar$, the appearance of a sharp and sudden volume reduction perfectly compatible with the volume discontinuity typical of a first order transition (see Fig. 3.3). The presence of the LDA-HDA phase transition has been later corroborated by other experimental works using Neutron Diffraction [55] and Raman Spectroscopy [56].

Once water has vitrified in one of its two amorphous states, the effect of heating glassy water is a spontaneous transition to cubic ice Ic around 150 K [45, 58]. This phenomenon implies that supercooled liquid water can not be achieved increasing temperature above the glass transition since nucleation to ice prevents the formation of this metastable liquid phase [59].

The presence of the nucleation temperature line and of the glass transition

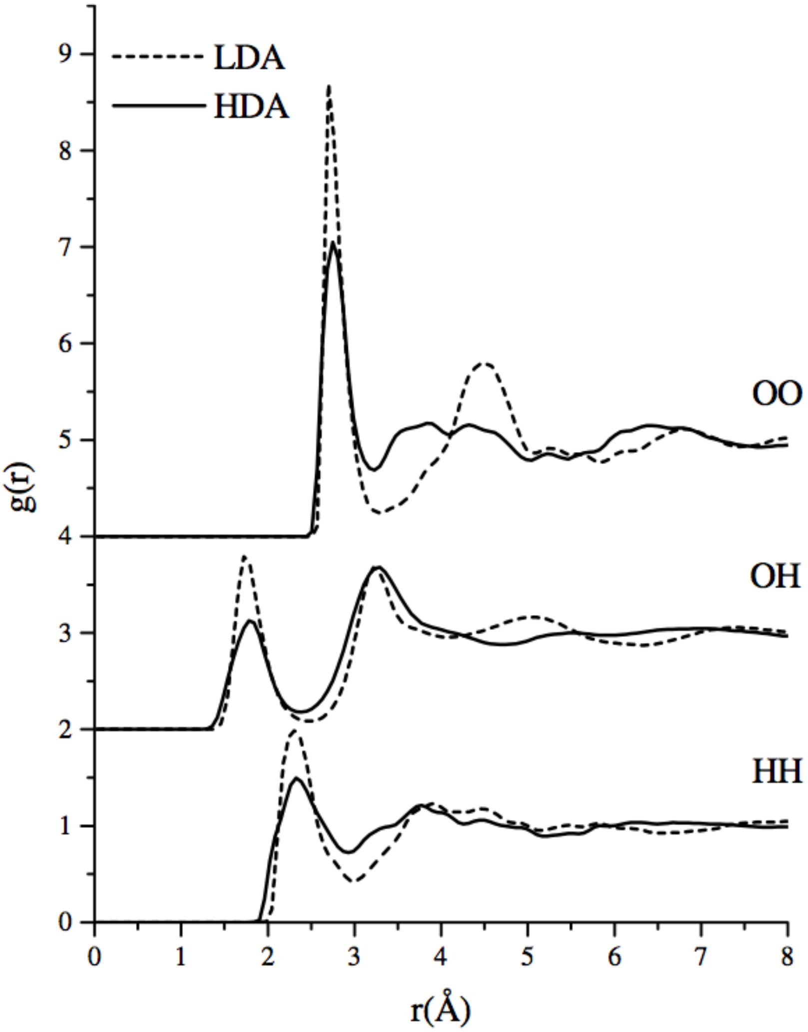

Figure 3.2: Oxygen-oxygen, oxygen-hydrogen and hydrogen-hydrogen RDF at T = 268 K, for LDL and HDL as calculated starting from neutron diffraction experimental data [54].

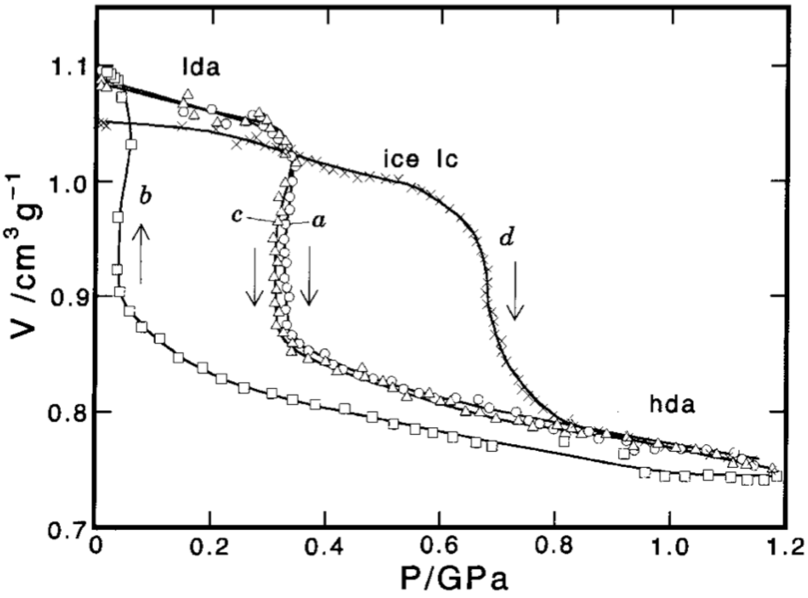

Figure 3.3: Evolution of volume in the thermodynamic path followed in Ref. [57] composed of compression (a), subsequent decompression (b) and compression (c) of amorphous phases during warming up to 135 K.

line, that both block the process of supercooling respectively upon cooling and heating the system, define a thermodynamic region, called "no man's land" [11, 12, 60], where it is very difficult to realize experimental measurements on the supercooled liquid state but not impossible in principle [61].

3.1.2 Supercooled Water Theoretical Scenarios

The discovery of glassy water polyamorphism and the existence of the LDA-HDA phase transition together with the thermodynamic and dynamical anomalies of liquid water have led to the development of several theoretical hypothesis [13, 36, 62–65] trying to explain the overall anomalous phenomenology of water in its stable and metastable state. The theoretical scenario that has by far received the greatest attention has been the Liquid-Liquid Critical Point (LLCP) Scenario [13].

3.1.2.1 The Liquid Liquid Critical Point Scenario

The hypothesis of the Liquid Liquid Critical Point was formulated for the first time by Poole, Sciortino, Essmann and Stanley on the basis of numerical simulations of the phase diagram of the ST2 water model [13] and is well

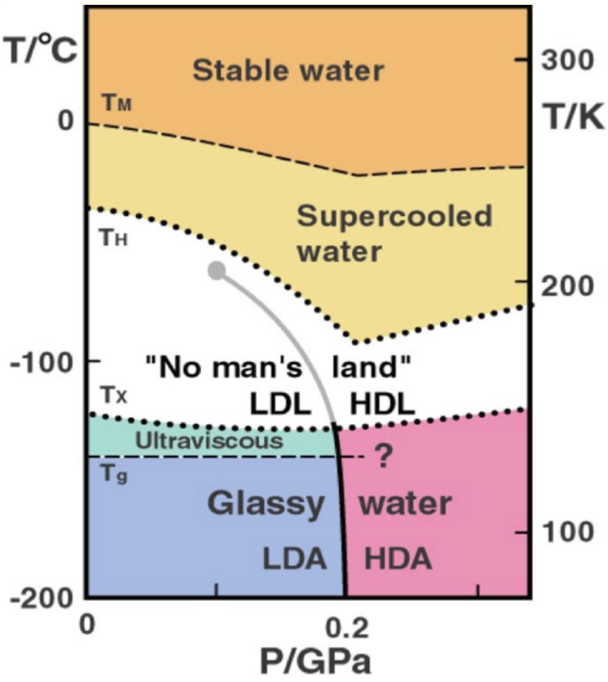

Figure 3.4: Main features of the LLCP scenario. The LDA and HDA are separated by a first order phase transition line. This line extends above the glass transition line in the so called no man's land and separates the two distinct liquid phases LDL and HDL. At the end of the coexistence line is situated the LLCP, above which the distinction between the two liquids disappears. T_H is the line of the homogeneous nucleation and T_M is the melting line. Figure from Ref. [10].

summarized by the picture in Fig. 3.4 [10]. The central idea of the LLCP scenario is the existence of a second order critical point located in the "no man's land" that would be the terminal point of a first order phase transition occurring between two different state of supercooled liquid water: the low density liquid water (LDL) and the high density liquid water (HDL). This transition is called liquid-liquid phase transition (LLPT) and would evolve in the low temperature and high pressure region into the observed transition between LDA and HDA. According to this scenario, LDA and HDA would be the correspondent vitreous phase of LDL and HDL respectively.

The presence of a LLCP explains on one hand the first order phase transition between HDA and LDA and on the other hand the anomalous increase of the thermodynamic response functions upon cooling [66]. The isothermal compressibility k_T and the isobaric specific heat c_P are, in fact, associated to the density and entropy fluctuations of the system through the relations:

$$< (\delta V)^2 >= V k_B T k_T \tag{3.1}$$

$$< (\delta S)^2 >= N k_B c_P \tag{3.2}$$

These quantities, as predicted by the theory of critical phenomena, become proportional to the fluctuations of the correlation length close to the second order critical point and consequently diverge asymptotically upon approaching it. Moreover, the experimentally observed phase transition between LDA and HDA would be the structurally arrested expression of the LDL-HDL equilibrium phase transition.

In presence of a first order phase transition the Clausius-Clapeyron equation holds:

$$\frac{dP}{dT} = \frac{\Delta s}{\Delta v} \tag{3.3}$$

where the left term represents the inclination of the coexistence line and Δs and Δv are respectively the difference in molar entropy and molar volume between the two coexisting states. Consequently, the uncommon negative slope of the hypothesized LLPT implies that HDL is a more disordered and entropic phase with respect to LDL that presents a more opened and structured local arrangement.

It should be underlined that, according to the LLCP scenario, a one phase region extends for temperatures above and pressure below the critical point. In this thermodynamic region, the distinction between LDL and HDL disappears and supercooled water exists as a liquid in a single phase. Similarly to the two phase region, also in the one phase region it is expected an asymptotic divergence of the density correlation length upon approaching the second order critical point. In particular, a locus of maxima of the correlation length appears moving towards the LLCP. This line is called Widom Line (WL) [67, 68] and it can be observed also for the ordinary liquid-vapour critical point [69]. Since close to the critical point the thermodynamic response functions become proportional to power laws of the correlation length, loci of maxima of k_T, c_P and other quantities related to the liquid fluctuations emerge in the one phase region. These loci progressively collapse on the Widom Line approaching the LLCP and, for this reason, can be considered a reasonable proxy for the Widom line in computational studies.

A huge amount of theoretical, computational [10, 67, 68, 70–87] and experimental [11, 12, 19, 88–91] works have been carried out in order to prove definitely the presence of the liquid liquid critical point. As mentioned before, it was the seminal computational work of Poole et al. [13] to led to the formulation of the LLCP hypothesis. These authors performed Molecular Dynamics simulations on ST2 water potential and analyzed several

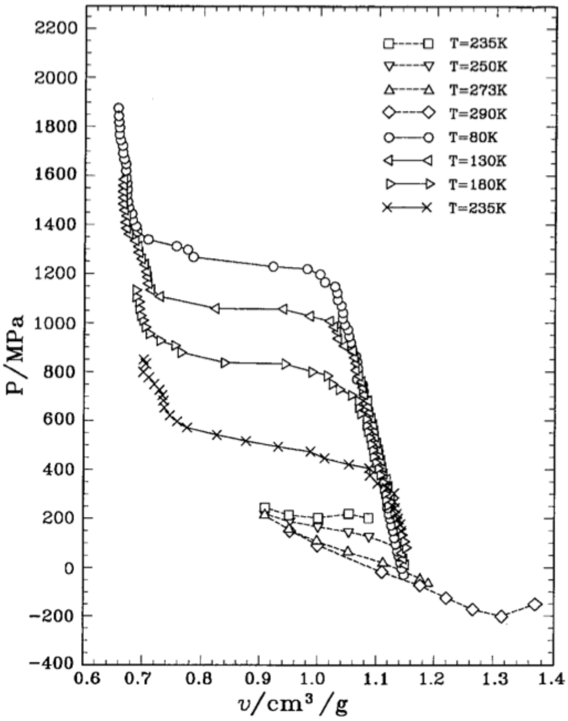

Figure 3.5: Results of isothermal compression of LDA (solid lines) and low temperatures isotherms (dashed lines) obtained from the Molecular Dynamics simulations on ST2 of Ref. [13]. The solid lines show an abrupt change in the volume typical of first order phase transition and the dashed lines exhibit inflection points that could be indicative of the presence of the LLCP. Figure from Ref. [7] and adapted from Ref. [13].

isotherms in the liquid and vitreous thermodynamic region. The high temperatures and low pressures liquid isotherms showed inflection points with a temperature dependence compatible with the presence of a second order critical point. Moreover non equilibrium isothermal compression of solid LDA exhibited a sharp and immediate increase of volume similar to the volume change occurring in first order phase transitions (see Fig. 3.5). Also the thermodynamic response functions increased asymptotically upon supercooling providing another proof of the existence of a LLCP.

Starting from ST2, Molecular Dynamics simulations on other water and water-like potentials were performed searching evidences to support the LLCP scenario. TIP4P [74, 80], TIP5P [67, 77, 82, 92] and ST2 [74, 76, 80, 81, 93, 94] present clearly a liquid liquid critical point and a first order liquid liquid phase transition. The LLPT has been also confirmed in ST2 by recent extensive computations based on free energy calculations [81, 95–104]. Also TIP4P/2005 manifests an anomalous increase in the isothermal compressibility and isobaric specific heat together with inflection points in the isotherms suggesting the presence of a LLCP [23]. The controversial interpretation of the results on Molecular Dynamics simulations on TIP4P by Tanaka et al. proposes also for this potential a LLCP [84, 105]. Free energy calculations on SPC/E [106] seem, moreover, to provide results compatible with the LLCP scenario.

Anomalous behaviour of the phase diagram both in the liquid stable and metastable state was found also in water-like potentials, such as the Jagla Model, that describes particle interactions with a spherically symmetric potential identified by two characteristic length scales. In particular, indications of the existence of LLPT, LLCP, increase of the thermodynamic response functions together with the density anomalies were detected for this potential [67, 70, 73, 107–113]. Free energy calculations have corroborated the existence of a LLCP in Jagla Potential [114].

From the experimental point of view, a decisive experiment promoting the idea of the LLCP was carried out by Mishima and Stanley [11, 12]. Through measurements on the melting line of metastable ice IV, Mishima and Stanley succeeded on tracing the liquid liquid phase transition and located the liquid liquid critical point around $T \sim 220$ K and $P \sim 100$ MPa [12]. Even if the experiment of Ref. [12] provides an important contribution in favor of the LLCP hypothesis, it is based on the observation of a sharp variation of the volume along the ice IV melting line that is also compatible with another theoretical scenario explaining water anomalies, the Singularity Free Scenario [36]. This fact makes this work a fundamental but not definitive proof of the LLCP scenario. An electron spin resonance experiment [91] found for bulk water results consistent with the coexistence of LDL and HDL phases in the deep supercooled region. Another method used to avoid crystallization of water in order to investigate the presence of two different state of supercooled liquid water is to confine it in small pores. Recent experiments using Neutron Diffraction technique on water confined in a nanoporous silica matrix, MCM-41 [19, 88–90], found results in agreement with the LLCP scenario. Zhang et al. [88] observed for the first time in confined D_2O the appearance of hysteresis in density, confirming the presence of a first order phase transition line. Recently Wang et al. [115] have found evidences of the existence of a liquid-liquid phase transition ending at a point located at $P = 1.29 \pm 0.34\ Kbar$ and $T = 213 \pm 3\ K$ that would correspond to the LLCP according to the LLCP scenario. A time-resolved optical Kerr effect investigation by Taschin et al. [116] has provided signs of the coexistence of two liquid structures of water, interpreted as LDL and HDL.

Theoretically speaking, several models were constructed in order to understand the microscopic origin of the two supercooled liquid phases of water and the thermodynamic anomalies of the supercooled regime [68, 71, 72, 75, 87, 117–119]. In particular, theoretical scaling analysis of the LLCP gives also a consistent scenario [66, 120, 121].

Even if further computational, experimental and theoretical investigations on the phase behaviour of water in the liquid and metastable supercooled state have to be performed to provide conclusive confirmations of the real existence of LLCP, the liquid liquid critical point scenario represents nowadays an elegant and reasonable explanation of water anomalies and opens the doors to an entire new research area on multiple-fluids critical phenomena. Besides the LLCP, other theoretical scheme flourished in the past years trying to justify the peculiar water phase diagram.

3.1.2.2 Other Scenarios

A theoretical scenario that is able to interpret glassy water polyamorphism and the anomalous increase of the thermodynamic response functions is the *Singularity Free* Scenario proposed by Sastry et al. [36]. In this scenario, the increase of k_T, c_P and of the magnitude of α_P upon cooling is not the consequence at higher T of the divergences of system fluctuations that occur approaching a critical point. On the contrary, the behaviour of these quantities is directly caused by the presence of the TMD line and its negative slope in the $P-T$ plane. Provided the following thermodynamic relations [36] (the subscript 'TMD' and 'P, at TMD' indicates a directional derivative along the TMD and a derivative calculated at constant pressure at the TMD, respectively):

$$\left(\frac{\partial K_T}{\partial T}\right)_{P,at\ TMD} = \frac{v^{-1}(\partial^2 v/\partial T^2)_{P,at\ TMD}}{(dP/dT)_{TMD}} \tag{3.4}$$

$$\left(\frac{\partial c_P}{\partial T}\right)_T = -T\left(\frac{\partial^2 v}{\partial T^2}\right)_P \tag{3.5}$$

the negative slope of the TMD and the positive concavity of the molar volume v as a function of temperature (that implies $(\partial^2 v/\partial T^2)_{P,at\ TMD} > 0$) cause the isothermal compressibility and isobaric specific heat to increase upon isobarically cooling and isothermally compressing the system respectively. No singularity is present and the thermodynamic response functions increase sharply because of the density anomaly, reaching a maximum finite value. It should be noticed that the line of maxima of k_T and c_P predicted in the singularity free scenario is not related to the maxima appearing in presence of a critical point and their heights do not necessary have a monotonic behaviour as happens by moving close to the LLCP. The anti-correlation between k_T and α_P finally explains also the increase of the absolute value of the expansion coefficient upon decreasing temperature isobarically. Calculations on lattice models have reproduced the situation depicted by the singularity free scenarios, with a sharp but finite increase of the response functions occurring more and more abruptly at higher pressure and maxima of k_T located at lower temperature upon increasing pressure. Giving a consistent explanation of water phase diagram, also the singularity free scenario can not be excluded as a possible interpretation of water anomalies.

Another scenario proposed in the past as the first unifying scenario but considered now obsolete is the *stability limit conjecture*, theorized by Speedy [62] in 1982. In this scenario the increase in the thermodynamic response functions was attributed to the approach to the limit of mechanical stability (LMS) line, where the supercooled liquid becomes unstable with respect to the vapour phase. This scenario predicted also the existence of a continuous limit of mechanical stability line bounding the superheated and the supercooled states, reverting to positive pressures for low temperatures. This behaviour of the LMS line would be anomalous, as in simple liquids the LMS line has a positive slope in all the phase diagram [5]. Subtle arguments of thermodynamic consistency basically ruled out this scenario [5] and furthermore no evidence of a retracing LMS line was found either in experiments or in computer simulations.

3.2 Supercooled Water Dynamics

Section 3.1 have shown how the collaborative work of theorists and experimentalists has been able to build a detailed picture of water thermodynamic behaviour in the liquid stable and metastable state. Nevertheless, less attention has been devoted to the dynamical aspects of this liquid. In this context, a milestone in the knowledge of water microscopic dynamics is represented by the seminal works of Ref. [14] and Ref. [15] that through Molecular Dynamics simulations on SPC/E water potential identified a two step relaxation scenario in the decay of the Self Intermediate Scattering Functions. The theoretical model able to explain this behaviour of the relaxation process in supercooled water is the Mode Coupling Theory (MCT) of glassy dynamics, formulated and developed by Goetze [16]. All the calculations exposed below are taken from Ref. [16] and references inside it.

3.2.1 The Mode Coupling Theory

The central idea of the Mode Coupling Theory is that at sufficiently low temperatures, particle dynamics is governed by a feedback mechanism that becomes so strong to cause the structural arrest of the system. In particular the deep coupling between single particle motion and the density fluctuations of the liquid leads the particle to be trapped in a "cage" formed by its nearest neighbors. This phenomenon, called "cage effect" is at the basis of slow structural rearrangement of liquids in the supercooled regime. The starting point of the MCT is the generalized Langevin equation.

3.2.1.1 The Theory

The simple temporal evolution of a phase space variable $A(t)$ that depends implicitly on the positions $\vec{r}_i$ and momenta $\vec{p}_i$ of a N particle system follows the equation:

$$\frac{d\mathbf{A}(t)}{dt} = \{\mathbf{A}(t), \mathcal{H}\} = i\mathcal{L}\mathbf{A}(t) \tag{3.6}$$

where $\mathcal{H}$ and $\mathcal{L}$ are respectively the Hamiltonian and the Lagrangian that govern the system. Defining a projection operator $\mathcal{P}$ along A as the operator that extracts the "A" character from the variable on which acts:

$$\mathcal{P} = (\mathbf{A}, ...)(\mathbf{A}, \mathbf{A})^{-1}\mathbf{A} \tag{3.7}$$

with $(\mathbf{A}, \mathbf{B}) \equiv \langle \mathbf{B}\mathbf{A}^* \rangle$, the equilibrium correlation function is identified by the inner product between two vectors $\mathbf{A}$ and $\mathbf{B}$ in the Liouville space. Eq. 3.6 can be transformed through a series of mathematical passages into the following equation:

$$\frac{d\mathbf{A}(t)}{dt} = i\mathbf{\Omega} \cdot \mathbf{A}(t) - \int_0^t d\tau \mathbf{K}(\tau) \cdot \mathbf{A}(t-\tau) + \mathbf{f}(t) \tag{3.8}$$

where $\mathbf{A}$ is the initial value $\mathbf{A} = \mathbf{A}(0)$, the *fluctuating random force* is defined as:

$$\mathbf{f}(t) \equiv e^{i(1-\mathcal{P})\mathcal{L}t} i(1-\mathcal{P})\mathcal{L}\mathbf{A} \tag{3.9}$$

the *memory function* matrix $\mathbf{K}(t)$ is:

$$\mathbf{K}(t) \equiv (f, f(t)) \cdot (\mathbf{A}, \mathbf{A})^{-1} \tag{3.10}$$

and the *characteristic frequency* matrix $\mathbf{\Omega}$ is:

$$i\mathbf{\Omega} \equiv (\mathbf{A}, i\mathcal{L}\mathbf{A}) \cdot (\mathbf{A}, \mathbf{A})^{-1} \tag{3.11}$$

The development of the generalized Langevin equation in Eq. 3.8 originates from the idea initially proposed by Langevin that particle dynamics within a liquid is characterized by two contributions with different time scales: the slow relaxation of the initial velocity of the molecules and the fast, instant collisions of particles with their surroundings. If $\mathbf{A}$ is a slow varying variable with time (quasi-hydrodynamic variable), the projection operator $\mathcal{P}$ on $\mathbf{A}$ represents an operator that extracts the slow "character" of the variable on which is applied. It follows that the random force $f(t)$ is the temporal evolution of the fast character of $\dot{\mathbf{A}}$ in the orthogonal fast space. $f(t)$ is not a force in the mechanical sense, being proportional to the molecule velocity, but corresponds in some sense to the fast contributions involved in particle dynamics. In this context, the memory function $\mathbf{K}(t)$ is a non local in time term that takes into account the previous history of particle trajectory and expresses the autocorrelation between the particle motion at time t and its past at earliest times. This means that, contrary to general Markovian processes, the instantaneous particle coordinates and velocities are determined not only by the state of the surrounding medium at the same time but also by the memory that the particle has of its path until that moment. It should be noticed that Eq. 3.8 shows that the time derivative of $\mathbf{A}$ is governed by two separate types of terms: the first two terms on the left are linear in $\mathbf{A}$ and represent the smooth contributions to the dynamics while the random force involves the effects of non linear and short-lived dynamical terms. This separation is useful for systems where quantities with different time scales participate to the dynamics as in case of liquid dynamics, that is characterized by impulsive and instantaneous forces whose correlations decay fast with time and slow relaxation processes. An appropriate choice of the variable $\mathbf{A}$, hence, allows to write the particle motion decoupling the fastly and slowly varying properties of the system. Defining the correlation matrix as:

$$\mathbf{C}(t) \equiv \langle \mathbf{A}(t)\mathbf{A}^*(0)\rangle = (\mathbf{A}, \mathbf{A}(t)) \tag{3.12}$$

Eq. 3.8 translates into the following equation for the correlation matrix:

$$\frac{d\mathbf{C}(t)}{dt} = i\boldsymbol{\Omega}\mathbf{C}(t) - \int_0^t d\tau \mathbf{K}(\tau) \cdot \mathbf{C}(t-\tau) \tag{3.13}$$

where the fluctuating force does not appear because of the orthogonality relation $(\mathbf{A}, \mathbf{f}(t)) = 0$.

Eq. 3.13 permits to determine an equation for the Self Intermediate Scattering Function (SISF) $F(\mathbf{q}, t)$ of liquids, defined as:

$$F_S(\mathbf{q}, t) = \frac{1}{N}\left\langle \sum_i e^{i\mathbf{q}\cdot\left[\mathbf{r}_O^i(t) - \mathbf{r}_O^i(0)\right]} \right\rangle, \tag{3.14}$$

where $\mathbf{r}_O^i(t)$ is the position of the oxygen atom at instant t. This function is a measure of the density fluctuations of the system and is directly related to the static structure factor $S(q) = F(q, 0)$.
For this purpose, the variable $\mathbf{A}$ is chosen to be:

$$\mathbf{A} = \begin{bmatrix} \delta\rho_{\mathbf{q}} \\ j_{\mathbf{q}}^L \end{bmatrix} \tag{3.15}$$

where $\delta\rho_{\mathbf{q}}$ is the Fourier Transform of the density save for a constant proportional to the uniform density $\rho = N/V$:

$$\delta\rho_{\mathbf{q}} = \sum_i e^{i\mathbf{q}\cdot\mathbf{r_i}} - (2\pi)^3 \rho\delta(\mathbf{q}) \tag{3.16}$$

and $j_{\mathbf{q}}^L$ the longitudinal component of the associated current:

$$j_{\mathbf{q}}^L = \frac{1}{m} \sum_i (\mathbf{q} \cdot \mathbf{p}_i) e^{i\mathbf{q}\cdot\mathbf{r}_i} \tag{3.17}$$

with m the particle mass. It should be noticed that, since modes with different $\mathbf{q}$ are independent, the equations that will be derived are valid for each $\mathbf{q}$. Moreover the choice of the longitudinal component $j_{\mathbf{q}}^L$ allows to express the current with a single component, fixing the axes along the direction of $\mathbf{q}$.
Substituting the definition of the variable $\mathbf{A}$ in Eq. 3.13, the terms involved in the equation reduce to:

$$\mathbf{C}(\mathbf{q}, t) = \begin{bmatrix} \langle \delta\rho_{-\mathbf{q}} \delta\rho_{\mathbf{q}}(t) \rangle & \langle \delta\rho_{-\mathbf{q}} j_{\mathbf{q}}^L(t) \rangle \\ \langle j_{-\mathbf{q}}^L \delta\rho_{\mathbf{q}}(t) \rangle & \langle j_{-\mathbf{q}}^L j_{\mathbf{q}}^L(t) \rangle \end{bmatrix} \tag{3.18}$$

$$i\boldsymbol{\Omega}_q = \begin{bmatrix} 0 & iq \\ i\frac{qk_BT}{mS(q)} & 0 \end{bmatrix} \tag{3.19}$$

$$\mathbf{K}(\mathbf{q}, t) = \begin{bmatrix} 0 & 0 \\ 0 & \frac{m\langle R_{-\mathbf{q}} R_{\mathbf{q}}(t) \rangle}{Nk_BT} \end{bmatrix} \tag{3.20}$$

where:

$$R_{\mathbf{q}} = \frac{dj_{\mathbf{q}}^L}{dt} - i\frac{qk_BT}{mS(q)} \delta\rho_{\mathbf{q}} \tag{3.21}$$

and $S(q)$ is the static structure factor. The correlations of the Fourier Transform of the density appearing in Eq. 3.18 correspond, save for an unphysical constant, to the Intermediate Scattering Functions of the liquid $F(\mathbf{q}, t) = \frac{1}{N} \langle \delta\rho_{\mathbf{q}}(t) \delta\rho_{-\mathbf{q}} \rangle$.

It follows that the lower left corner of the matricial Eq. 3.13 becomes:

$$\frac{d^2F_S(\mathbf{q},t)}{dt^2}+\frac{q^2k_BT}{mS(q)}F_S(\mathbf{q},t)+\int_0^t dt'K(\mathbf{q},t-t')\frac{d}{dt'}F_S(\mathbf{q},t')=0 \qquad (3.22)$$

Eq. 3.22 represents the equation of motion of an harmonic oscillator with frequency $\Omega_q^2=q^2k_BT/mS(q)$ dumped by a time-retarded frictional force proportional to the memory function $K(\mathbf{q},t-t')=m\langle R_{-\mathbf{q}}R_{\mathbf{q}}(t-t')\rangle/Nk_BT$. Moreover the dependence of the microscopic frequency from the static structure factor implies that, as it will be shown later, the static properties of the system are the input quantities for the Mode Coupling equations of the Self Intermediate Scattering Function.

Before going on, it should be underlined that Eq. 3.22 has been derived from totally general assumptions that are not specific of glass-formers liquids. Nevertheless, even if it is an exact equation it is not solvable. In order to gain predictions on the dynamical behaviour of supercooled liquids, several approximations have to be done for determining a reasonable expression of the memory function that could take into accounts the slow structural relaxation discussed in the previous Section. The sets of passages originally developed by Goetze and his collaborators [122] to write explicitly the memory function are based on two main approximations. The first one is that, suspecting that fast random force was actually coupled to the slow modes of the system $\delta\rho_{\mathbf{k}_1}\delta\rho_{\mathbf{k}_2}$ and had a residual slow character, the random force is substituted with its projection onto a subspace spanned by its dominant slow product modes. The second approximation consists of factorizing all the four point correlation functions into products of two point ones. The result from these and other manipulations is the following expression for the memory function:

$$K(\mathbf{q},t)=\frac{\rho^2k_BT}{2Nm}\sum_{\mathbf{k}}\left|V_{\mathbf{q}-\mathbf{k},\mathbf{k}}\right|^2F(\mathbf{k},t)F(\mathbf{q}-\mathbf{k},t) \qquad (3.23)$$

with:

$$V_{\mathbf{q}-\mathbf{k},\mathbf{k}}\equiv\{(\hat{\mathbf{q}}\cdot\mathbf{k})c(k)+\hat{\mathbf{q}}\cdot(\mathbf{q}-\mathbf{k})c(|\mathbf{q}-\mathbf{k})\} \qquad (3.24)$$

The two-mode approximated vertex function $V_{\mathbf{q}-\mathbf{k},\mathbf{k}}$ depends only on the wavevectors $\mathbf{q}$ and $\mathbf{k}$ and can be computed from the static structure factor through the Ornstein-Zernike relation $S(k)=1/(1-\rho c(k))$.

It has to be underlined that the presence in the formulation of the memory function of the product $F(\mathbf{k},t)F(\mathbf{q}-\mathbf{k},t)$ implies that $K(\mathbf{q},t)$ decades with the same time scale of density correlators. Surprisingly, despite the removal of the slow component of the memory function through the projection operator, this "fast" quantity reveals coupled dynamically with the slow modes of motion.

The expression of Eq. 3.23 for the memory function is not complete. Eq. 3.23, in fact, represents only the long-time contribution to the total memory function, contribution that becomes progressively more important for temperatures and pressures in the deep supercooled region. Since the earliest time interval of the dynamics is characterized by instantaneous collisions between particles, it is worth to describe the short time term of the total memory function as a function sharply peaked at $t = 0$, in particular as a Dirac δ function:

$$K^{(0)}(\mathbf{q}, t) = \nu(k)\delta(q) \tag{3.25}$$

Including also the effects of the short time collisions in the memory function, the full version of $K(\mathbf{q}, t)$ is composed of the sum of the short and long time terms:

$$K(\mathbf{q}, t) = \nu(q)\delta(t) + \Omega_q^2 K^L(\mathbf{q}, t) \tag{3.26}$$

where long time memory function of Eq. 3.23 has been factorized extracting the frequency Ω_q^2.
Overall the non-linear equation 3.22 can be rewritten as:

$$\frac{d^2F_S(\mathbf{q},t)}{dt^2}+\Omega_q^2F_S(\mathbf{q},t)+\nu(q)\frac{d}{dt}F_S(\mathbf{q},t)+\Omega_q^2\int_0^\infty dt'K^L(\mathbf{q},t-t')\frac{d}{dt'}F_S(\mathbf{q},t')=0 \tag{3.27}$$

Eq. 3.27 and Eq. 3.23 are the so-called Mode Coupling Equations and are a closed set of coupled equations from which the full time evolution of the Self Intermediate Scattering Function can be determined. The only initial input necessary for solving these equation is the static structure factor, that introduces the temperature and density dependence of the solution and can be computed from knowledge of the interaction potential between molecules. It is clear from Eq. 3.27 that the feedback mechanism mentioned previously comes from the quadratic dependence of the memory function from the density correlator itself. This means that the instantaneous density fluctuations of the system are non-linearly related to its previous history through the sum in Eq. 3.23. The deep implications of the Mode Coupling Equations can be understood applying a further approximation. Since the vertex function gives the largest contribution when the reciprocal vector has the value $\mathbf{q} \sim \mathbf{q}_{max}$ of the first peak of the static structure factor, the substitution of the sum on the wavevectors space with the single value $\mathbf{q}_{max}$ reduces Eq. 3.27 to:

$$\frac{d^2F_S(t)}{dt^2} + \Omega^2F_S(t) + \nu\frac{d}{dt}F_S(t) + \Omega^2\lambda\int_0^\infty dt'\left[F_S(t-t')\right]^2\frac{d}{dt'}F_S(t') = 0 \tag{3.28}$$

where λ is a "control parameter" called *exponent parameter* that takes into account the state parameters of the system such as temperature and density and depends on the static structure factor. With this approximation the SISF has become a function dependent only on time. The analytical solution of Eq. 3.28 shows that for particular values of Ω and λ, which corresponds to a fixed temperature and density, a sharp phase transition occurs from an ergodic phase where the system is able to structurally relax and rearrange to a non ergodic state where the liquid dynamics is completely arrested. In this second phase the non linear coupling of density fluctuations with the memory function is so strong that particles are totally blocked at fixed positions.

For each density, the temperature at which the ergodic to non ergodic crossover happens is called Mode Coupling Temperature T_C and marks the transition between the thermodynamic region where the supercooled system is still in liquid state and the phase at which the liquid has developed into an amorphous solid. At T_C the liquid has vitrified transforming into a glass. This ideal glass phase transition can be seen formally analyzing the solution of Eq. 3.28 in the Laplace space. It has been demonstrated, in fact, that defining the order parameter f as:

$$\lim_{t \to \infty} F_S(t) = f \tag{3.29}$$

a relation exists between the order parameter and the exponent parameter:

$$\frac{f}{1-f} = \lambda f^2 \tag{3.30}$$

the solution to which is shown in Fig. 3.6 for each value of λ. Fig. 3.6 shows that the order parameter curve as a function of λ displays a sharp bifurcation at a critical value of the exponent parameter $\lambda = 4 = \lambda_c$. For values of λ below λ_c, f is constantly zero, meaning that the SISF decays to zero for $t \to \infty$ and the density fluctuations fully relax. On the contrary, when λ is greater than λ_c the density correlators tend asymptotically to finite positive constant values and the density fluctuations do not disappear also at long times. In this non ergodic phase, the system is a glass.

To conclude, the scenario depicted by Mode Coupling Theory establishes that in glass formers liquids the non linear coupling between the single particle motion and the density fluctuations of the medium becomes so strong to cause the structural arrest of the system for temperatures close to the Mode Coupling Temperature T_C. The theory therefore defines a (ρ, T) locus of crossovers from an ergodic to a non ergodic phase which is identified with the glass transition line.

Besides giving important information about slow dynamics of liquids in the supercooled region, the Mode Coupling equations are highly predictive and

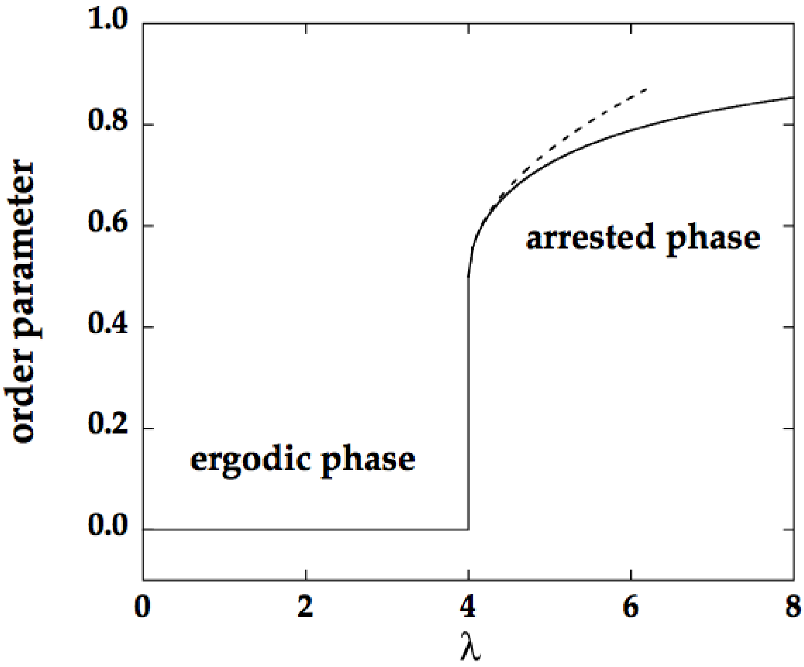

Figure 3.6: Dependence of the order parameter f on the exponent parameter λ as predicted by Mode Coupling Theory. The solid curve represents the solution of Eq. 3.28 and the dashed line correspond to solution to Eq. 3.30. At a critical value $\lambda_c = 4$ the system crosses from an ergodic to a non ergodic arrested phase.

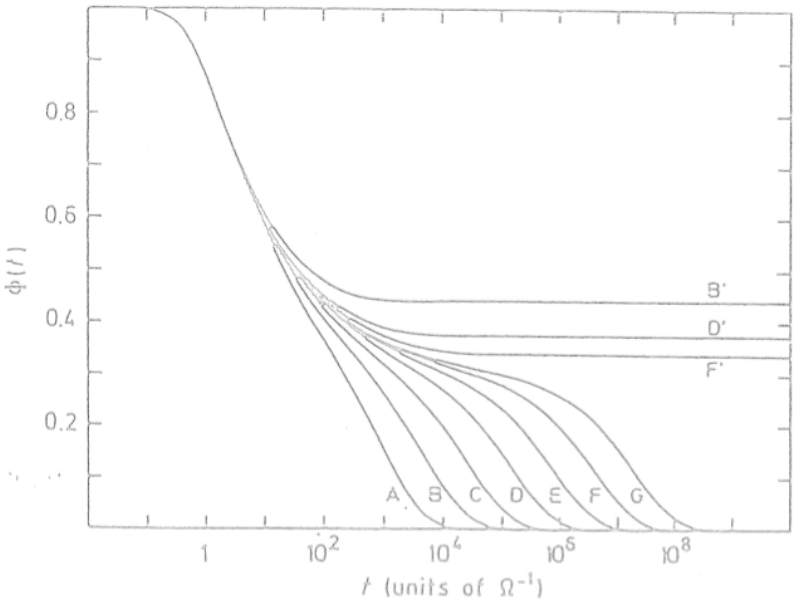

Figure 3.7: Time dependence of the correlation functions as computed from a schematic model without hopping processes. The different curves correspond to different values of the coupling parameter. From Ref. [123].

provide the theoretical basis of the two step relaxation scenario found at first in Ref. [14] and Ref. [15] in SPC/E water potential.

3.2.1.2 The cage effect

The full time and temperature dependence of the solutions to the approximated Mode Coupling Equations are important not only for the glass transition theory but also for explaining the phenomenological behaviour of liquids upon supercooling.

Fig. 3.7 is a sketch of the Self Intermediate Scattering Functions solution to Eq. 3.28 upon varying the exponent parameter λ. For this model computed in Ref. [123] different λ correspond to different temperatures of the system. The SISF exhibit a two step relaxation scenario perfectly in agreement with observations from Neutron Scattering experiments. At the microscopic earliest times, the SISF has a quadratic dependence on time typical of ballistic motion. In this regime, in fact, particles move within the liquid without interacting with the others and the SISF decay with time. At intermediate times, in the so-called β relaxation regime, a simple inflection point appearing in the high temperature range (curve B) transforms into a constant plateau upon cooling the system (curve G). The reason for the existence of this plateau, which is an expression of the so-called "cage" effect, is the following: due to the feedback mechanism between the density correlators and the memory function, the coupling between the single particle and the density fluctuations becomes so strong at lower temperatures that the slow rearrangement of the surrounding molecules causes a progressive increase of structural relaxation times and arrest temporarily the average particle motion. In this transient temporal regime, particles remain trapped in a "cage" formed by its nearest neighbors and are confined in a limited space region for all the duration of the plateau. Only in the long time regime the SISF enters in the so-called α relaxation regime where the thermal fluctuations of the system allow the cages to dissolve and break up and particles are free again to explore the liquid in diffusive regime. As it is clear from the Figure, on approaching the critical temperature T_C the predicted dynamics is more and more stretched towards longer time scales and the length of the plateau increases, suggesting that particles stay blocked inside the cages for grater time. When T reaches the Mode Coupling Temperature value, the SISF do not decay any more to zero and the β relaxation regime is the only relaxation process to survive. At these temperatures, the cages are completely "frozen" and do not disappear also at long times trapping permanently particles in the finite cage volume. The finite positive asymptotic limit of the SISF, therefore, evidences that the the liquid has entered in the non ergodic glassy phase and molecules are not more able to rearrange being enclosed in rigid, fixed cages. According to MCT, below T_C (curve F', D', B') the height of the plateau increase proportionally to the difference $\sqrt{T_C - T}$ and the β regime occurs at shorter and shorter times upon cooling, as displayed in Fig. 3.7 and confirmed by Neutron Scattering experiments on polymer glass former [124].

The dynamics of supercooled water has revealed to follow the behaviour theoretically predicted by Mode Coupling theory both experimentally and computationally, exhibiting SISF with the two step relaxation and the cage effect explained by the theory. Earliest experimental confirmations of MCT were showed in Ref. [125] and later time resolved spectroscopy experiments have confirmed that water behaves à la Mode Coupling [116] and that T_C coincides with the singular temperature of the apparent divergences both of the thermodynamic response functions and of the dynamical properties of water [17]. From the computational point of view, simulations on different water potentials such as TIP4P in bulk [126] and aqueous solutions [127] and SPC/E confined water [20, 25, 128, 129] have also validated the general trend of the SISF expected by MCT. Apart of giving a general theoretical framework for the glass transition and the two different relaxation processes, MCT provides also important qualitative predictions about the specific dependence of the Self Intermediate Scattering Functions on time, on the wavevector $\mathbf{q}$ and on the static structural properties of the system. Next Section will be devoted to these predictions.

3.2.1.3 MCT Predictions and Tests

One of the most relevant goal of the MCT is the theoretical derivation of the β and α relaxation processes manifesting in glassy dynamics. In this context, the Mode Coupling equations are important not only for the ergodic to non-ergodic phase transition but allow also to extract the qualitative behaviour of the β relaxation regime, that is predicted to be:

$$\frac{F_S(\mathbf{q},t)}{S(q)} = f^c_{\mathbf{q}} + h_{\mathbf{q}}\epsilon^{\frac{1}{2}} g^{\pm}_{\epsilon}(t/t_\epsilon) \tag{3.31}$$

The quantity $f^c_{\mathbf{q}}$ is the *ergodicity factor* and corresponds to the first point at which the SISF does not decay to zero anymore. $h_{\mathbf{q}}$ is the *critical amplitude* and it is independent of temperature and time while $\epsilon = \lambda - \lambda_c/\lambda_c$ and t_ϵ represent the distance from the critical parameter (and hence from the critical temperature T_C) and the characteristic time scale of the regime respectively. The sign ± is related to the positive or negative values of ϵ. It should be noticed that Eq. 3.31 states implicitly that a *factorization property* holds. The temporal dependence of the SISF, in fact, enters only through the q-indipendent function g. This means that the temporal and spatial correlations in the β regime are completely independent differently from other types of dynamical processes. Tests on the factorization property of MCT solution has been performed in simulations of Lennard Jones systems [130] and colloidal suspensions [131]. According to MCT, the temperature dependence of the β scale time t_ϵ should diverge asymptotically as a power law upon approaching the ideal glass transition temperature T_C:

$$t_\epsilon = t_0|\epsilon|^{\frac{-1}{2a}} \tag{3.32}$$

with $0 < a < 1/2$. This trend is evident in Fig. 3.7 where, on increasing and decreasing temperature towards T_C from below and above T_C respectively, the correspondent time at which the SISF enter in the β regime moves to larger values. Light Scattering experiments have found a similar divergence [131, 132].

The exact computation of the universal function $g(t/t_\epsilon)$ could be, in principle, carried out by starting from the exponent parameter λ and hence from the static structure factor. Nevertheless, this calculus is rather complex and MCT provides useful predictions on the explicit form of $g(t/t_\epsilon)$, even if they are correct only in leading order in ϵ. In particular, in the early β relaxation regime, that corresponds to the interval where the SISF has not yet entered the plateau but is close to it, the time dependence of $g(t/t_\epsilon)$ can be written as:

$$g_\epsilon^{\pm}(t/t_\epsilon) \sim (t/t_\epsilon)^{-a} \tag{3.33}$$

where a is the same exponent of Eq. 3.32. The longer time behaviour of the β regime, where the SISF exited from the cage regime and has just entered in the second slow α relaxation, is well described by the so-called Von Schweidler law (VSL):

$$g_\epsilon^{-}(t/t_\epsilon) \sim (t/t_\epsilon)^{b} \tag{3.34}$$

with b another critical exponent called the Von Schweidler exponent and where the subscript $-$ indicates that this regime is absent in the non ergodic glassy phase.

Even if MCT does not give a representation of the glass transition in term of the theory of critical phenomena, a relation between the exponents a, b, and λ exists and connects these critical parameters through a scaled equation:

$$\lambda = \frac{\Gamma^2(1+b)}{\Gamma(1+2b)} = \frac{\Gamma^2(1-a)}{\Gamma(1-2a)}, \tag{3.35}$$

Eq. 3.35 permits to extract the entire set $\{a, b, \lambda\}$ from the knowledge of only one of its elements. The power law behaviour of Eq. 3.33 and Eq. 3.34 together with the satisfaction of Eq. 3.35 have been found in Light Scattering experiments [131, 132] and computer simulations of water [15, 126] and other [133] potentials.

Although the solutions of the Mode Coupling Equations lead to an approximate description of the β relaxation regime, the main theoretical prediction derived from these equations concerns the structural relaxation time of the supercooled liquid and its relation with the Mode Coupling Temperature T_C. In order to understand the deep implications of this prediction, the meaning of T_C in terms of the structural relaxation time must be discussed. Being defined as the ideal glass transition temperature, T_C represents the temperature at which the liquid is not more able to rearrange and relax even at long time and the molecules are completely arrested and "frozen" in a disordered solid state. Consequently, T_C is the temperature at which the liquid structural relaxation time τ diverges, together with the connected self diffusion coefficient D and viscosity η. At T_C the time that the system takes to rebalance and relax is in principle infinite. Since the physical definition of the relaxation time is the time necessary to the density fluctuations to dissolve, τ is identified by the characteristic time of decay of the SISF's α regime. It follows that an analysis of the MCT solutions for the Intermediate Scattering Functions at different values of the exponent parameter λ provides the full dependence of the α relaxation time τ from the temperature and density of the system. According to MCT, τ increases asymptotically upon approaching T_C as the following power law:

$$\tau^{-1} \propto (T - T_C)^{\gamma} \tag{3.36}$$

where γ is larger than 1.5 and should be a universal exponent. A dramatic slowing down of the dynamics is therefore predicted to happen at temperature near T_C. A large amount of experimental [17, 18, 125] and computational studies on water [14, 15, 20, 25, 126–129] have proved the power law behaviour of Eq. 3.36.

Also simulations on hard-sphere potentials [131] and Lennard Jones Binary Mixture [130, 134, 135] exhibit a similar increase of the relaxation time on approaching the Mode Coupling Temperature.

As in the β regime, also for the α regime MCT equations produce the qualitative form of the long time SISF. In particular, the temporal dependence of the correlators in the α interval is expected to be:

$$F_S(\mathbf{q}, t) \propto \Psi(t/\tau(T)) \tag{3.37}$$

with τ the α relaxation time. This equation expresses the validity of the *time-temperature superposition principle* (TTSP) in the α regime. Since the SISF is function of the rescaled time $t/\tau(T)$, plotting the density correlators for different temperatures versus $t/\tau(T)$, all the SISF collapse on a single master curve independent from the single value of T. The TTSP has been found to be valid in several computer simulations on Lennard Jones binary mixture [134] and water potentials [15, 126].

Differently from the β regime, the simplified model represented by the approximated MCT equations predicts a purely exponential decay for the master curve in contrast to the behaviour observed both experimentally and computationally. The SISF in the α regime, in fact, reveals to be well fitted by the so-called Kohlrausch-Williams-Watts (KWW) function:

$$F_S(Q, t) = A(Q) exp[-(t/\tau)^{\beta}] \tag{3.38}$$

with β the Kohlrausch exponent of the stretched exponential decay, τ the structural relaxation time and $A(Q)$ the Lamb-Mossbauer factor corresponding to the height of the plateau [16] and directly related to the radius of the cage.

It has been shown that the overall curves of the Intermediate Scattering Functions in liquids following the MCT can be fitted with the formula [14,

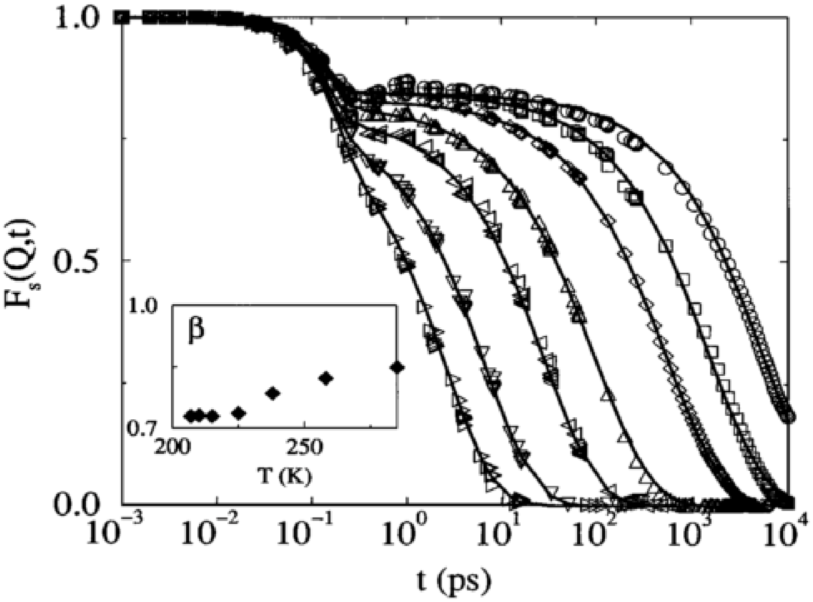

Figure 3.8: Self intermediate scattering functions for different temperatures calculated at the maximum of the static structure calculated from MD simulations on SPC/E water potential. Symbols are the data calculated from simulations in the temperature range from $T = 206.3$ K (circles) to $T = 284.5$ K (rightward triangles). The solid lines are the fits to Eq. (3.39). The inset shows the T dependence of the exponent β associated with the slow relaxation.

15]:

$$f(Q,t) = (1 - A(Q))exp[-(t/\tau_s)^2] + A(Q)exp[-(t/\tau)^{\beta}] \tag{3.39}$$

The first term of Eq. 3.39 describes the quadratic dependence on time of the earliest time dynamical regime, where molecules move ballistically. The short time τ_s represents therefore the characteristic time scale of the fast component of relaxation process. The stretched exponential decay in the second term of the fitting formula expresses the slow structural α relaxation typical of supercooled liquid dynamics, during which density fluctuations progressively vanish with a characteristic time τ. An example of the agreement between the fitting formula and the SISF computed from Molecular Dynamics simulations on SPC/E water potential [14, 15] is displayed in Fig. 3.8.
The β and α relaxation regime theoretically predicted and described by MCT are not two separate and independent contributions of the SISF.

Even if they have two different time scales, the characteristic exponents introduced by the theory are related each other through the following equation:

$$\gamma = 1/2a + 1/2b \tag{3.40}$$

where γ, a and b are respectively the power law exponent of the α relaxation time and the parameters of the β regime. Eq. 3.40 is important because it allows to extract information on the time dependence of the β relaxation from measurements of the temperature dependence of the α relaxation time and vice versa. Moreover it should be noticed that, consequently to this equation, the time τ and t_ϵ introduced previously are directly connected.

In conclusion, Mode Coupling Theory is nowadays the most important analytical theory able to derive from a set of closed, self consistent equations, the slowing down of the relaxation time, the cage effect and the two step relaxation scenario observed experimentally and computationally in supercooled liquid water.

Nevertheless, the MCT predictions reveal to be valid in a finite range of temperature. In the deep supercooled regime near the MCT temperature T_C, deviations from MCT behaviour begin to occur. The reason for these deviations is that some terms neglected because of the approximations applied to determine the MCT equations become progressively important on approaching T_C and cause a general change in the temperature dependence of the SISF. In particular the singularity at the ideal glass transition temperature is smeared out by the presence of phenomena not taken into account by MCT in its ideal formulation. These activated processes are able to restore ergodicity to the system also below T_C and are called *hopping processes*. They represent a secondary relaxation mechanism through which particles are able to jump out the walls of their cages even if they have not dissolved. In view of hopping phenomena, the MCT temperature T_C is no more the temperature at which the system is structurally arrested and the α relaxation time diverges but marks the transition of relaxation mechanism from the MCT diffusion mechanism to the hopping mechanism. In the next Section, the effect of hopping phenomena on supercooled water dynamics will be discussed.

3.2.2 From the fragile to the strong liquid across the Widom line

As discussed in the previous Section, MCT predicts a power law increase of the structural relaxation time of supercooled liquids asymptotically diverging at the Mode Coupling Theory temperature T_C. Following Angell's classification of glass forming liquids [136], elaborated originally using the viscosity, liquids whose dependence of self diffusion coefficient D on temperature is well described by MCT power law are said "fragile" liquids [64, 137–140]. More in general, a fragile liquid exhibits a behaviour of viscosity as a function of T/T_G, where T_G is the experimental temperature of structural arrest of the system, that can be often fitted by the empirical Vogel-Fulcher-Tamman (VFT) law:

$$D = D_0 e^{\left(-\frac{B}{T-T_0}\right)} \tag{3.41}$$

where B and T_0 are fitting parameters. Fragile liquids are only one of the two broad classes of liquids defined on the basis of their viscosity. Liquids that present an Arrhenius exponential increase of diffusion coefficient of the form:

$$D = D_0 e^{\left(-\frac{E_A}{k_B T}\right)} \tag{3.42}$$

are said "strong" liquids, with E_A the activation energy. The difference between fragile and strong liquids is evident in Fig. 3.9 where the shear viscosity η vs T_G/T is plotted for three glass forming liquids in the so-called Arrhenius plot. Fragile liquids show a marked change in the curvature and a dramatic increasing of the viscosity upon approaching the experimental glass transition temperature T_G. On the contrary, strong liquids have a linear plot indicating that the dynamical transport properties of the system are dominated by "activated" processes.

As mentioned in the previous Section, the presence of activated hopping processes in supercooled liquid dynamics is neglected in the Mode Coupling Theory. These phenomena cause a deviation in the deep supercooled regime in the dependence of the structural relaxation time on temperature, that moves from the fragile power law behaviour predicted by MCT to the strong Arrhenius trend. This change from the high temperature fragile character to the low temperature strong character is called *fragile to strong crossover* (FSC).

Water exhibits a fragile to strong crossover widely investigated both computationally and experimentally. Molecular Dynamics simulations on SPC/E water [142] have found a fragile to strong crossover, later confirmed by other computer simulations on bulk water for ST2 and TIP5P [67] and on bulk and aqueous solution for TIP4P [126, 127] and Jagla potential, a primitive model [67, 143, 144]. Signatures of the existence of the FSC have been found also in computer simulations of confined water [14, 20]. From the experimental point of view, evidences of a fragile to strong crossover have been observed in experiments on confined water [19, 90, 145–148] that additionally found that this crossover as a function of pressure is pointing to the

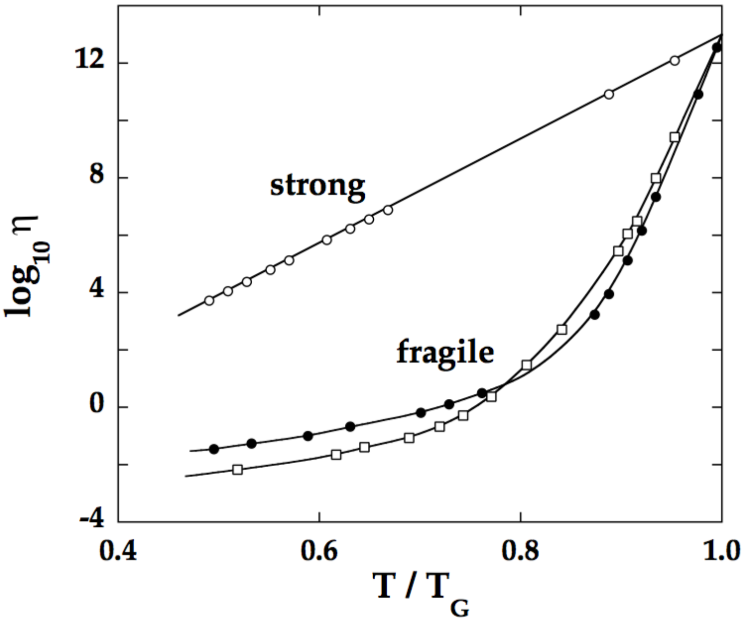

Figure 3.9: Arrhenius plot of the shear viscosities (in poise) of three glass-forming liquids, showing the difference in behaviour between strong and fragile glass formers. Open circles: silica; squares: o-terphenyl; filled circles: an ionic melt of composition $[KNO_3]_0.6[Ca(NO)_3)_2]_{0.4}$. Figure from Ref. [141].

region where the LLCP has been predicted to be located [11, 12, 19, 146]. In Fig. 3.10 is shown the logarithm of the relaxation time as a function of 1/T measured for water confined in MCM-41 silica pores [19]. The crossover from non-Arrhenius behaviour at high temperature, fitted here using the VFT law, to Arrhenius behaviour at low temperature is clearly visible. The experimental investigation of the FSC is hampered in bulk water by the homogeneous nucleation.

The Fragile to Strong Crossover is not a phenomenon purely dynamical. Relation between the appearance of the FSC in correspondence of crossing of the Widom Line has been found both in computer simulations and experiments.

The FSC has been found to happen at the crossing of the Widom line for ST2, TIP5P and Jagla model [67]. Besides, it was shown by computer simulations that water in hydrophilic confinement has a bulk-like behaviour and that upon supercooling the FSC occurs in correspondence with a peak of the specific heat which can be considered to a good approximation as a proxy for the Widom line [20, 25, 149]. The FSC has been found to occur upon crossing the Widom line also for TIP4P bulk water [126], for TIP4P aqueous solutions of electrolytes [127] and for solvophobic solutions [143]. Connection between FSC and WL has been confirmed also experimentally [19, 90, 145, 146, 150]. Experiments in confinement have also shown a peak of the specific heat in correspondence of the FSC [147].

The deep meaning of the Fragile to Strong Crossover, its microscopic origin in the dynamics and its relation with the thermodynamic aspects of water phase diagram are still nowadays matter of debate. Next Chapters will be devoted to the investigation of this dynamical crossover both in bulk and confined water through Molecular Dynamics simulations in order to provide new insights for a better comprehension of the FSC in water.

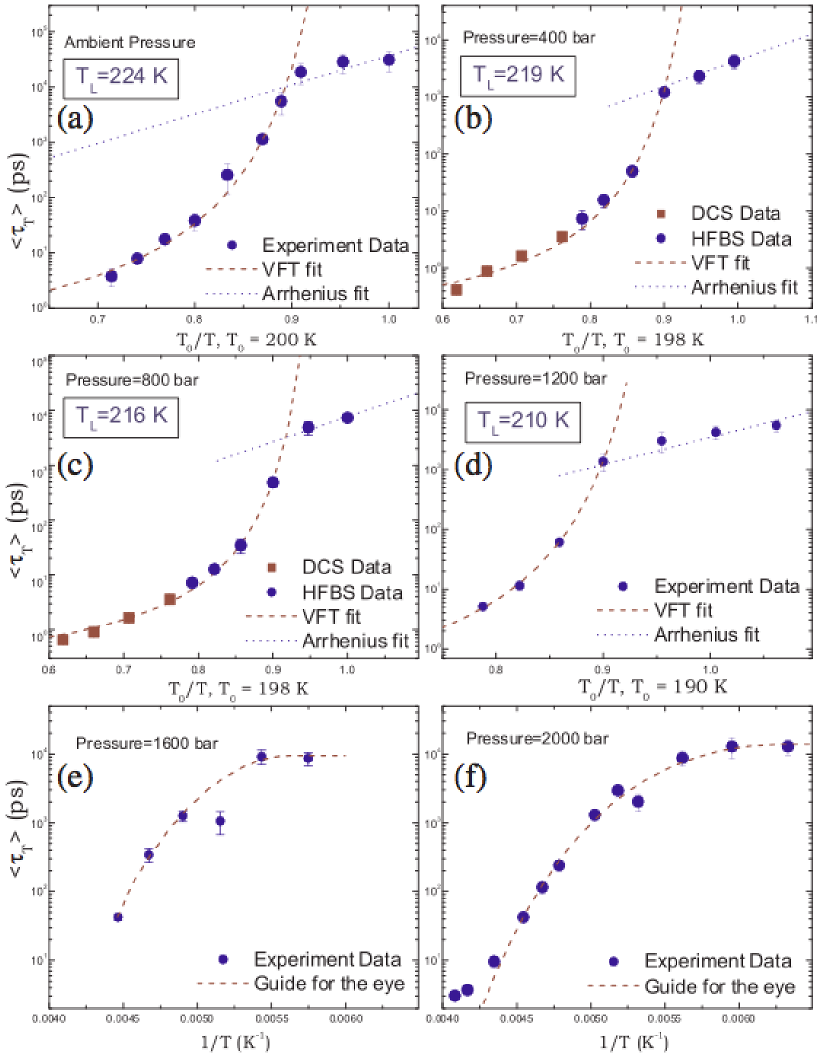

Figure 3.10: Average translational relaxation time τ_T as a function of 1/T for water confined in silica MCM-41 pores at several pressures. Data and Figure from Ref. [19].

4

Molecular Dynamics Simulations

Computer simulations have a dominant role in the study of the physics of liquid matter. After the first pioneering works [151–153], computer simulations techniques have evolved following the progressive increased availability of computing power and nowadays they are the preferred theoretical methods for the investigation of the properties of liquids. This happens partly because the equations describing the statics and the dynamics of liquids cannot often be solved analytically and the approximations used to deal with them do not always work well. In the case of the static properties for example, the Ornstein-Zernike equation can only be solved approximately. The two most used approximations are the Percus-Yevick and the hypernetted chain approximations but when compared to the experimental results they do not always give encouraging results [141]. This chapter covers the general concepts of the Molecular Dynamics (MD) technique. The first section, Sec. 4.1, deals with the main steps of this simulation method. In the following sections details about the integration algorithm, Sec. 4.2, thermostats and barostats in MD, Sec. 4.3, and the Ewald summation method, Sec. 4.4, are discussed. Sec. 4.5 is devoted to a discussion about the computation of dynamical observables performed in this PhD Thesis.

4.1 The MD technique

Classical MD is a deterministic simulation method that allows the calculation of thermodynamic, static and dynamic properties of a many-body system [154]. The motion of the particles (atoms or molecules) that constitute the system is determined solving Newton's equations. With a fixed number of particles the Hamiltonian of the simulated system is in general given by:

$$H = \sum_{i=1}^{N} \frac{\mathrm{p}_i^2}{2m} + U(\mathrm{r}_1,\ \mathrm{r}_2,\ \ldots,\ \mathrm{r}_N) = \sum_{i=1}^{N} \frac{\mathrm{p}_i^2}{2m} + \sum_{i=1}^{N} \sum_{j>i}^{N} u(|\mathrm{r}_i - \mathrm{r}_j|) \tag{4.1}$$

where N is the total number of particles and U is the many-body interaction potential. In the right-hand side of the equation U is assumed to be approximated with the sum of the radial potentials u between pairs of particles.

The particles are subject to Newton's laws of motion:

$$m_i \ddot{\mathbf{r}}_i = \frac{d\mathbf{p}_i}{dt} = \mathbf{F}_i = -\nabla_{\mathbf{r}_i} U \tag{4.2}$$

$$\mathbf{v}_i = \dot{\mathbf{r}}_i = \frac{\mathbf{p}_i}{m_i} \tag{4.3}$$

Given the positions and the velocities of the particles at time t, the equations of motion are integrated with discrete time steps δt and the positions and the velocities of the particles at time $t+\delta t$ are computed. The trajectories of the particles are thus determined in a deterministic way. Details about the integration algorithm are given in the next Section. From the microscopic motion it is possible to evaluate macroscopic quantities using statistical mechanics. In the MD technique the validity of the *ergodic hypothesis* is implied. Considering a generic thermodynamic quantity A, then under the ergodic hypothesis

$$\langle A \rangle = \int A(\mathbf{r}^N,\ \mathbf{p}^N) \rho[H(\mathbf{r}^N,\ \mathbf{p}^N)] d\mathbf{r}^N d\mathbf{p}^N = \overline{A} = \lim_{t\to\infty} \frac{1}{t} \int_0^t A(\mathbf{r}^N,\ \mathbf{p}^N) dt' \tag{4.4}$$

the average calculated over the ensemble is identical to the average calculated over time steps. In MD this hypothesis holds when the simulation time exceeds by far the characteristic time of molecular motion. Simulation runs are usually divided into two parts. During the equilibration runs the system is evolved until equilibrium is reached and the thermodynamic properties and in particular the energy of the system remain constant over time. This can be done by rescaling the velocities, as explained in Sec. 4.3. In the production runs, the trajectories are accumulated and then average quantities are computed.

If runs are performed in the microcanonical ensemble, the total energy of the system $E = K + U$ is conserved. Methods to deal with MD in different ensembles are discussed in Sec. 4.3. In the NVE ensemble the temperature can be calculated from the equipartition theorem by the relation

$$T = \frac{2}{3} \frac{\langle K \rangle}{k_B} = \frac{1}{3} \frac{\sum_{i=1}^{N} m_i v_i^2}{k_B N} \tag{4.5}$$

while the pressure can be calculated using the virial theorem [154], with P given by:

$$P = \frac{Nk_BT + \langle \mathcal{V} \rangle}{V} \tag{4.6}$$

where $\mathcal{V} = \frac{1}{3}\sum_{i=1}^{N} \mathbf{r}_i \cdot \mathbf{F}_i$ is the virial.

Suppose that the simulation box is cubic and the edge of the box is L (thus $V = L^3$). To avoid introducing artifacts due to the presence of the surfaces of the cube, it is necessary to implement periodic boundary conditions. The central simulation box is replicated in all directions forming an infinite lattice. As a consequence a particle leaving the central box corresponds to its image entering the box from the opposite side. With the *minimal image convention*, a reference particle in the central box interacts only with the particles and the image particles contained in a cube centered on the reference particle and with the same dimensions of the simulation box. The presence of the periodic boundary conditions makes the whole system invariant to translation, implying the total linear momentum to be conserved. This further conserved quantity reduces the number of degree of freedom of the system to $3N - 3$ and consequently modifies the equipartition theorem.

Usually the interaction potential is not calculated for all distances but a truncation is introduced. Only the interaction distances for which $r_{ij} = |\mathbf{r}_i - \mathbf{r}_j| < r_{\text{cut}} \leq L/2$ are retained for the computation of the interactions. With the cut-off, one needs to introduce long range corrections to the interaction potential. For short range potentials, as the Lennard-Jones (LJ) potential, the standard corrections [154] for the potential energy and for the virial are given respectively by:

$$u_{ij}^{\text{corr}} = 2\pi \frac{N_i N_j}{V} \int_{r_{\text{Cut}}}^{\infty} g_{ij}(r) u_{ij}(r) r^2 dr \tag{4.7}$$

$$\mathcal{V}_{ij}^{\text{corr}} = -2\pi \frac{N_i N_j}{V} \int_{r_{\text{Cut}}}^{\infty} g_{ij}(r) \frac{\partial}{\partial r} u_{ij}(r) r^3 dr \tag{4.8}$$

where $g_{ij}(r)$ is the pair radial distribution function (RDF) between particle i and particle j. It is usual to take $g_{ij}(r) = 1$ for $r > r_{\text{cut}}$. For long range potentials, as the electrostatic potential, special care is required. The Ewald summation method for the treatment of the electrostatic interactions is discussed in Sec. 4.4.

4.2 MD integration algorithms

In order to calculate the trajectories of the particles subject to Newtons's laws, Eq. 4.2-4.3, an integration algorithm is necessary. The integration time step must be much less than the time taken by the molecule to cover a distance equal to its own length. Typically $\delta t = 10^{-15}\mathrm{s} = 1$ fs for phenomena that take place at the picoseconds or nanoseconds scale. Supposing that, as in the case of water, the particles are rigid molecules, the motion can be separated into translational and rotational motion.

The integration of the translational motion is quite straightforward. The most common algorithm is called *leap-frog* algorithm and it is derived from Verlet's algorithm [154]. The latter considers the Taylor expansion for the position, the velocity and the acceleration of a molecule

$$\mathbf{r}_i(t+\delta t) = \mathbf{r}_i(t) + \mathbf{v}_i(t)\delta t + \frac{1}{2}\mathbf{a}_i \delta t^2 + ... \tag{4.9}$$

$$\mathbf{v}_i(t+\delta t) = \mathbf{v}_i(t) + \mathbf{a}_i(t)\delta t + \frac{1}{2}\mathbf{b}_i \delta t^2 + ... \tag{4.10}$$

$$\mathbf{a}_i(t+\delta t) = \mathbf{a}_i(t) + \mathbf{b}_i(t)\delta t + ... \tag{4.11}$$

Taking $\mathbf{r}_\mathrm{i}(t-\delta t) = \mathbf{r}_\mathrm{i}(t) - \mathbf{v}_\mathrm{i}(t)\delta t + \frac{1}{2}\mathbf{a}_\mathrm{i}\delta t^2 + \dots$ and summing it to Eq. 4.9 the velocity term from the equation for the position can be eliminated, obtaining:

$$\mathbf{r}_i(t+\delta t) = -\mathbf{r}_i(t-\delta t) + 2\mathbf{r}_i(t) + \mathbf{a}_i \delta t^2 + \mathcal{O}(\delta t^4) \tag{4.12}$$

and making the algorithm faster. In the Verlet procedure the velocity can be recovered calculating

$$\mathbf{v}_i(t) = \frac{\mathbf{r}_i(t+\delta t) - \mathbf{r}_i(t-\delta t)}{2\delta t} \tag{4.13}$$

Verlet's algorithm is fast and robust but it does not allow an accurate computation of the velocities. This can be amended with the leap-frog algorithm.

Given the quantities $\mathbf{r}_i(t)$, $\mathbf{a}_i(t)$ and $\mathbf{v}_i(t-\frac{1}{2}\delta t)$ a two step iteration is made, in which first the velocities are updated through

$$\mathbf{v}_i(t+\frac{1}{2}\delta t) = \mathbf{v}_i(t-\frac{1}{2}\delta t) + \mathbf{a}_i(t)\delta t \tag{4.14}$$

then the positions of the particles are calculated with:

$$\mathbf{r}_i(t+\delta t) = \mathbf{r}_i(t) + \mathbf{v}_i(t+\frac{1}{2}\delta t)\delta t \tag{4.15}$$

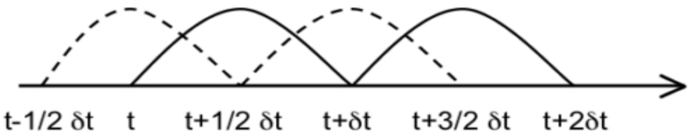

Figure 4.1: Schematic representation of the leap-frog algorithm. Dashed lines represent the first step, Eq. 4.14, with the calculation of the velocities while solid lines represent the second step, Eq. 4.15, with the calculation of the positions.

The forces are calculated after the second step and the new accelerations can be put into Eq. 4.14 to begin a new iteration. A diagram of the leap-frog iteration algorithm is depicted in Fig. 4.1.

The leap-frog algorithm yields more accurate positions. They are in fact calculated using a velocity at a time closer to $t + \delta t$. The forces are computed taking the derivative of the potential generated by the distribution of particles ensuing from Eq. 4.15. Velocities at time t can be simply obtained from the relation

$$\mathbf{v}_i(t) = \frac{\mathbf{v}_i(t + \frac{1}{2}\delta t) - \mathbf{v}_i(t - \frac{1}{2}\delta t)}{\delta t} \tag{4.16}$$

The integration of the rotational motion of molecules requires a more complex treatment. The vector τ_i, the torque with respect to the centre of mass of the molecule positioned at r_i, is defined by

$$\tau_i = \sum_a (\mathbf{r}_{ia} - \mathbf{r}_i) \wedge \mathbf{F}_{ia} = \sum_a \mathbf{d}_{ia} \wedge \mathbf{F}_{ia} \tag{4.17}$$

where $\mathbf{d}_{ia}$ denotes the position of the atom a within the molecule i with respect to its centre of mass. The orientation of a rigid body in the space can be defined by a rotation matrix that consents the transformation from the frame of reference of the laboratory to the one of the centre of mass.

This matrix is usually defined in terms of three independent angular parameters, the *Euler angles* $(\varphi,\ \theta,\ \psi)$. A quadri-dimensional vector, with unitary norm, can be defined as a function of the Euler angles. This vector is called *quaternion* and it permits to have convergent equations of motion. Defined $\mathbf{q}$ as

$$\mathbf{q} = (q_0,\ q_1,\ q_2,\ q_3) \tag{4.18}$$

with $q_0^2 + q_1^2 + q_2^2 + q_3^2 = 1$, the rotation matrix can be written in terms of q. It reads

$$R = \begin{pmatrix} q_0^2 + q_1^2 - q_2^2 - q_3^2 & 2(q_1 q_2 + q_0 q_3) & 2(q_1 q_3 - q_0 q_2) \\ 2(q_1 q_2 - q_0 q_3) & q_0^2 - q_1^2 + q_2^2 - q_3^2 & 2(q_2 q_3 + q_0 q_1) \\ 2(q_1 q_3 + q_0 q_2) & 2(q_2 q_3 - q_0 q_1) & q_0^2 - q_1^2 - q_2^2 + q_3^2 \end{pmatrix} \tag{4.19}$$

and if $\hat{\mathbf{d}}_{ia}$ is the position of the atom a in the center of mass frame, its position in the laboratory frame is obtained by $\mathbf{d}_{ia} = R^T \hat{\mathbf{d}}_{ia}$. The quaternion for each molecule satisfies the equations of motion:

$$\begin{pmatrix} \dot{q}_0 \\ \dot{q}_1 \\ \dot{q}_2 \\ \dot{q}_3 \end{pmatrix} = \frac{1}{2} \begin{pmatrix} q_0 & -q_1 & -q_2 & -q_3 \\ q_1 & q_0 & -q_3 & q_2 \\ q_2 & q_3 & q_0 & -q_1 \\ q_3 & -q_2 & q_1 & q_0 \end{pmatrix} \begin{pmatrix} 0 \\ \omega_x \\ \omega_y \\ \omega_z \end{pmatrix} \tag{4.20}$$

where $(0,\ \omega_x,\ \omega_y,\ \omega_z)$ are the components of the angular velocity vector ω in the centre of mass frame. This system does not possess singularities and it can be solved with a procedure similar to the one applied for the integration of the translational motion. To solve the rotational motion the following equation can be used:

$$\frac{d\mathbf{J}}{dt} = \frac{d}{dt}(I\omega) = \tau \tag{4.21}$$

where $\mathbf{J}$ is the total angular momentum of the molecule, I the moment of inertia matrix and τ the torque of the molecule (for convenience here the subscript i indicating each molecule is dropped). This equation is evidently coupled to Eq. 4.20. Having stored $\mathbf{J}(t - \frac{1}{2}\delta t)$, $\mathbf{q}(t)$ and $\tau(t)$ the equations for the rotational motion can be solved iteratively, first updating the angular momentum through:

$$\mathbf{J}(t) = \mathbf{J}(t - \frac{1}{2}\delta t) + \tau(t)\frac{1}{2}\delta t \tag{4.22}$$

Then the $\dot{\mathbf{q}}$ can be calculated from Eq. 4.20 and a guess for $\mathbf{q}(t + \frac{1}{2}\delta t)$ is given by:

$$\mathbf{q}(t + \frac{1}{2}\delta t) = \mathbf{q}(t) + \dot{\mathbf{q}}(t)\frac{1}{2}\delta t \tag{4.23}$$

The last two are auxiliary equations to estimate $\mathbf{q}(t + \frac{1}{2}\delta t)$ and calculate $\dot{\mathbf{q}}$ at the half-step time. Now the new $\mathbf{J}$ and $\mathbf{q}$ can be calculated through the relations:

$$\mathbf{J}(t + \frac{1}{2}\delta t) = \mathbf{J}(t - \frac{1}{2}\delta t) + \tau(t)\delta t \tag{4.24}$$

$$\mathbf{q}(t + \delta t) = \mathbf{q}(t) + \dot{\mathbf{q}}(t + \frac{1}{2}\delta t)\delta t \tag{4.25}$$

4.3 Thermostats and barostats in MD

In Sec. 4.1 it has been shown that the basic MD algorithm is thought in the microcanonical NVE ensemble. However it is possible to implement algorithms that simulate the presence of a thermostat and/or a barostat. Therefore MD can be performed in different ensembles such as the canonical NVT ensemble or the isothermal-isobaric NPT ensemble.

For the thermostat, the most common techniques are known as Nosé- Hoover [155], Berendsen [156] and Gaussian constraint [157]. Only the first one reproduces exactly the averages and fluctuations in the canonical ensemble. The others give properties that differ from the averages in the canonical ensemble, typically of $\mathcal{O}(1/N)$ [154]. In most cases this accuracy is enough and indeed the Berendsen algorithm is by far the most used in MD simulations. In the Berendsen algorithm the velocities are rescaled through $\dot{\mathbf{r}}_i \rightarrow s\dot{\mathbf{r}}_i$ and the change in temperature per time step in terms of the rescaling parameter s is given by:

$$s = [1 + \frac{\delta t}{\tau_T}(\frac{T_0}{T} - 1)]^{1/2} \tag{4.26}$$

where τ_T is the time constant of the coupling to the external bath and T_0 is the desired temperature.

In general the coupling of the system to a thermostat and/or a barostat can be effectively obtained also adding terms to the Lagrangian of the system, thus modifying the equations of motions. The general Lagrangian of a system is

$$\mathcal{L} = \frac{1}{2} m \sum_{i=1}^{N} |\dot{\mathbf{r}}_i|^2 - U \tag{4.27}$$

In the case of a thermostat, a thermal bath is inserted and the velocities are rescaled writing $\dot{\mathbf{r}}_i \rightarrow s\dot{\mathbf{r}}_i$. The new Lagrangian in terms of the rescaled quantities is

$$\mathcal{L} = \frac{1}{2} m \sum_{i=1}^{N} s^2 |\mathbf{r}_i|^2 - U + \frac{Q}{2} s^2 - (3N+1) k_B T_0 \ln s \tag{4.28}$$

where Q is the “mass” associated with the thermal bath. The modified equations of motions that are obtained are of the kind

$$\ddot{\mathbf{r}}_i = -\frac{1}{m_i s^2} \frac{\partial U}{\partial \mathbf{r}_i} - \frac{2\dot{s}}{s} \dot{\mathbf{r}}_i \tag{4.29}$$

$$Q\ddot{s} = \frac{1}{s} \left[\sum_i m_i s \dot{\mathrm{r}}_i^2 - (3N+1) k_B T_0 \right] \tag{4.30}$$

With this method the energy of the system is not conserved but the energy of the total system constituted by the system plus the thermal bath is conserved.

Beyond the canonical ensemble, another common working ensemble is the isothermal-isobaric NPT ensemble. In analogy with what seen for the temperature, algorithms can be implemented to fix the pressure, adjusting dynamically the volume and in case the shape of the simulation box. The most common algorithms for the introduction of a barostat are known as Hoover [158] and Berendsen [156].

4.4 Ewald summation

For long range interactions, such as the electrostatic interactions, the cutoff plus corrections method described in Sec. 4.1 is not sufficient to achieve accuracy. In this case, special care is needed in dealing with potential truncation and long range contributions. As a matter of fact the inadequate treatment of electrostatic interactions can lead to severe artifacts in the results of the simulations [81]. There exist several methods for the treatment of the electrostatic interactions. In the following the general ideas of the most used method, the Ewald summation method, are described.

Taking into account the periodic boundary conditions, the electrostatic energy term of the interaction potential can be written as

$$U_E = \frac{1}{2}\sum_{i=1}^{N} q_i \phi_E(\mathbf{r}_i) \tag{4.31}$$

and ϕ_E is given by

$$\phi_E = \sum_{j=1}^{N}\sum_{\mathbf{R}} \frac{q_j}{|\mathbf{r}_{ij} + \mathbf{R}|} \tag{4.32}$$

where $\mathbf{R} = \mathbf{n}L, \mathrm{n} = (n_x,\ n_y,\ n_z)$, with $n_x, n_y, n_z \in \mathbb{Z}$. The sum is performed with the convention that $i \neq j$ if $\mathbf{R} = 0$.

By adding and subtracting screening charges, the sum can be broken into two parts, $U_E = U_{\mathrm{SR}} + U_{\mathrm{LR}}$. The first part contains the original point charges screened by diffuse clouds of opposite charges; this part becomes short ranged and can be evaluated in the real space. The second part compensates for the added screening charges and it is generated by the sum of the screening charge densities (with opposite charge); it is evaluated in the Fourier space. The screening charges are typically taken with a Gaussian distribution:

$$\rho_s(r) = -q_i(\frac{\alpha}{\pi})^{3/2} e^{-\alpha r^2} \tag{4.33}$$

First the long range part of the sum must be calculated. Having taken the screening charges as in Eq. 4.33, the compensating charge distribution can be written as

$$\rho_c(\mathbf{r}) = \sum_{j=1}^{N} \sum_{\mathbf{R}} q_j (\frac{\alpha}{\pi})^{3/2} \exp[-\alpha|\mathbf{r} - (\mathbf{r}_j + \mathbf{R})|^2] \tag{4.34}$$

and its Fourier transform is given by

$$\tilde{\rho}_c(\mathbf{k}) = \int_V d\mathbf{r} e^{-i\mathbf{k}\cdot\mathbf{r}} \rho_c(\mathbf{r}) = \sum_{j=1}^{N} q_j e^{-i\mathbf{k}\cdot\mathbf{r}_j} e^{-k^2/4\alpha} \tag{4.35}$$

The field generated by this charge distribution can be calculated using the Poisson's equation in the Fourier space, $k^2\tilde{\phi}(\mathbf{k}) = 4\pi\tilde{\rho}(\mathbf{k})$. Anti-transforming the field thus obtained and plugging it into the long range part of the sum, it follows:

$$U_{\mathrm{LR}} = \frac{1}{2} \sum_{i=1}^{N} q_i \phi_c(\mathbf{r}_i) = \frac{1}{2V} \sum_{\mathbf{k}\neq 0} \frac{4\pi}{k^2} |\tilde{\rho}(\mathbf{k})|^2 e^{-k^2/4\alpha} \tag{4.36}$$

where $\tilde{\rho}(\mathbf{k}) = \sum_{i=1}^{N} q_i e^{-i\mathbf{k}\cdot\mathbf{r}_i}$. This part of the potential contains spurious self-interactions terms as the point charges at $\mathbf{r}_i$ interact with the compensating charges also at $\mathbf{r}_i$. The self interactions terms represent the potential at center of the Gaussian charge distributions and they are to be subtracted from the final expression to recover the correct Coulombic energy.

Now the short range part of the sum is calculated. Using the Poisson's equation in the real space $-\nabla^2\phi(\mathbf{r}) = 4\pi\rho(\mathbf{r})$ it is possible to demonstrate that the screening potential can be written as

$$\phi_s(r) = \frac{q_i erf(\alpha^{1/2} r)}{r} \tag{4.37}$$

where erf is the error function. It is defined by

$$erf(x) = \frac{2}{\pi^{1/2}} \int_0^x e^{-t^2} dt \tag{4.38}$$

The self-interaction terms correspond to $\phi_{\mathrm{self}} = \phi_s(0) = 2(\frac{\alpha}{\pi})^{1/2} q_i$ and the total self-interaction energy becomes

$$U_{\mathrm{self}} = (\frac{\alpha}{\pi})^{1/2} \sum_{i=1}^{N} q_i^2 \tag{4.39}$$

which must be subtracted from the total electrostatic energy. Using the result 4.37, the short range part of the sum can be rewritten as

$$U_{\mathrm{SR}} = \frac{1}{2}\sum_{\mathbf{R}}\sum_{i\neq j}^{N} q_i q_j [\frac{1}{|\mathbf{r}_{ij}+\mathbf{R}|} - \frac{erf[\alpha^{1/2}|\mathbf{r}_{ij}+\mathbf{R}|]}{|\mathbf{r}_{ij}+\mathbf{R}|}] =$$

$$= \frac{1}{2}\sum_{\mathbf{R}}\sum_{i\neq j}^{N} q_i q_j \frac{erfc[\alpha^{1/2}|\mathbf{r}_{ij}+\mathbf{R}|]}{|\mathbf{r}_{ij}+\mathbf{R}|} \tag{4.40}$$

with the *erfc* function defined by

$$erfcc(x) = \frac{2}{\pi^{1/2}}\int_x^{+\infty} e^{-t^2}dt \tag{4.41}$$

Putting all the terms together the final result is obtained:

$$U_E = U_{\mathrm{SR}} + U_{\mathrm{LR}} - U_{\mathrm{self}} = \frac{1}{2}\sum_{\mathbf{R}}\sum_{i\neq j}^{N} q_i q_j \frac{erfc[\alpha^{1/2}|\mathbf{r}_{ij}+\mathbf{R}|]}{|\mathbf{r}_{ij}+\mathbf{R}|}$$

$$+ \frac{1}{2V}\sum_{\mathbf{k}\neq 0}\frac{4\pi}{k^2}|\tilde{\rho}(\mathbf{k})|^2 e^{-k^2/4\alpha} - (\frac{\alpha}{\pi})^{1/2}\sum_{i=1}^{N} q_i^2 \tag{4.42}$$

The original sum has been thus separated into two parts. The short range sum is performed in the real space while the long range sum is performed in the Fourier space. The tuning of the parameter α results particularly important in determining the convergence of the integrals. In order to get fast convergence α should be large in the real space and small in the Fourier space. A balance of these needs is usually considered and typically α is set to values of the order of 5/L [154], taking a number of wave vectors of the order of ten for the computation of the sums over $\mathbf{k}$.

4.5 Dynamical Observables

In the analysis that will be discussed in the next Chapters, some dynamical observables have been calculated by means of personal programs implemented in *C* and executed in parallel with the Message Passing Interface (MPI) architecture. In particular it has been calculated the Self Intermediate Scattering Function, defined as:

$$F_S(Q,t) = \frac{1}{N}\left\langle \sum_i e^{i\vec{Q}\cdot\left[\vec{r}^{\,i}_O(t)-\vec{r}^{\,i}_O(0)\right]} \right\rangle, \tag{4.43}$$

and the Van Hove Self Correlation Functions:

$$G_S(\vec{r},t) = \frac{1}{N}\left\langle \sum_{i=1}^{N} \delta(\vec{r} + \vec{r}_O^{\,i}(0) - \vec{r}_O^{\,i}(t)) \right\rangle, \tag{4.44}$$

where N is the number of molecules and $\vec{r}_O^{\,i}$ the position of the oxygen atom recorded directly in the atomic trajectories of the MD simulation. For both the quantities the choice of the bin of uncertainty Δr is choose equal to 0.001 Å. The parallelization of the program has been implemented assigning to each processor the computation of the SISF (or the VHSCF) of a group of N/N_{CPU} particles, where N_{CPU} is the number of processors used. The average time for the calculation of a single Intermediate Scattering Function of 20 ns is approximately 10 days with 32 processors. The same computation using one single core would be around 320 days.

5

Molecular Dynamics of Supercooled Bulk Water: The Fragile to Strong Crossover

In this Chapter the results obtained for the MD simulations of TIP4P/2005 bulk water are presented. In particular the dynamical behaviour of the system is analysed, testing the range of validity of Mode Coupling Theory (MCT) for the TIP4P/2005 potential [159] and investigating the origin of the deviation from the MCT regime to the Arrhenius regime revealed by the occurrence of the Fragile to Strong Crossover in the deep supercooled region [159, 160]. The details of the MD simulations are given in Sec. 5.1. In Sec. 5.2.1 the Self Intermediate Scattering Functions of the oxygen atoms and the relative study of particle dynamics in terms of the Mode Coupling Theory is presented. In Sec. 5.2.2 the Fragile To Strong Crossover in TIP4P/2005 is studied. Sec. 5.2.3 is devoted to the analysis of the connection between the Fragile to Strong Crossover and the Widom line, showing an important relation between water dynamics and thermodynamics. The microscopic origin of the Fragile to Strong Crossover and the appearance of hopping processes in the deep supercooled regime are explored through the calculations of the Van Hove Self Correlation Functions of the oxygen atoms in Sec. 5.3.

5.1 TIP4P/2005 Bulk Water: Simulation Details

In order to study the dynamical properties of supercooled bulk water and their relation with the thermodynamic aspects of its phase diagram, a box of 512 water molecules was simulated at four different densities, $\rho = 0.95$ g/cm^3, $\rho = 0.98$ g/cm^3, $\rho = 1.00$ g/cm^3 and $\rho = 1.03$ g/cm^3. The box lengths are respectively 25.26 Å, 25.00 Å, 24.83 Å and 24.59 Å. All the sim-

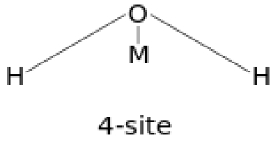

Figure 5.1: Geometry of the TIP4P/2005 molecule.

ulations are performed at constant volume in the mild and deep supercooled regime with a temperature range from 300 K to 195 K. The interactions between the water molecules are represented by the TIP4P/2005 potential, that describes the molecule as composed of two positively charged hydrogens with $q_H = 0.5564e$, one neutral oxygen which interacts as a single Lennard-Jones pole with $\sigma = 3.159$ Å and ϵ/k_B=93.2 K and a negatively charged imaginary site M with $q_M = -2q_H$ placed along the bisector $H - O - H$ and coplanar with the oxygen and hydrogens at distance 0.1546 Å from the oxygen (see Fig. 5.1).

TIP4P/2005 [21] is currently one of the most popular and realistic water model potential. TIP4P/2005 exhibits a TMD curve [22] perfectly in agreement with the experimental one and reproduces accurately several aspects of the phase diagram of stable water at low temperature like ice polymorphism [21]. In the supercooled region, it manifests an anomalous increase of thermodynamic response functions [22] and a line of maxima of the isobaric specific heat and isothermal compressibility in the one phase region proving the existence of a WL that terminates at the LLCP [23]. It is also interesting that TIP4P/2005 and TIP4P show a slope of the diffusion coefficients as function of temperature in good agreement with experiments. TIP4P/2005 values of the diffusion coefficients are close to the experimental values, while TIP4P predicts faster diffusion coefficients [24]. For the sake of completeness, it should be mentioned that water's anomalous properties have been investigated not only through classical MD water potentials but also through several quantum potentials implemented in *ab initio* molecular dynamics simulations [161]. Even if this kind of potentials takes into account quantum effects involved in liquids thermodynamics and dynamics, it is still difficult from a computational point of view to perform long time simulations using the *ab initio* approach.

The totality of the MD simulations are made with parallel Gromacs package 4.5.5. The Coulomb interactions have been implemented with the Ewald method, with a truncation of the potential at 9.5 Å and through the use of the Particle Mesh Ewald (PME) algorithm with a Fourier spacing of 1 Å and a fourth degree polynomial. The system has been equilibrated with

Berendsen thermostat. In order to verify the correct equilibration of the system, at the lowest temperatures calculated the box has been reheated quickly to higher temperatures and progressively cooled down until the initial temperature controlling if it has reached the same minimum of energy.

5.2 TIP4P/2005 water dynamics: Mode Coupling Theory and Fragile to Strong Crossover

5.2.1 Intermediate Scattering Functions and Mode Coupling Theory

As explained in Sec. 3.2, several dynamical aspects of water in the supercooled regime have been proved to be in agreement with the predictions of Mode Coupling Theory [16] both experimentally [17, 18] and computationally [14, 15, 126]. Among the measurable properties of the system that can be exploited to test the validity of MCT in water dynamics, the Self Intermediate Scattering Functions (SISF) provide important information on the temporal evolution of particles motion [14, 15]. In order to verify if TIP4P/2005 bulk water dynamics follows MCT, the oxygen SISF have been calculated for all the values of temperature and density mentioned in Sec. 5.1. Being defined as:

$$F_S(Q,t) = \frac{1}{N}\left\langle \sum_i e^{i\vec{Q}\cdot\left[\vec{R}^i_O(t)-\vec{R}^i_O(0)\right]} \right\rangle, \tag{5.1}$$

the SISF have been computed at the first peak of the oxygen-oxygen static structure factor $Q_0 = 2.25$ Å^{-1} where the MCT peculiar features of these correlators are more visible. The results are shown in Fig. 5.2.

As predicted by MCT, all the SISF exhibit a two step relaxation composed of a fast decay at short time scale and a slow structural decay at long times. This aspect of the correlators is directly related to the "cage effect" mentioned in Sec. 3.2.1.2 typical of liquids slow dynamics. At microscopic times, particles move ballistically without interacting each other and the correspondent SISF decrease as a Gaussian function with time. Entering the intermediate temporal region, the ballistic decay is progressively substituted by a slowly varying regime, the β relaxation regime, that begins to emerge as an inflection point at higher temperature and evolves into a constant plateau upon decreasing temperature. In this regime, particles are trapped in a cage formed by their nearest neighbors and the self density fluctuations

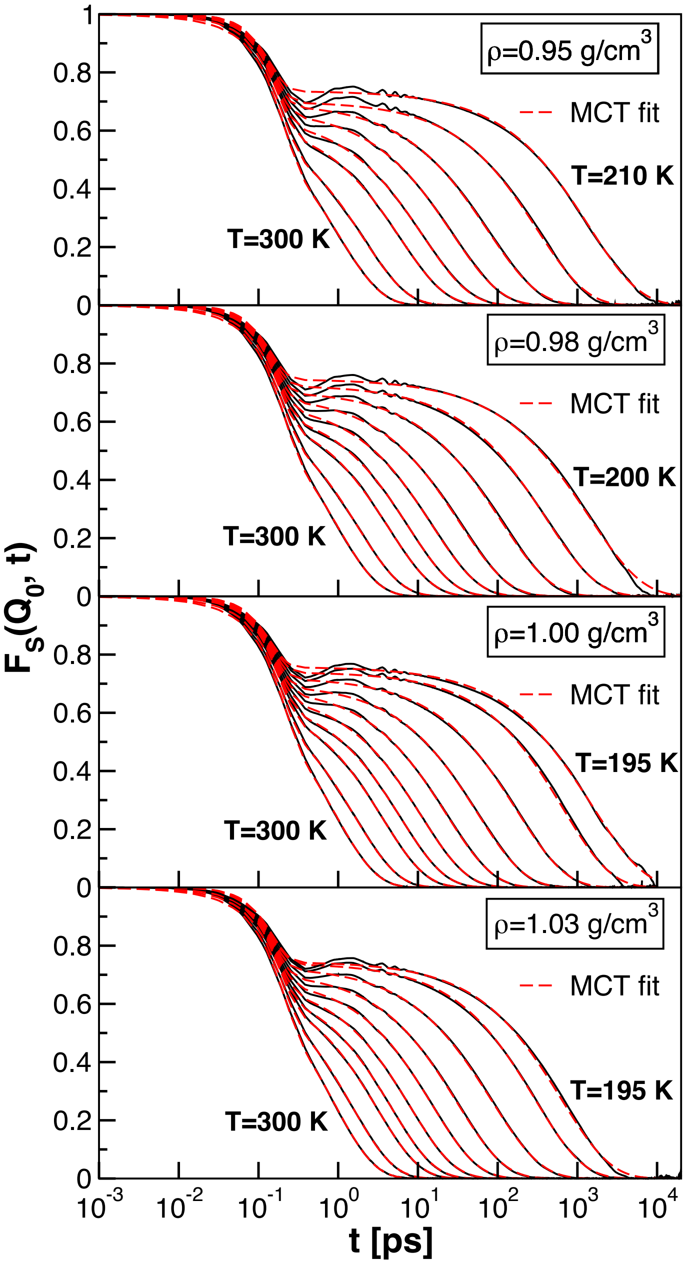

Figure 5.2: Oxygen Self Intermediate Scattering Functions for different temperatures calculated at the maximum of the static structure factor for the four different densities indicated. The temperatures investigated for $\rho = 0.95$ g/cm^3 are T=300, 280, 260, 250, 240, 230, 220, 210 K. For $\rho = 0.98$ g/cm^3 we added T=200 K and for $\rho = 1.00$ g/cm^3 and $\rho = 1.03$ g/cm^3 we further added T=195 K. The black solid lines are the MD results and the dashed red lines are the fits to Eq. 5.2.

T(K)	A	τ_s(ps)	τ(ps)	β
300	0.6836	0.2073	0.9216	0.8395
280	0.6636	0.1947	1.615	0.8044
260	0.6464	0.1836	3.607	0.8014
250	0.6523	0.1778	6.072	0.7853
240	0.6716	0.1699	10.95	0.7567
230	0.6889	0.1618	22.55	0.7356
220	0.7000	0.1585	55.31	0.7252
210	0.7216	0.1514	173.7	0.7065
200	0.7400	0.1473	658	0.7200
195	0.7580	0.1410	1547	0.6652

Table 5.1: Fitting parameters of the SISF with Eq. 5.2 for the density $\rho = 1.00$ g/cm^3.

remain approximately steady since the molecules motion is confined inside a finite spatial region. Only at long time scale, thermal fluctuations induce the cages dissolvation allowing the particles to diffuse within the liquid with Brownian motion and to enter in the so called α relaxation regime. In this regime, the SISF display a second decay characterized in its late part by a stretched exponential and the system is finally able to structurally rearrange itself.

It was shown in Ref. [14, 15] that for liquids with a dynamics well described by MCT the Self Intermediate Scattering Functions can be fitted with the formula:

$$F_S(Q,t) = (1 - A(Q))exp[-(t/\tau_s)^2] + A(Q)exp[-(t/\tau)^\beta], \tag{5.2}$$

where the first exponential represents the fast component of the SISF decay and the second stretched exponential describes the slow part of the system relaxation. $A(Q)$ is the Lamb-Mossbauer factor [16] corresponding to the height of the plateau, τ_s and τ are respectively the time scale characteristic of the short time fast relaxation and α relaxation and β is the Kohlrausch exponent of the long time exponential decay. All the SISF calculated in the present work are well fitted by Eq. 5.2, as shown in Fig. 5.2, proving that MCT is valid also for TIP4P/2005 bulk water. The values of the parameter of the fits for density $\rho = 1.00$ g/cm^3 are reported in Table 5.1. As expected from MCT, τ and β have a strong temperature dependence. The increase of τ and the decrease of β from values near 1 to smaller values by cooling the system indicate clearly that the dynamics is progressively slowing down and the cage has less and less capability to relax. At lower temperatures the

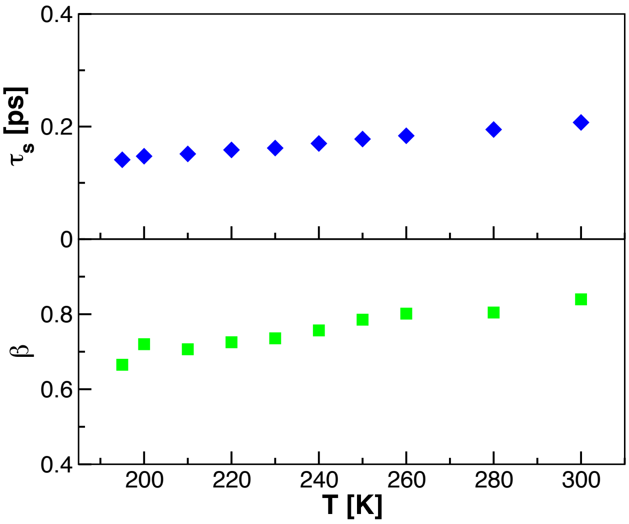

Figure 5.3: Behaviour of the short relaxation time τ_s and of the exponent of the α relaxation stretched exponential β vs the temperature at $\rho = 1$ g/cm^3.

liquid is more structural arrested and with less mobility and consequently the self time correlations decay as a stretched exponential with an exponent β much shorter than the gaussian value $\beta = 1$ typical of Brownian particle diffusion in the high temperature range. The τ_s extracted from the fitting procedure is rather constant, as visible in Fig. 5.3 where also the trend of β is displayed as a function of temperature at $\rho = 1$ g/cm^3.

Moreover, the slowing down of the cage breaking rate by decreasing temperature causes the particle to stay trapped inside the cage for longer times, as confirmed by the increasing length of the plateau in the SISF intermediate time region.

Besides the temperature dependence of liquid dynamics in the supercooled regime, it is also interesting to analyse what happens to the particle motion by varying density at fixed temperature. In Fig. 5.4 the SISF of the four densities investigated at $T = 210$ K are plotted.

Even if all the densities exhibit the two step relaxation scenario typical of supercooled liquids, the SISF in Fig. 5.4 decay slower and slower as density is isothermally decreased. This phenomenon is a direct consequence of the so called diffusion anomaly [22, 40–43, 142]. In general, the isothermal compression of a simple liquid induces a loss of fluidity and an overall slowing

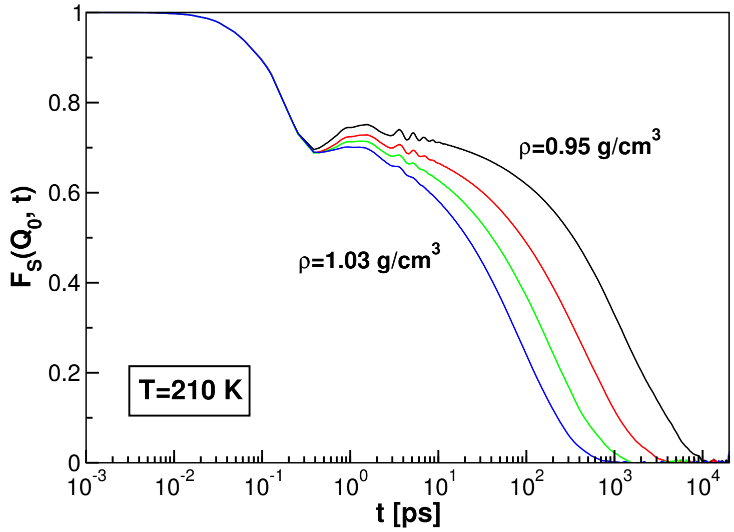

Figure 5.4: Oxygen Self Intermediate Scattering Functions calculated at the maximum of the static structure factor for the four different densities investigated at the same temperature T=210 K.

down of particle dynamics that reflects in a decrease of the self diffusion coefficient and an increment of the structural relaxation time. Differently from most liquids, water self diffusion coefficient presents an anomalous behaviour [40], decreasing upon decreasing density in the range from $\rho = 0.95$ g/cm^3 to $\rho = 1.15$ g/cm^3. In the supercooled regime, in fact, the increase of density or pressure is associated to an increase of breaking of the hydrogen bonds (HB) between the water molecules, that restores fluidity and allows the particles to diffuse free from their nearest neighbors. This dissolution of the HB network corresponds to an increment of the system capability to rebalance and rearrange itself, as shown in Fig. 5.4, where at higher densities the SISF decay faster indicating a greater mobility of liquid particles. The anomalous slowing down of the dynamics and the correspondent increase of the structural relaxation time by lowering density is displayed for all the temperature investigated in Fig. 5.5. According to the interpretation of the LLCP and the coexistence of two phases of liquid water it can be deduced that decreasing density isothermally corresponds to penetrate in the LDL phase of supercooled water and for each temperature lower densities coincide with systems more structured and "frozen" with values of τ greater and greater. Moreover, the rate of increase of the α relaxation

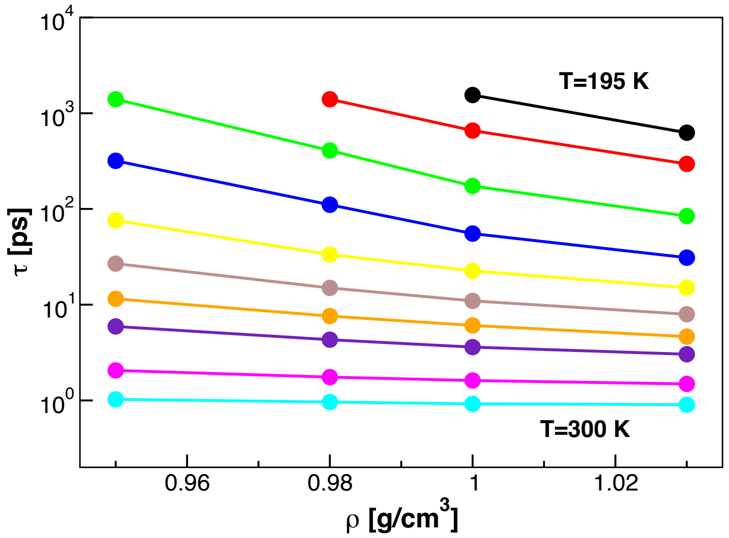

Figure 5.5: Isothermal curves of α relaxation time as a function of densities investigated from T=300 K to T=195 K.

time with decreasing density along each isotherm grows progressively upon cooling the system, as visible from the logarithmic scale of the plot. This trend indicates that, upon decreasing density, the continuous slowing down and freezing of the particle dynamics is quicker at lower temperatures. By comparisons with the results obtained with the TIP4P potential [126, 162], it should be noticed that the structural relaxation times at the same temperature and density extracted from the SISF computed in this work are definitively greater, revealing a general "stretching" of the overall dynamics in the TIP4P/2005 potential. A snapshot of the α relaxation times determined for TIP4P [126] and TIP4P/2005 at the same thermodynamic conditions is shown in Fig. 5.6. The possible origin of this behaviour will be discussed later.

Although the analysis of the TIP4P/2005 bulk water dynamics through the computation of the oxygen Self Intermediate Scattering Functions has shown several dynamical aspects in agreement with MCT, a further inspection needs to be conducted in order to test the real temperature and density range of validity of the MCT predictions. This is what will be examined in the next Section.

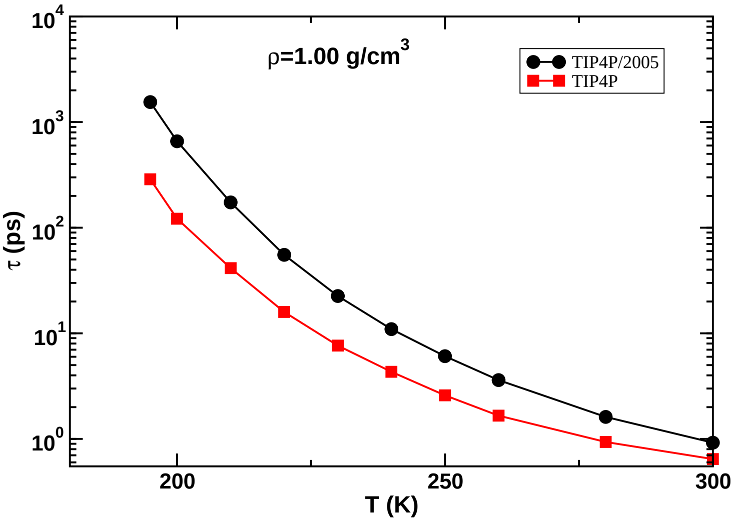

Figure 5.6: Values of the α relaxation times extracted for TIP4P [126] and for TIP4P/2005 at the same temperature and density. A general slowing down of the dynamics in TIP4P/2005 is evident.

5.2.2 The Fragile to Strong Crossover

Starting from the generalized Langevin equation, one of the goal of the MCT is to predict not only the two step relaxation typical of glassy dynamics but also several phenomenological properties of supercooled liquids. As already mentioned in Sec. 3.2.1.3, one of these properties is the dependence from temperature of the α relaxation time that, according to MCT, should follow a power law:

$$\tau \sim (T - T_C)^{-\gamma}, \tag{5.3}$$

with T_C the Mode Coupling temperature at which the system should pass from an ergodic phase to a dynamically arrested glassy phase and γ an exponent that should be independent from the system studied. In real liquids, and in particular in real water, particles have the capability to diffuse and rearrange within the liquid in a finite time interval also below the hypothesized value of the MCT temperature T_C. This disagreement with Eq. 5.3 is caused by the occurrence, approaching T_C, of a different mechanism in the structural relaxation process that has not been taken into account in the ideal formulation of MCT. In the deep supercooled regime, in fact, although the thermal fluctuations are not more sufficient to break

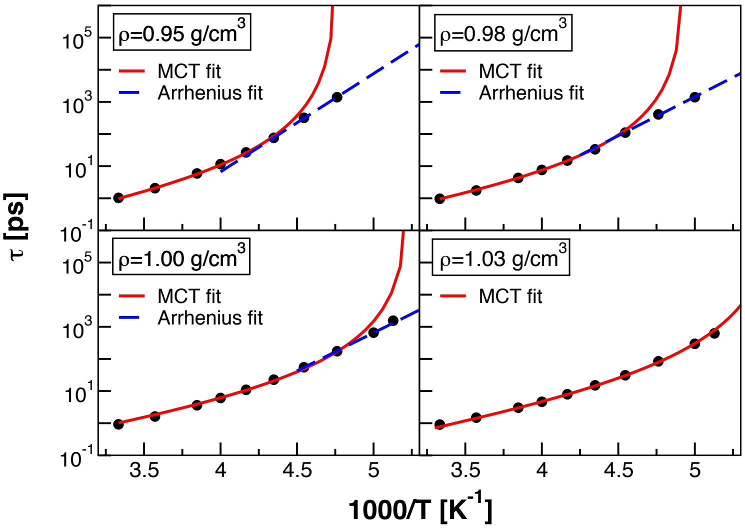

Figure 5.7: Complete behaviour of the α relaxation time τ versus the inverse of the temperature for the four different densities investigated. The red lines are the fit with Mode Coupling power law, see Eq. 5.3. The blue lines are the fit with the Arrhenius function, see Eq. 5.4.

and dissolve the cages formed in the intermediate temporal region, particles are able to escape from the cages jumping out through activated processes called "hopping processes" [163, 164]. The presence of these phenomena allows the system to relax even if the cages are completely frozen and restore the ergodicity otherwise lost under T_C. It has been already discussed in Sec. 3.2.2 that the appearance of hopping processes generates a change in the temperature dependence of the α relaxation time that deviates from the power law of Eq. 5.3 to an exponential Arrhenius law:

$$\tau = \tau_0 e^{E_A/k_B T}, \tag{5.4}$$

where E_A is the activation energy of hopping processes. This Fragile to Strong Crossover (FSC) marks the temperature at which the cages begin to be fixed and frozen and hopping starts to be the dominant mechanism of the structural relaxation. Fig. 5.7 shows the τ extracted from the SISF for the four densities computed as a function of temperature in the range investigated. The red lines represent the high temperature MCT fit with Eq. 5.3 and the blue lines represent the low temperature Arrhenius fit with Eq. 5.4. The values of the fit parameters are listed in Table 5.2, where T_C is

$\rho[g/cm^3]$	$T_C[K]$	γ	$E_A[kJ/mol]$	T_L [K]
0.95	209.898	2.982	58.454	230
0.98	202.628	2.858	46.349	220
1.00	190.829	2.939	45.291	210
1.03	179.687	3.354	-	-

Table 5.2: Fitting parameters of the MCT Eq. 5.3 and Arrhenius Eq. 5.4 for each density and correspondent fragile to strong crossover temperatures.

the Mode Coupling Temperature and T_L is the FSC temperature. The fits of MCT are done excluding high temperatures values at which water does not yet follow the supercooled liquid dynamics. Except for the higher density $\rho = 1.03$ g/cm^3, the other densities investigated exhibit a Fragile to Strong Crossover at a temperature T_L that is always higher than the correspondent MCT temperature T_C. This can be understood considering that hopping phenomena begin to occur when cages are still able to relax and become progressively the primary relaxation mechanism only below the temperature of ideal structural arrest T_C. It should be noticed that the values of MCT temperature T_C and of the FSC temperature T_L increase monotonically for decreasing density, in agreement with water diffusion anomaly. As said above, in fact, for each temperature lower densities have structures more rigid and with slower dynamics than higher densities and consequently are "closer" to the strong regime. Therefore the Fragile to Strong Crossover from a state where water diffusion properties have a fragile character to a region where water behaves as a strong liquid happens at higher temperature for smaller densities with respect to greater densities. A clear panoramic of these deviations from MCT is displayed in Fig. 5.8 where the inverse of the α relaxation time as a function of $T - T_C$ is plotted in the log-log plane for the four densities investigated.

In order to obtain a further confirmation of the thermodynamic range of validity of the MCT determined by the previous analysis of the α relaxation time, the time-temperature superposition principle (TTSP) represents another prediction of MCT verifiable through the computation of the SISF. For times in the late β relaxation regime, i.e. in the time interval where the density correlator is dropping below the plateau and entering in the α relaxation regime, MCT hypothesizes that SISF should follow the so called von Schweidler law (VSL):

$$\phi_Q(t/\tau) = f_Q - h_Q \cdot (t/\tau)^b, \tag{5.5}$$

where f_Q is the ergodicity factor, h_Q is the amplitude and the exponent b is the von Schweidler exponent. Eq. 5.5 means that the Intermediate Scat-

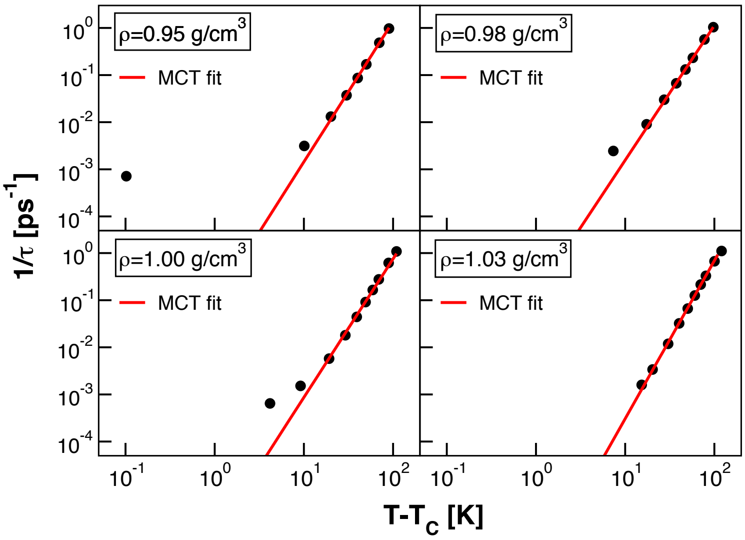

Figure 5.8: Log-log plot of the inverse of the α relaxation time $1/\tau$ versus $T-T_C$ for the four different densities investigated. The red line is the MCT fit, see Eq. 5.3. For each panel only the temperatures $T > T_C$ can be shown.

tering Functions of supercooled liquids have a universal dependence from the rescaled time t/τ independently from the specific value of temperature evaluated and should collapse on a single master curve if plotted as a function of the ratio t/τ. To test the validity of the TTSP for TIP4P/2005 bulk water, for all the densities investigated the SISF have been rescaled in their time dependence with the correspondent τ and fitted with Eq. 5.5. The SISF as a function of t/τ and the results of the fits with the VSL equation (red lines) are plotted in Fig. 5.9 for the four densities simulated.

For each density, it is evident that the TTSP holds in the thermodynamic range of validity of MCT. The values found for $\rho = 1$ g/cm^3 are $f_Q = 0.734$, $h_Q = 0.4907$ and $b = 0.4949$ similar to the values found for other potentials [15, 126]. Besides providing important predictions on the shape of the relaxation curves of the density correlators, MCT foresees also the existence of a connection between the β relaxation and the structural properties of the system, that should be related through the following non linear equation:

$$\lambda = \frac{\Gamma^2(1+b)}{\Gamma(1+2b)} = \frac{\Gamma^2(1-a)}{\Gamma(1-2a)}, \tag{5.6}$$

where b is the Von Schweidler exponent, a is the characteristic exponent

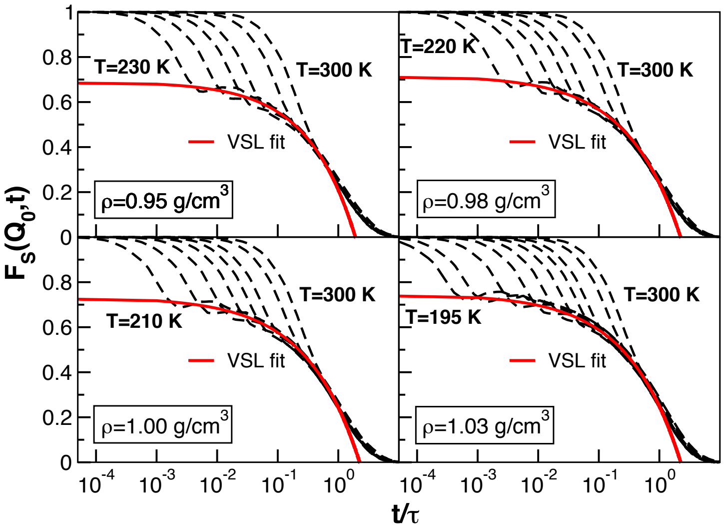

Figure 5.9: SISF vs scaled time t/τ for four different densities in the range of temperatures where MCT holds. The red lines are the von Schweidler law fits, see Eq. 5.5.

of the early part of the β relaxation and λ is the exponent parameter, a quantity that can be extracted from the static structure factor. This aspect together with the following scaling equation that relates the α and β relaxation:

$$\gamma = \frac{1}{2a} + \frac{1}{2b}, \tag{5.7}$$

allows to further verify the validity of MCT comparing the exponent parameter obtained independently from Eq. 5.6 and Eq. 5.7. In particular, after having calculated a from Eq. 5.7, the parameter λ has been derived separately from a and b. For density $\rho = 1$ g/cm^3, the results are $\lambda = 0.83$ from a and $\lambda = 0.79$ from b. These values are in fairly good agreement, the slight difference can be caused by the presence of hopping phenomena, which are known to begin to occur also in the range of validity of MCT.

In conclusion, the analysis conducted above has revealed a remarkably good accord between the results of TIP4P/2005 bulk water dynamics obtained from the SISF and the Mode Coupling Theory predictions, confirming the MCT power law dependence of α relaxation times and the time-temperature superpositions principle in the mild supercooled regime. Nevertheless, all the densities investigated except $\rho = 1.03$ g/cm^3 present, in the deep supercooled region, a deviation of the structural relaxation times from the fragile MCT behaviour to the strong Arrhenius behaviour that is caused by the appearing of hopping phenomena. This Fragile to Strong Crossover, as already discussed in Sec. 3.2.2, has been associated in previous works to the existence in the one phase region of the Widom Line [20, 25, 67, 126, 127, 143, 147, 149]. The question that remains to be elucidated is if this connection between these two characteristics of the thermodynamics and the dynamics of supercooled water subsists also for the TIP4P/2005 potential.

5.2.3 Dynamics and Thermodynamics: The Fragile to Strong Crossover at the Widom Line

Section 5.2.2 has shown that the temperature dependence of the α relaxation times for densities $\rho = 0.95$ g/cm^3, $\rho = 0.98$ g/cm^3 and $\rho = 1.00$ g/cm^3 deviates from the fragile MCT power law to the strong Arrhenius exponential law at $T_L = 230$ K, $T_L = 220$ K and $T_L = 210$ K respectively. Several computational and experimental works have found the existence of a Fragile to Strong crossover and a correspondence between the occurrence of this FSC and the crossing of the Widom Line (WL) in different systems and water potentials. As already explained in Sec. 3.1.2.1, the Widom Line is defined as the line of maxima of the correlation length that emanates from the LLCP as an extension in the one phase region of the first order liquid-liquid phase transition (LLPT). Having a negative slope in the $P - T$ plane, the LLPT separates the high temperature high density liquid from the low temperature low density liquid. Within this scenario, the coincidence between the WL and the FSC can be understood as described in the following: on one hand the WL represents the extension in the one phase region of the LLPT, a negatively sloped coexistence line that separates HDL from LDL; on the other hand the FSC determines a dynamical border between a supercooled liquid region more fluid and dynamically faster which has, as displayed in Fig. 5.4, a high density structure, and a phase in the deep supercooled regime where the liquid is more structural arrested and less dense. The WL and the FSC, therefore, mark together thermodynamically and dynamically the passage of the system from a fragile high density state to a strong low density phase.

The dynamical results presented in Sec. 5.2.2 evidence the absence of the Fragile to Strong Crossover at density $\rho = 1.03$ g/cm^3. In order to motivate this absence through the presence of the Widom Line already determined in the TIP4P/2005 by Abascal and Vega in Ref. [23] the isochoric specific heat $c_V = (\partial U/\partial T)_V$ has been calculated for all the state points investigated.

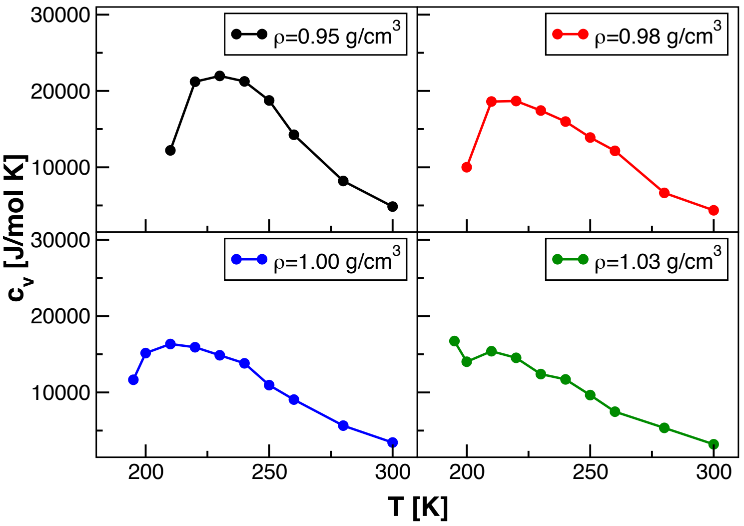

Figure 5.10: Plot of the isochoric specific heat, c_V , for the four different densities investigated as a function of temperature. For each density under the critical density, $\rho_C = 1.012\ g/cm^3$, a maximum appears. For the density $\rho = 1.03\ g/cm^3$, above the critical density, c_V continues to increase upon lowering temperature down to the lowest temperature investigated.

In agreement with what expected in presence of a second order critical point, TIP4P/2005 potential displays a locus of maxima of the isothermal compressibility [23], roughly coincident with the minima of expansivity and collapsing in a range of circa 30 K with the maxima of c_V computed in this work. This suggests that the choice of c_V maxima as a proxy of the Widom Line is reasonable. The values of c_V for the four densities analysed in the range of temperature simulated are plotted in Fig. 5.10. Except for $\rho = 1.03$ g/cm^3, the three lower densities have a single maximum of c_V. It should be noticed that, in contrast with what happens commonly in critical phenomena, the values of these maxima decrease for increasing density, i.e. coming nearer to the region of larger fluctuation and the critical point. This behaviour can be justified in the same manner of Ref. [165], where the maxima of the isobaric specific heat decrease anomalously approaching the LLCP in TIP5P. The isochoric specific heat, in fact, can be written by definition as the sum of two different contributions:

$$c_V = \left(\frac{\partial U}{\partial T}\right)_V = \left(\frac{\partial U}{\partial T}\right)_P + \left(\frac{\partial U}{\partial P}\right)_T \left(\frac{\partial P}{\partial T}\right)_V . \tag{5.8}$$

The second term of the sum can be recombined through the use of the Maxwell relation:

$$\left(\frac{\partial P}{\partial T}\right)_V = \left(\frac{\partial S}{\partial V}\right)_T \tag{5.9}$$

and exploiting the chain rule for the partial derivatives:

$$\left(\frac{\partial U}{\partial P}\right)_T = \left(\frac{\partial U}{\partial V}\right)_T \left(\frac{\partial V}{\partial P}\right)_T . \tag{5.10}$$

By means of these transformations, the isochoric specific heat can be finally written as:

$$\left(\frac{\partial U}{\partial T}\right)_V = \left(\frac{\partial U}{\partial T}\right)_P - \left(\frac{\partial U}{\partial V}\right)_T \left(\frac{\partial V}{\partial T}\right)_P \tag{5.11}$$

As confirmed by the increase of the α relaxation time upon lowering density shown in Fig. 5.5, the thermodynamic state points simulated lie in the region of diffusion anomaly, that implies:

$$\left(\frac{\partial V}{\partial T}\right)_P < 0 \tag{5.12}$$

Moreover, from the calculation of the internal energy as a function of volume along the isotherms in the region investigated:

$$\left(\frac{\partial U}{\partial V}\right)_T < 0 \tag{5.13}$$

in agreement also with Ref. [74]. Since the term $(\partial U/\partial T)_P$ corresponds to the isobaric specific heat c_P apart a constant and, as a thermodynamic response function, diverges positively moving close to the LLCP, Eq. 5.12 and Eq. 5.13 reveal that the c_V is composed of two contributions that diverge asymptotically with opposite sign approaching the critical point. Therefore, the anomalous decrease of the values of the maxima could be due to cancellation effects.

In order to explore a possible connection between the Fragile to Strong Crossover found in the previous Section and the existence of the Widom Line in the phase diagram of TIP4P/2005 supercooled water, the state points at which the FSC occurs and the location of the maxima of c_V used as proxy of the WL have been compared. The results of this analysis is displayed in Fig. 5.11, where the LLCP, the c_V maxima, the FSC and the TMD curve of TIP4P/2005 are plotted in the $\rho - T$ plane. The temperatures of maxima of the isochoric specific heat for each density except the highest coincide within statistical fluctuations with the points of the Fragile

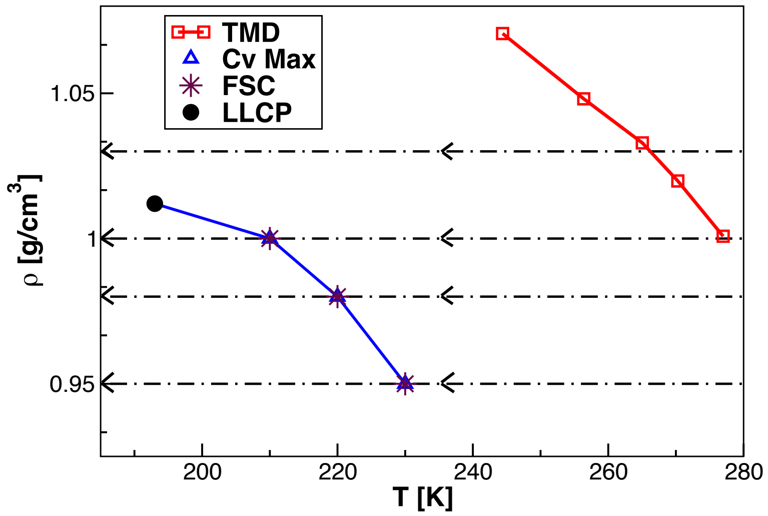

Figure 5.11: Results in the $\rho - T$ plane. The horizontal dashed lines indicate the different isochores calculated with MD simulations. c_V maxima are empty triangles, Fragile to Strong Crossovers are stars, the LLCP is the full circle and the TMD are squares, the continuos lines are guides for the eye.

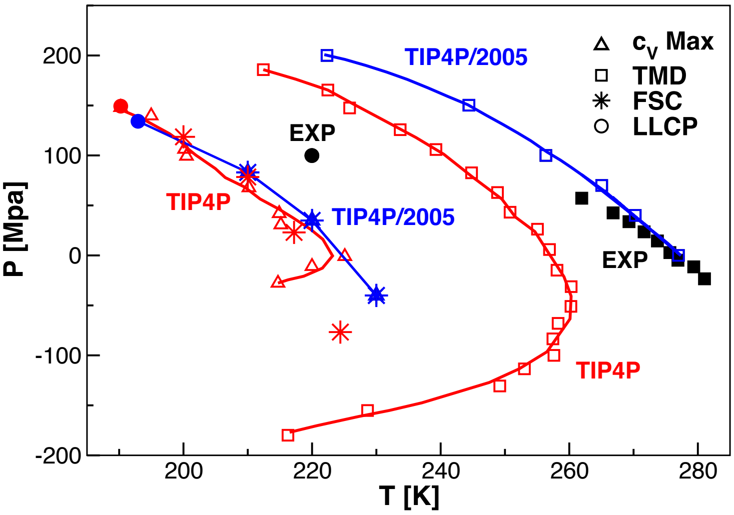

Figure 5.12: Plot in the $P-T$ plane of the maximum of response functions c_V (triangle up) together with the FSC (stars) and TMD lines (squares) for TIP4P (red symbols and lines) [86, 126] and TIP4P/2005 (blue symbols and lines) potentials. TIP4P/2005 TMD is from Ref. [23]. Black squares are experimental results for the TMD line. LLCP are filled circle symbols. The experimental LLCP refers to the estimated value in Refs. [11, 12].

to Strong Crossover. This relation between the WL and the FSC represents an important property of supercooled water phenomenology, proving that dynamics and thermodynamics are not two aspects totally separated and independent of the system: the dynamical deviation of the liquid from the fragile fast behaviour to the strong slow regime is directly associated to the crossing of the WL, a purely thermodynamic curve marking the passage between the high density and low density liquid phase of supercooled water. In the light of these considerations, the absence of the FSC and of a maximum of c_V for $\rho = 1.03$ are perfectly explained with the fact that this density lies above critical density, the LLCP of the TIP4P/2005 being located at T=193 K, P=135 MPa, $\rho = 1.012$ g/cm^3 in Ref. [23].

In Fig. 5.12 the significant thermodynamic curves together with the FSC for the potentials TIP4P and TIP4P/2005 in the $P-T$ plane are reported. The experimental curve of the TMD is also reported in the available range. TIP4P/2005 potential presents a TMD curve in agreement with experiments in contrast with TIP4P, that exhibits a TMD rigidly shifted at lower temperatures. Despite these differences in the high temperature range, the two potentials reveal a similar phase diagram in the mild and deep supercooled regime, locating the LLCP, FSC and WL approximately in the same $P-T$ region. The result is that the TIP4P/2005 shows a phase diagram of the stable and metastable regime "expanded" compared to the TIP4P and an overall dynamics definitively slower at equal temperature as already discussed in previous works [24, 126]. The similarity between the TIP4P and the TIP4P/2005 only in the supercooled region could be attributed to the different charge distribution of the water molecule. Even if the TIP4P/2005 provides a realistic description of the molecular orientational order [24] with a crystalline phase in good agreement with experiments, in the deep supercooled region this improvement with respect to TIP4P could tend to progressively become less relevant, leading to analogous predictions of the peculiar phenomena in this thermodynamic region.

To conclude, the analysis of the TIP4P/2005 bulk water dynamics through the calculation of the Intermediate Scattering Functions have confirmed the validity of the Mode Coupling Theory in the mild supercooled regime and has shown the presence of a Fragile to Strong Crossover upon penetrating in the deep supercooled phase. This dynamical deviation has been proved to be related to the crossing of the Widom Line, bringing to light an important connection between dynamics and thermodynamics.

5.3 The microscopic origin of the Fragile to Strong Crossover: Hopping Phenomena

In Sec. 5.2.2 it has been mentioned that the change of the structural relaxation time from the MCT power law behaviour to the exponential Arrhenius trend is caused by the appearance of hopping phenomena. Given the importance of the FSC both from the thermodynamic and dynamical point of view, a better comprehension of these activated processes and of how they influence water dynamics could furnished a new insight on the low temperature aspects of the supercooled metastable state. This kind of study on the same system described in Sec. 5.1 will be fully examined in the next Sections.

5.3.1 Van Hove Self-Correlation Functions

Previous Sections have been devoted to the investigation of water dynamics through the computation of the SISF. Even if this quantity provides a good picture of particle motion, other mathematical instruments can be exploited

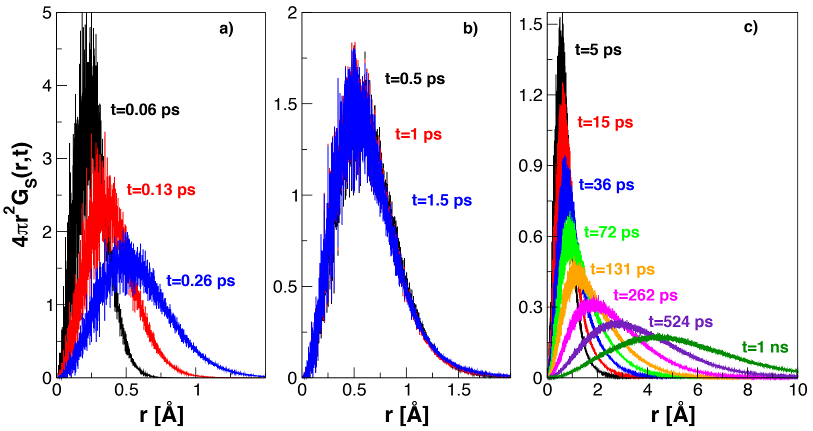

Figure 5.13: Radial Van Hove Self Correlation functions at $T = 220$ K for density $\rho = 1.00$ g/cm^3 for various instants of time. The VHSCF are displayed in a) the ballistic time interval, b) the intermediate "cage" regime and c) the long time diffusive regime.

to explore liquid dynamics. One of these is the oxygen Van Hove Self-Correlation Function (VHSCF), defined as:

$$G_S(\mathbf{r},t) = \frac{1}{N}\left\langle \sum_{i=1}^{N} \delta(\mathbf{r} + \mathbf{r}_O^i(0) - \mathbf{r}_O^i(t)) \right\rangle, \tag{5.14}$$

where N is the number of particles of the system. The VHSCF represents the probability that a particle had covered a distance $\mathbf{r}_O(0) - \mathbf{r}_O(t)$ in a time interval t and gives a detailed characterization of the average molecule evolution both in space and time. In order to evaluate in which way hopping intervenes in the Fragile to Strong Crossover, the radial version $4\pi r^2 G_S(r,t)$ of the oxygen VHSCF for the three subcritical densities $\rho = 0.95$ g/cm^3, $\rho = 0.98$ g/cm^3 and $\rho = 1.00$ g/cm^3 have been calculated for several values of time in the range of temperature from 300 K to 190 K. The results of these calculations for $\rho = 1.00$ g/cm^3 at various instants of time representative of the three regime typical of supercooled liquids dynamics are presented in Fig. 5.13.

The progression of the VHSCF with time reflects the "cage" effect, as already discussed in Ref. [15]. At the initial times (panel *a*), the particle moves within the liquid completely free from the interactions with the other ones exploring portions of space greater and greater with time. This ballistic motion results in a VHSCF with a strong gaussian character that moves its peak at larger distance and extends progressively its tail upon increasing time, indicating that the molecule is going away from its original position. The spread of the radial VHSCF on the x-axis stops temporarily in the intermediate temporal region (panel *b*) where the function remains fixed in time and collapses on a single curve. At these instants of time, the particle is confined in a finite spatial region around the position of the peak and trapped in the cage formed by its nearest neighbors. The evolution with time of the Van Hove functions starts again at long times (panel *c*) when the cages dissolve and the molecules can diffuse within the liquid with Brownian motion. Probing new spatial region more and more distant, in this regime particles exhibit peaks of the VHSCF that translate spatially at higher values of distance upon increasing time, with an overall shape of the VHSCF that expands and tends to go back to a Gaussian whose variance is controlled by the diffusion coefficient D.

Besides giving a complete description of the average molecular trajectory in time, the analysis of the VHSCF can be employed to obtain information on particle motion inside the cage.

The most intuitive way of thinking about the cage confining potential is to suppose that the interactions with the molecule's nearest neighbors act on the whole as a three-dimensional harmonic force. Following this hypothesis, already formulated in Ref. [15], the correspondent VHSCF should have a Gaussian behaviour:

$$G_S(\mathbf{r},t) = \left(\frac{m\omega^2}{4k_BT\pi}\right)^{3/2} e^{-M\omega^2\mathbf{r}^2/4k_BT}, \tag{5.15}$$

where m is the oxygen mass and ω is the angular frequency of the oscillation. In the range of temperature where the cage effect is more evident and for each of the three densities analyzed the radial VHSCF in the cage regime have been fitted with the radial version of Eq. 5.15. Fig. 5.14 shows the result of the fit for $T = 220$ K and $\rho = 1.00$ g/cm^3. As in Ref. [15], the fit displays clearly that in the cage regime the VHSCF follows accurately the Gaussian of Eq. 5.15 at small distances near the position of the peak but progressively deviates its tail from the curve of the fit. This behaviour on one hand confirms the harmonic character of the radial Van Hove function for small oscillation around the center of the cage and on the other evidences the importance of anharmonic contributions at the edge of the cage.

The values of the oscillation frequency ω extracted from the fitting procedure by Eq. 5.15 are shown in Fig. 5.15 as a function of temperature for all the isochores analysed. For what concerns the temperature dependence, for each density the value of ω increases monotonically upon cooling

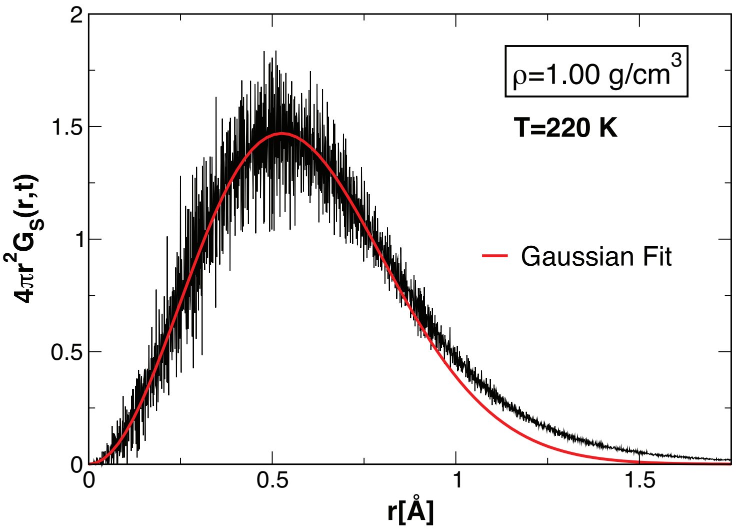

Figure 5.14: Radial Van Hove Self Correlation Function calculated at $T = 220$ K for $\rho = 1.00$ g/cm^3. The black data are the MD results and the red line is the fit to Eq. 5.15.

the system. Considering that the oscillation frequency is, by definition, directly proportional to the modulus of the elastic constant of the harmonic potential $k = m\omega^2$, this trend depicts the cage as gradually more rigid and more attractive upon diminishing the temperature. Moreover, at fixed temperature the frequency grows decreasing density. This phenomenon is once again related to the diffusion anomaly: low density structures have less capability to rearrange and cages more "frozen" and obstructive; higher density presents a faster dynamics and cages that dissolve easier with time. It should be noticed that, on approaching the correspondent Mode Coupling Temperature T_C determined in the previous Section, the slope of the ω curves for all the three densities flattens. A possible explanation of a similar behaviour is that close to T_C the dynamics is almost structurally arrested and the cages completely blocked; in this "glassy" phase the cage harmonic potential becomes progressively temperature invariant and does not modify anymore its properties.

Overall, the outcomes of the fits of the radial VHSCF to Eq. 5.15 at several temperatures and $\rho = 1.00$ g/cm^3, are compared in Fig. 5.16. The plot evidences a peculiar behaviour of the cage radius. Upon decreasing temperature, in fact, the VHSCF become narrower and sharper with a standard

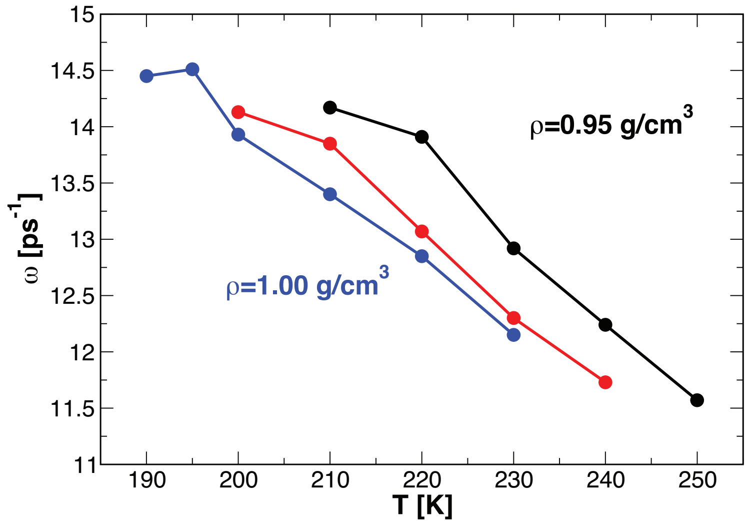

Figure 5.15: Values of the pulsations obtained by fitting the radial VH-SCF with Eq. 5.15 at the temperature where the cage freezes for longer times the particle motion. Each curve represents one of the three densities investigated, from the lower density $\rho = 0.95$ g/cm^3 (black line) to the higher density $\rho = 1.00$ g/cm^3 (blue line).

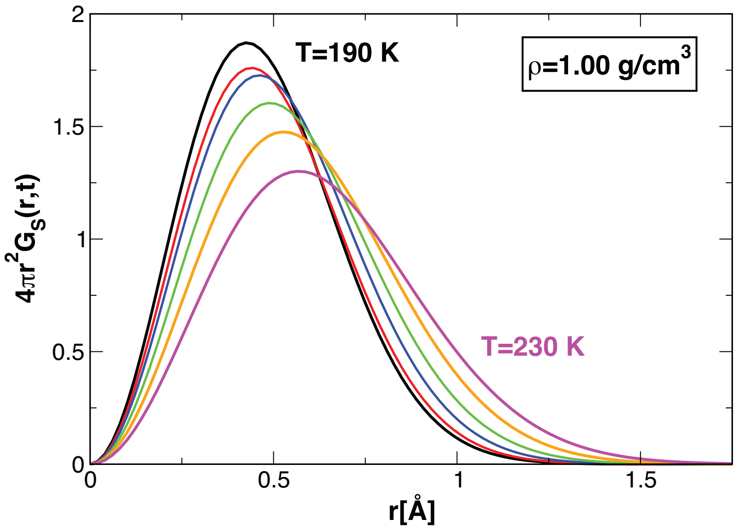

Figure 5.16: Fits to Eq. 5.15 of the radial Van Hove correlation functions at $\rho = 1.00$ g/cm^3 at the values of temperatures investigated from $T = 230$ K to $T = 190$ K. For each temperature the VHSCF is computed during the cage time interval.

deviation $\sigma = \sqrt{\frac{2k_BT}{m\omega^2}}$ smaller and smaller in agreement with the increase of the oscillation frequency. By considering σ as an approximate measure of the particle's mean square displacement inside the cage, this means that the cage radius reduces itself by lowering temperature, as predicted by Mode Coupling Theory. Consequently, even if the global arrangement of the molecules within the liquid maintains the same density upon supercooling, the strengthening of the hydrogen bonds leads to a contraction of the volume of the cage trapping the particle.

In pursuing the goal of a better comprehension of hopping processes, the Van Hove Self Correlation Function reveals a useful mathematical instrument not only for the study of the properties of the cage regime but also for a deep examination on the mechanisms responsible of the system's structural relaxation. Next Section will be devoted to the analysis of the VHSCF in the long time regime inquiring in details on the relation between the Fragile to Strong Crossover and the emergence of hopping phenomena.

5.3.2 Hopping Phenomena and Fragile to Strong Crossover

As already seen in Sec. 5.2.2 the dynamics of TIP4P/2005 bulk water is well described in the mild supercooled regime by Mode Coupling Theory. Accordingly to this theory, the system's structural relaxation is founded on the Brownian diffusion of the particles within the liquid after the dissolvation of the cages formed in the intermediate transient regime. The time τ characteristic of this α relaxation follows the power law of Eq. 5.3, diverging asymptotically at T_C. At this temperature, in fact, the system moves from a state where the cages break down and reform continuously allowing it to rearrange to a phase where the cages are completely blocked and the system has vitrified. Results of Sec. 5.2.2 have shown that for the three subcritical densities simulated, the liquid is able to structurally relax also below the relative Mode Coupling Temperature exhibiting an Arrhenius increase of the relaxation time. This discrepancy with MCT is caused by the appearance in the deep supercooled regime of activated hopping processes that restore the ergodicity to the system below the ideal glass transition temperature T_C and that are not taken into account in the initial version of MCT. Even if the the cages are still frozen, the molecule has a non zero probability to escape from it jumping out. This process gives on one hand the chance to the particles to diffuse again within the liquid and on the other introduces a new mechanism of system's relaxation different from the MCT relaxation. Hopping phenomena occur gradually upon lowering temperature. They begin to emerge at temperatures above the Mode Coupling Temperature and approaching T_C progressively become the dominant mechanism of the

long time scale dynamics, being the α relaxation predicted by MCT more and more arduous to realize upon cooling. Once reached T_C, the cages are definitively arrested and the only way for the system to relax is by hopping. Sec. 5.2.2 have shown that the manifestation of hopping processes reveals in the Fragile to Strong Crossover of the structural relaxation time, characterized by a deviation of the temperature dependence from the MCT power law to the exponential Arrhenius law of Eq. 5.4 typical of activated processes.
Given the primary role that hopping has in the main aspects of water dynamics, a more detailed investigation on the intrinsic functioning at the basis of these phenomena and a qualitative description of the behaviour of these processes upon varying temperature and density could be improved the current knowledge of liquid dynamics at temperatures in the deep supercooled regime. The study of the Van Hove Self Correlation Functions at long times provides a direct observation of the eventual presence of hopping. As it will be shown later, in fact, while in the high temperature range the VHSCF exhibit a distribution typical of the α relaxation, at sufficiently low temperatures the emergence of hopping processes is revealed by the appearance of one or more weak extra peaks superposing to the stronger peak of the α relaxation. In Fig. 5.17 the long times VHSCF for the three densities investigated at three values of temperatures, one 10 K above and two 10 K and 20 K below their respective crossover temperature T_L (whose values are listed in Table 5.2) are presented. The results of the computation of VHSCF show an overall behavior similar for each density.

Above the crossover temperature (left panel of each density), the VHSCF broaden in space and display non zero values at distances larger and larger upon increasing time, as expected in the α regime. First changes begin to occur already at temperatures 10 K below the FSC (central panel of each density). For all the three densities simulated, in fact, the VHSCF do not translate and keep the principle peak of the α relaxation at a fixed position, indicating that for these instant of times particles are still trapped in the cage. It is only at very long times that the VHSCF begin to deviate from the α relaxation character and a weak double peak starts to rise deforming the shape of the distribution, as clear for example in the VHSCF at 1 ns for $\rho = 0.95$ g/cm^3 in the central panel.

This behaviour of the correlation functions represents a decisive result in the comprehension of the microscopic origin of the Fragile to Strong Crossover. For each isochore studied, activated hopping processes begin to happen and to manifest in the VHSCF in correspondence of the transition of the supercooled liquid from the fragile MCT phase to the strong Arrhenius regime. In the light of these considerations, the FSC can be interpreted as a passage from a high density structure, where the faster dynamics and the greater

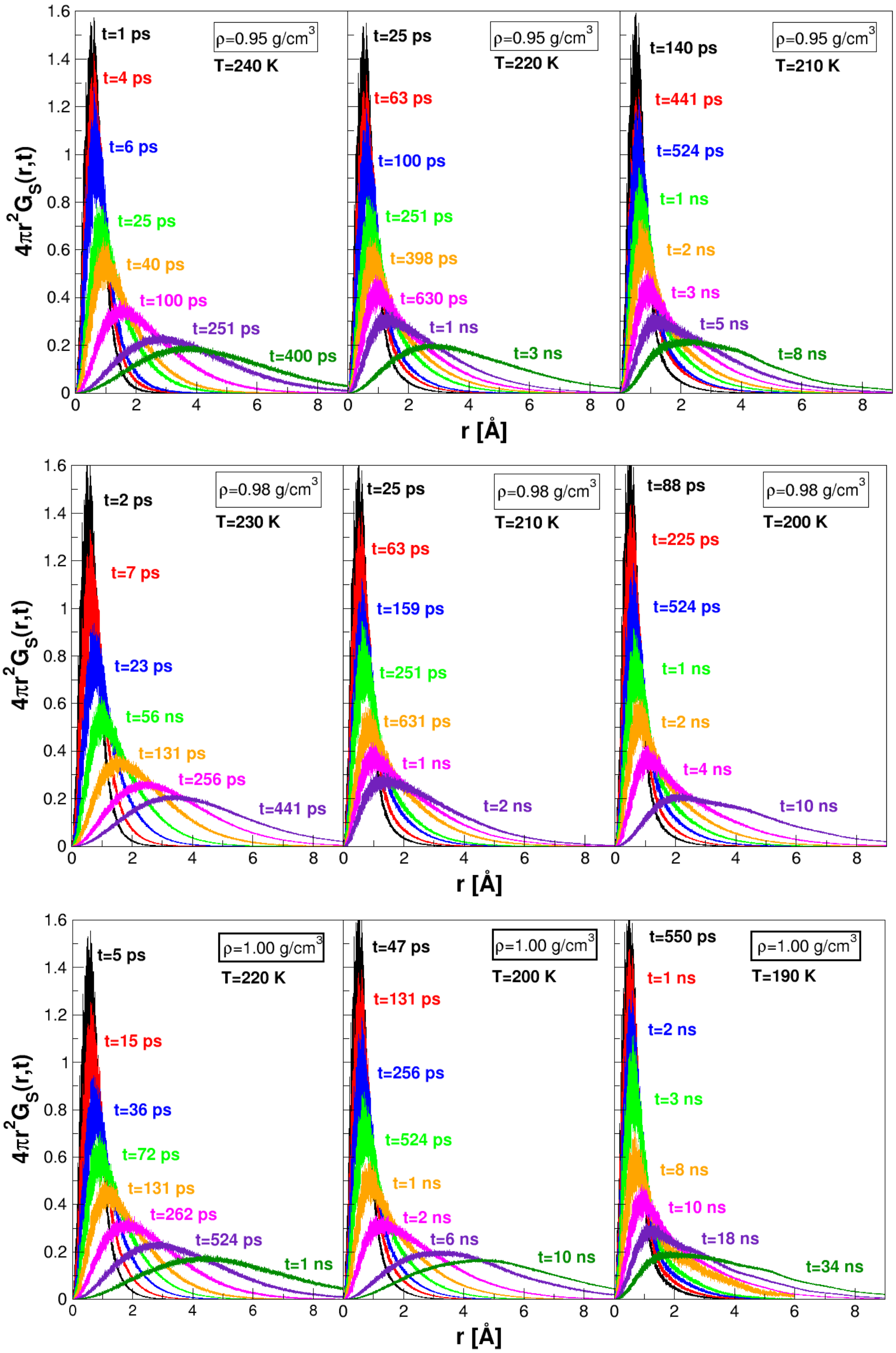

Figure 5.17: Radial Van Hove Self Correlation Function in the long time diffusive regime calculated for $\rho = 0.95$ g/cm^3, $\rho = 0.98$ g/cm^3, $\rho = 1.00$ g/cm^3. For each density, the VHSCF are shown at $T > T_L$, $T < T_L$ and $T = T_C$, with T_L and T_C the respective crossover temperature and MCT temperature reported in Table 5.2.

fluidity is guaranteed by the relaxation of the cages and the consequent Brownian diffusion of the molecules, towards an open low density configuration where the slower relaxation mechanism is determined by multiple jumps of the particles outside frozen cages.
Observing the right panels of Fig. 5.17, it is evident from the static position of the α peak that at $T = T_C$ the cages are completely arrested and hopping is the dominant relaxation process with a peak clearly visible as a shoulder in the VHSCF (see 8 ns, 10 ns and 34 ns respectively for $\rho = 0.95$ g/cm^3, $\rho = 0.98$ g/cm^3 and $\rho = 1.00$ g/cm^3).
Finally, it should be noticed that, upon lowering temperature, the VHSCF with the same height of the peak correspond to times longer and longer, indicating that the liquid capability to rearrange itself is reduced. Moreover, for each panel, comparing VHSCF with the same height of the peak for different densities Fig. 5.17 shows that the temporal range of the structural relaxation shifts towards times more and more large increasing density.
Since VHSCF associated to different thermodynamic state points with distributions quantitatively similar describe the same relative instant of time of the dynamics, last observation reveals that even if all the densities are at the same distance in temperature from their crossover temperature, the particles dynamics is slower at higher densities. Consequently, it is not the distance from the Fragile to Strong Crossover to determine the behavior of the liquid dynamics but the absolute temperatures.
The direct relation between the FSC and the occurrence of hopping phenomena discussed in this Section makes important to examine in depth the mechanism underlying these processes and, in particular, how it is influenced by the variation of temperature and density. In order to carry out this analysis the VHSCF at very long time must be calculated, as it will be shown in the following Section.

5.3.3 Hopping Phenomena and Radial Distribution Functions

The computation of the Van Hove correlators at instant of times large enough to reach a number of jump statistically significant provides a detailed insight on the evolution of hopping processes and its dependence from density and temperature. In the latest part of the dynamics, in fact, hopping peaks become more pronounced and visible allowing a systematic study of these activated phenomena. In Fig. 5.18 the VHSCF together with the oxygen-oxygen radial distribution function $G_{OO}(r)$ computed for the three densities at their Mode Coupling Temperature T_C are plotted. The $G_{OO}(r)$ are rescaled by a factor in order to make more easy the comparison.

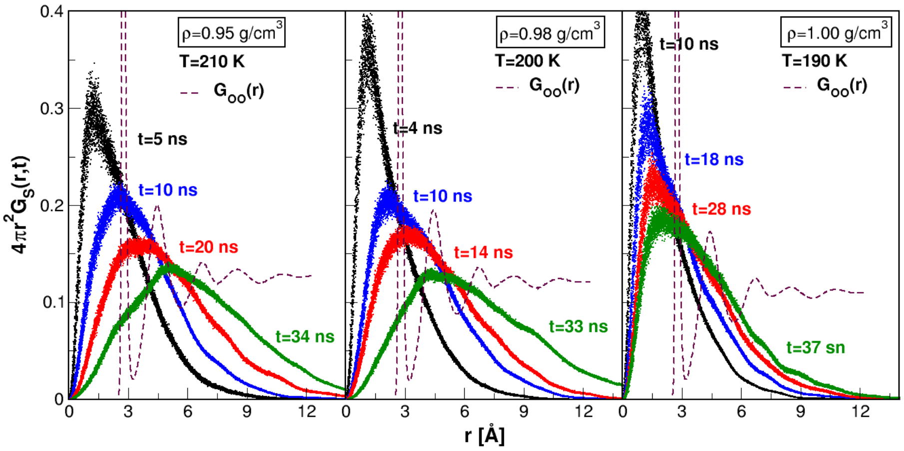

Figure 5.18: Radial Van Hove Self Correlation Function in the long time diffusive regime calculated for $\rho = 0.95$ g/cm^3, $\rho = 0.98$ g/cm^3, $\rho = 1.00$ g/cm^3. For each density, the VHSCF are shown at $T = T_C$, with T_C the respective Mode Coupling Temperature reported in Table 5.2. The $G_{OO}(r)$ at T_C are also reported and rescaled to make the comparison more clear.

Fig. 5.18 shows clearly that hopping is the dominant process at T_C and provides a picture of the evolution of hopping phenomena with time. At the earliest time, the VHSCF exhibits only one sharp peak, revealing that the particle is still trapped in the frozen cage. At greater times, this peak lowers without shifting its position and simultaneously a second evident peak rises at 2.5 Å. It is worth highlighting that the appearance of this double peak occurs in correspondence to the first peak of the $G_{OO}(r)$. Since the $G_{OO}(r)$ identifies the local structural order around each particle, the coincidence of the hopping peak with the peak of the $G_{OO}(r)$ points out that a large amount of particles have jumped out from the cage and reached the nearest region available, i.e. the first shell of the radial distribution function. Besides the second peak, multiple peaks begin to emerge in correspondence to the other peaks of the $G_{OO}(r)$. At longer times, these further peaks grow and become more pronounced, while the peak at the first shell progressively vanishes. This means that, upon increasing time, particles explore greater distances, jumping consecutively from one shell to the following. In principle, hopping peaks should increase and decrease their height remaining locked in correspondence to the peaks of the radial distribution function. Nevertheless, Fig. 5.18 displays a slight shift of the peaks of the VHSCF at very long times. This effect is probably due to a residual particle diffusion so that there is a convolution of hopping effects and the Gaussian typical

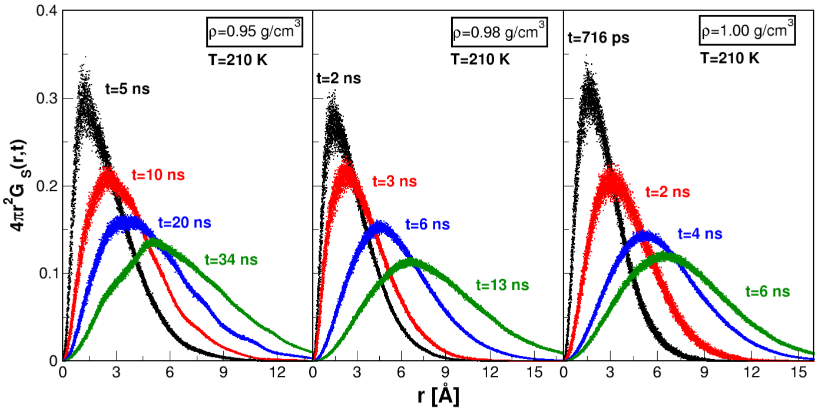

Figure 5.19: Radial Van Hove Self Correlation Function in the long time diffusive regime calculated for $\rho = 0.95$ g/cm^3, $\rho = 0.98$ g/cm^3, $\rho = 1.00$ g/cm^3 at the same temperature $T = 210$ K.

of Brownian motion.

The comparison of VHSCF with the same height of Fig. 5.18 allows to extrapolate information on the hopping rate upon varying density. At the lowest density $\rho = 0.95$ g/cm^3 and at time $t = 10$ ns (blue line) the dominant peak of the correlation function is the first hopping peak, with the "cage" peak almost completely vanished. Seeing at a quantitative similar probability distribution for $\rho = 1.00$ g/cm^3, the VHSCF at $t = 28$ ns exhibits a stage of evolution of hopping processes significantly less advanced, with a minor number of particles jumped out from the cage as evident by the main α peak and by the weakness of the multiple hopping peaks. Considering that the study of VHSCF with the same height corresponds to the analysis of same relative times in the system dynamics, the trend shown in Fig. 5.18 reveals that hopping is more favoured at lower densities and it occurs with a faster rate by decreasing density. In agreement with the remark done in the previous Section about an overall slower dynamics at lower densities, the higher hopping rate of $\rho = 0.95$ g/cm^3 is a consequence of the smaller mobility of the system at lower densities. In order to carry out a quantitative analysis of the hopping rate, it would be interesting to explore more in detail the dependence of the values of the hopping peaks as a function of time.

Besides investigating the behaviour of the VHSCF at the Mode Coupling temperature, the results of the calculation of the spatial correlators at fixed temperature upon varying density are plotted in Fig. 5.19, where the long times VHSCF for the three densities at $T = 210$ K are shown. Compatibly with the diffusion anomaly [22, 39–43], VHSCF with the same height are associated to times longer and longer decreasing density, manifesting a more arrested and slower dynamics at lower densities. Moreover, at the same temperature T=210 K there is a monotonic behaviour of the hopping strength with density, as displayed by the growing sharpness and intensity of the hopping peaks upon decreasing density. At $\rho = 0.95$ g/cm^3, hopping peaks are well visible and sharp. Upon increasing density, hopping phenomena reduce their intensity and frequency, as shown at $\rho = 0.98$ g/cm^3 and $\rho = 1.00$ g/cm^3 where the peaks are progressively smoother and less detectable. This trend is again a confirmation of the interpretation of hopping phenomena as the cause of the FSC. At fixed temperature, higher densities are farther from their respective T_C and have penetrated less in the low density region than lower densities. Indeed, increasing density isothermally corresponds to move away from the region where hopping is the dominant dynamical process and get closer to the phase where $\tau(T)$ is still well described by Eq. 5.3. The fact that hopping is favored where water is less dense directly connects to the fact that in TIP4P/2005 bulk water the FSC was found upon crossing the Widom line. This line, in fact, separates two regions where the molecular arrangement is described respectively by HDL or LDL. Therefore, upon crossing the Widom line hopping rate is higher where water is less dense and consequently the dynamics crosses from fragile to strong. Besides the dynamical properties of bulk water in the supercooled regime, interesting information on this anomalous liquid can be determined also through the study of water in confined geometries. This research field is important both for its relevance in many technological and biological processes and for the effect of confinement of making accessible regions of the supercooled phase diagram of water not achievable in the bulk state. Next Chapter will be devoted to this kind of analysis, focusing on the structural aspect of water in MCM-41 and on a possible relation between dynamics and thermodynamics also in confined systems.

6

Supercooled Confined Water in MCM-41

The study of the thermodynamic and dynamical properties of water in confinement is a research area of relevant interest in chemical, biological and physical field. The role and properties of interfacial water in contact with hydrophilic or hydrophobic surfaces is central in many biological systems, such as living cells, biopolymers, membrane and a wide variety of gel-forming substances [166]. Water has a key role also in the process of protein folding [167]. Moreover, the effect of confinement on supercooled water is to avoid crystallization at temperatures where bulk water would instantaneously convert to stable ice. The prevention of the nucleation process in confinement allows to reach values of temperatures and pressures otherwise inaccessible for bulk water, providing a chance to get information about the thermodynamics and dynamics in the *no man's land*. Therefore, the analysis of how water's interactions with substrates modify its phase diagram is particularly relevant in connection with the recent debate about the existence of a liquid-liquid critical point (LLCP) in supercooled water and it permits to understand to what extent confined water can reproduce the properties of bulk water under supercooled conditions that are quite difficult to reach in experiments for the bulk. In this chapter the results obtained from the MD simulations of water confined in MCM-41 are presented, focusing on the structural properties of water inside this confining geometry and investigating the possible existence of a relation between structural, dynamical and thermodynamic properties of this system [168].

A brief review of the phenomenology of water confined in MCM-41 is discussed in Sec. 6.1. The details of the MD simulations are given in Sec. 6.2. In Sec. 6.3 the layering effects due to the confinement and the analysis of the structural characteristics of water inside the pore is carried out through the calculation of the radial distribution functions (RDF). In Sec. 6.4 these results are further examined in term of the excess entropy, following the idea of a connection between thermodynamics and dynamics in supercooled wa-

Figure 6.1: Schematic diagram of MCM-41 materials. Figure from Ref. [176].

ter. Finally, a preliminary study on TIP4P/2005 water confined in MCM-41 is introduced in Sec. 6.5.

6.1 Phenomenology of water confined in MCM-41

A large amount of studies have been carried out to investigate the consequences of confinement on water properties [9] and the possibility to analyze its behaviour in the deep supercooled regime [169]. Experiments have shown that supercooled conditions that are inaccessible in bulk water can be reached under confinement [19, 88, 150, 170, 171]. Computationally, supercooled confined water has been investigated in the "no man's land" by several works [20, 25, 128, 129, 149].
Among the different typologies and geometries of surfaces examined in order to understand how the thermodynamic and dynamical features modificate in presence of an interacting substrate [172–175], confinement of water in hydrophilic environments has been widely explored. Within this research area, MCM-41 (Mobile Crystalline Material) ordered mesoporous material is one of the most interesting confining structures to study since on one hand it allows to investigate bulk-like water properties through the analysis of confined water thanks to its strong hydrophilicity and on the other hand it has a wide range of application in many technological processes being easily tailored in structure, composition and pore size. MCM-41 is obtained from assemblies of organic molecules that function as a template around which the silica grows and nucleates packing into the same geometrical structure of the organic array. The results is multiple hexagonal channels of amorphous SiO_2 arranged in an ordered space-filling array (see Fig. 6.1).

The thermodynamics and dynamics of supercooled water confined in MCM-41 has been dealt with both experimentally and computationally.

Evidences of a liquid-liquid phase transition ending at a point located at $P = 1.29 \pm 0.34\ kbar$ and $T = 213 \pm 3\ K$ in water confined in MCM-41 have been found in recent experiments using Neutron Diffraction technique [115] supporting the idea of the existence of a liquid-liquid critical point. Later density measurements confirm this findings [88]. Moreover, several experimental works aimed to the examination of the dynamical characterization of water confined in this hydrophilic mesoporous material have been performed [177, 178]. In particular, from Quasi-Elastic Neutron Scattering (QENS) [19, 90, 146, 148] and Nuclear Magnetic Resonance measurements [145] on water confined in MCM-41 the occurrence of a FSC was found. From the computational point of view, extensive computer simulations of SPC/E water embedded in a model of MCM-41 were performed by Gallo et al. [20, 25, 149]. It was evident from these simulations that water at contact with the hydrophilic substrate suffers a layering effect with the formation of a double layer of almost immobile molecules. This bound water resides on average in a range of circa 0.3 nm from the confining surface and it is not detected in QENS experiments. The presence of this stack of molecules bound to the surface acts as a screen from the strongly hydrophilic substrate interaction for the inner water molecule arranged in the layer close to center of the pore (free water). In fact, molecule belonging to this layer are more mobile and not involved in the formation of hydrogen bonds with the interface, and they were found to behave like bulk water upon cooling. In particular, through calculations of Intermediate Scattering Functions, it was found that the dynamics of confined free water can be interpreted in the framework of the MCT like in glass formers upon confinement [163]. Moreover the extraction of the α relaxation time from the long time decay of the SISF has showed a temperature dependence of the α relaxation time that exhibits a Fragile To Strong Crossover in agreement with experiments [20, 25] at temperature $T_L \sim 215$ K. T_L also coincides with a maximum in the specific heat indicating once again an important connection between dynamics and thermodynamics. It should be mentioned that similarities with studies on MCM-41 confined water have been observed in computer simulations on water confined in Vycor, another porous silica glass [128, 129, 179–181]. Specifically, the layering effect and the possibility to recover bulk water properties in molecules at the central inner layer have been confirmed also in this system. Experimental results on the dynamics of nanoconfined water in Vycor have been obtained also by Transient Grating Spectroscopy [182, 183] and time-resolved optical Kerr effect spectroscopy [184–186].

Next Section will be devoted to the study of the static properties of supercooled SPC/E water confined in MCM-41 simulated in Ref. [20], analysed through the calculations of the radial distributions functions. The results of the computation will be examined focusing on a possible connection between structure, thermodynamics and dynamics in this system and connecting the entropic behaviour of water inside the confining pore with its local structural order. This kind of analysis is relevant not only for a better comprehension of the effect of hydrophilic confinement on water phase diagram but it provides also an important indication of a relation between the thermodynamic and dynamical features of supercooled confined water.

6.2 Molecular Dynamics of confined water: the model

In order to investigate the structural features of water confined in MCM-41, a cylindrical hydrophilic silica pore of diameter 15 Å has been constructed analogously to Ref. [20]. The procedure for the construction of this system starts from a cubic cell of silica with a box length of 42.78 Å and a density of 0.0662 Å, where the silica atoms interact each other through the potential of Vessal et al [187] and arranged in such a way to reproduce the β cristobalite crystalline structure. The box is instantaneously melted at 6000 K and then equilibrated up to 3000 K. A rapid quenching is then performed by quickly lowering the temperature of the system with a cooling rate of 10^{13} K/s until the ambient temperature $T = 300$ K is reached and the silica is in the glassy state. The result of this procedure is therefore a cubic cell of amorphous solid silica. Inside this cell, a cylindrical pore is carved by eliminating all the atoms lying within a distance of 7.5 Å from the central axis of the cube, a value chosen to make contact with experiments [19, 146]. After the cavity was cut out and relaxed for a few picoseconds, silicon atoms with less than four oxygen neighbors are excluded from the cell. The remaining oxygen atoms can be classified in Non Bridging Oxygen atoms (NBO), where only one silicon neighbor is present and Bridging Oxygen atoms (BO) with two silicon neighbors. The NBO oxygens are saturated with hydrogen ions, acidic hydrogens (AHs), reproducing exactly the experimental saturation with hydrogen atoms of surface oxygen atoms whose valences are not saturated, done before inserting water in the sample. Finally the pore is filled with water molecules. The final block of material is composed of 1496 Silicons, 3064 Bridging Oxygens, 28 Non Bridging Oxygen, 28 acidic Hydrogens. The pore contains 380 SPC/E water molecules and during the simulation all of the atoms of the confining matrix are kept rigid. Fig. 6.2

is a snapshot of the cylindrical pore.

Interactions between water molecules are represented by the SPC/E potential [26], a three site rigid model where two sites correspond to two positively hydrogen atoms with point charge $q_H = 0.4238e$ and one site corresponds to a negative oxygen atom with $q_O = -2q_H = -0.8476e$. The OH distance is set at 0.1 nm and the angle HOH is equal to the tetrahedral angle 109.47°. SPC/E is one of the most used water potential both for the study of bulk water and water near extended surfaces. Due to its under-structured characterization of the water molecule, SPC/E water phase diagram results shifted to lower values of pressure and temperature. The Temperature of Maximum Density line has been extensively analyzed in numerous thermodynamic works [13, 74, 85, 188, 189] and it has been located by these authors approximately 20-30 K below the experimental TMD. From the dynamical point of view, pioneering studies on the dynamical behaviour of SPC/E water interpreted in terms of the Mode Coupling Theory have been introduced in Ref. [14, 15] followed by further dynamical calculations [142, 190]. Moreover, SPC/E shows diffusion coefficients in good agreement with the experimental results on water, as observed by several authors [26, 191–193] and from calculations on configurational entropy [40].

Water molecules interact with the substrate atoms using the empirical potential model by Brodka and Zerda [194], whose parameters are those used and tabulated in Ref. [20]. This potential consists of Coulomb interactions, where different fractional charges are assigned for each site of the silica molecule, and (12-6) Lennard Jones interactions between the water oxygen atoms and the BO and NBO oxygens of the surface.

Periodic boundary conditions are applied to the cubic box. The shifted force method was adopted with a cutoff at 0.9 nm for all the interactions. The size of the initial cubic box length was chosen by taking into account already the cut-off of the potentials. As in the previous work it is used a number of $N_w = 380$ water molecules to get an average density of 1.00 g/cm^3 in the inner part of the pore. Temperatures ranging from T = 300 K to T = 200 K are simulated. Simulations also on the bulk water with the SPC/E potential are performed. The Molecular Dynamics was performed with 512 molecules at the density of 1.00 g/cm^3, equivalent to the average density of the free water confined in the pore. The temperature range was from T = 300 K to T = 190 K. For bulk water the cutoff of the potentials was taken at 0.95 nm. For the Coulomb interactions the Ewald method was implemented and the Particle Mesh Ewald (PME) algorithm was used. Both for confined and bulk water a time step of 1 fs is used. The results presented here were obtained by using the parallel Gromacs package 4.5.5 [195]. The equilibration is performed by means of the Berendsden thermostat. Production runs are

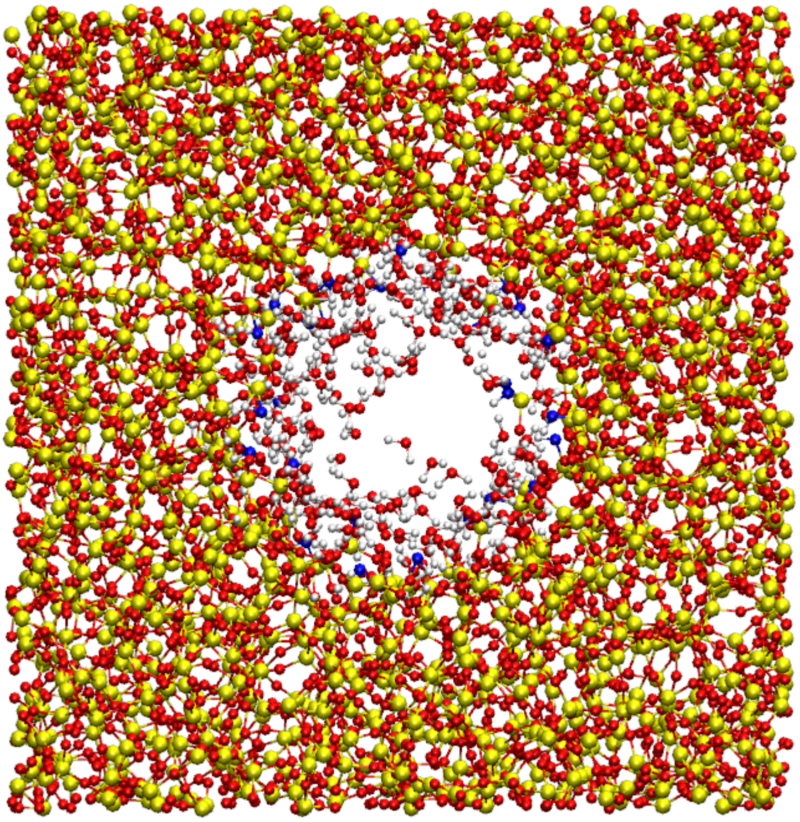

Figure 6.2: Snapshot of the silica confining pore simulated in this work. Red, yellow and blue points are respectively the oxygen, the silicon and hydrogen atoms. Few water molecules are present inside the pore.

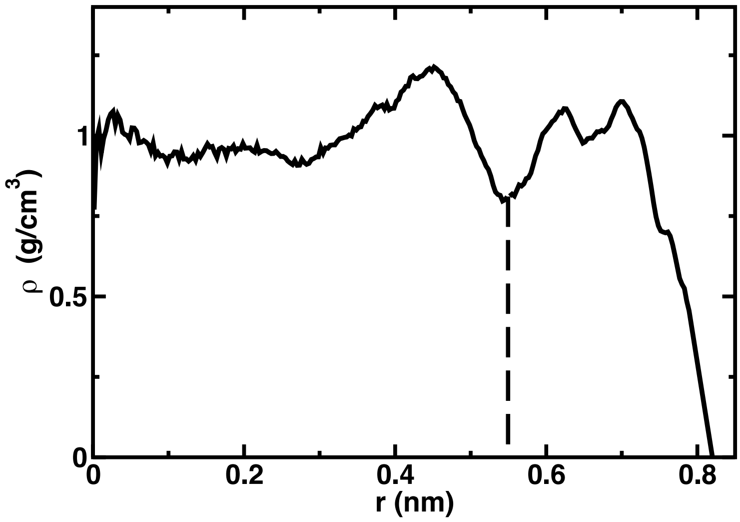

Figure 6.3: Density profile along the pore radius. Figure from Ref. [20].

done in the microcanonical ensemble.

6.3 Layering effects and structural properties of confined water

The study of structural, thermodynamic and dynamical aspects of confined water begins from the identification of which properties extracted from water in the confining structure can be considered an hint of the behaviour of bulk water. In order to answer to this question the density profile of the water molecules calculated along the pore radius for the system described above has been determined in Ref. [20] and it is plotted in Fig. 6.3. The figure shows clearly the presence of different layers. As already discussed in Ref. [20], the strong hydrophilicity of the surface causes the formation a double layer close to the internal walls of the pore. Water molecules lying on average inside this layer are subject to the attractive interactions with the substrate atoms and they form hydrogen bonds with the bridging oxygen of the silica (silanols). The commonly shown reaction mechanism for the creation of silanols predicts the formation of an HB bond between the hydrogen of water molecule and the oxygen at the vertex of the siloxane group $Si-O-Si$ and the breaking of the siloxane group itself [179, 196].

Consequently this water close to the surface has less mobility and is more dynamically restricted, showing a dramatic slowing down of the motion with a subdiffusive regime at long times already at room temperature [149]. On contrary, water in the cylindrical region $0 < R < 0.55$ nm, the free water, presents features similar to bulk water. The bound water layer, in fact, acts as a screen from the effect of interactions with the substrate and leaves water in the inner core free to move within the liquid without constraints.

The study discussed below is centered on analysis of molecules in the free water region, whose characteristics in structure and dynamics are analogous to simple bulk water. In particular the radial distribution functions have been calculated for the free water molecules. It should be noticed that the computation of RDF in confining rigid matrices is not a straightforward task. RDF of confined particles, in fact, suffer finite volume effects and distortions due to the particular geometry of the confining structure. The radial distribution function is, by definition, a measure of the deviation of local density from the value it would have if particles were non interacting. Following this definition, the spherical RDF can be written explicitly as:

$$g_{ab}^{(s)}(r) = \frac{n_{ab}^{(2)}}{n_b \cdot \Delta v(r)} \tag{6.1}$$

where $n_{ab}^{(2)}$ represents the average number of atoms (or sites) b that are found in a spherical shell at distance r from an atom (or site) a, $n_b = N_b/V_c$ is the average density of the atoms (or sites) b in the cell of volume V_c and $\Delta v(r)$ is the volume of the spherical shell. The problem with Eq. 6.1 lies in the normalization $n_b = N_b/V_c$ that implicitly supposes the ideal gas distribution of non interacting particles to be homogeneous in all directions. While this hypothesis is reasonable in systems with periodic boundary conditions in all the directions, confined systems have to be considered separately, because of excluded volume effects and the dependence of the global symmetry on the specific geometry of the confining matrix. For this reason, the correct normalization of the RDF of free water confined in MCM-41 is the uniform radial distribution function of the correspondent ideal gas confined inside a cylindrical rough surface. It follows that this distribution is the product of an homogeneous function $g_u(r)$ corresponding to the distribution of non interacting particles inside a confined cell of simulation with cylindrical geometry and a correction factor $f_c(r)$ that takes into account the irregularity of the internal wall of the pore and the presence of the periodic boundary condition on z axis of the pore. Therefore, the complete free water RDF containing all the corrections due to the confinement in MCM-41 can be evaluated as:

$$g_{ab}(r) = \frac{g_{ab}^{(s)}(r)}{f_c(r) \cdot g_u(r)} \tag{6.2}$$

where, of course, $g_{ab}(r)$ would be equal to $g_{ab}^{(s)}(r)$ in the normal bulk case. Since the function $g_u(r)$ expresses the correction coming from the cylindrical geometry of the system, it is reasonable approximate $g_u(r)$ with the Fourier transform of a cylindrical form factor, as already done in Ref. [180] for extracting the RDF from simulation of water in Vycor:

$$g_u(r) = \frac{V_{cyl}}{(2\pi)^3} \int d^3Q P_{cyl}(Q) e^{iQ\cdot r} \tag{6.3}$$

with V_{cyl} the volume of the cylinder and

$$P_{cyl}(Q) = \int_0^1 d\mu \left[j_0 \left(\frac{\mu Q L}{2} \right) \right]^2 \left[\frac{2 j_1 (Q R_c \sqrt{1-\mu^2})}{Q R_c \sqrt{1-\mu^2}} \right]^2 \tag{6.4}$$

where $j_n(x)$ are the Bessel's functions of order n, R_c is the radius of the cylinder and L its height. By imposing that the RDF must go asymptotically to oscillate around the constant unity value it is possible to find that $f_c(r)$ is an asymptotic linear correction weakly dependent on r. In Fig. 6.4 we report as examples the $g_{OO}^{(s)}(r)$ as obtained from the simulation, the correction factors and the final $g_{OO}(r)$ for $T = 300$ K and $T = 220$ K.
We computed the site-site RDF for the free water at decreasing temperatures from $T = 300$ K down to $T = 200$ K. In Fig. 6.5, Fig. 6.6, Fig. 6.7 and Fig. 6.8 we show $g_{OO}(r)$, $g_{OH}(r)$ and $g_{HH}(r)$ for few chosen temperatures as obtained after the corrections. We compare with the same functions of bulk SPC/E water at 1 g/cm^3.
Fig. 6.5 displays that the behaviour of the Oxygen-Oxygen Radial Distribution Functions of free water upon decreasing temperature is similar to the trend of bulk water, reported in the inset of the figure. Overall, all the peaks and the minima of the RDF become sharper and sharper by lowering temperature, with the values of maxima and minima that increase and decrease respectively. This behaviour is compatible with a local arrangement of free water molecules more tetrahedrally ordered and structured in multiple shells at low temperatures also in confinement, as it happens in bulk. These feature is present also in the experimental bulk RDF upon cooling [197, 198]. The position of the peaks remains unaltered by cooling the system, differently from the first minimum whose position shifts towards lower distances as in the bulk.

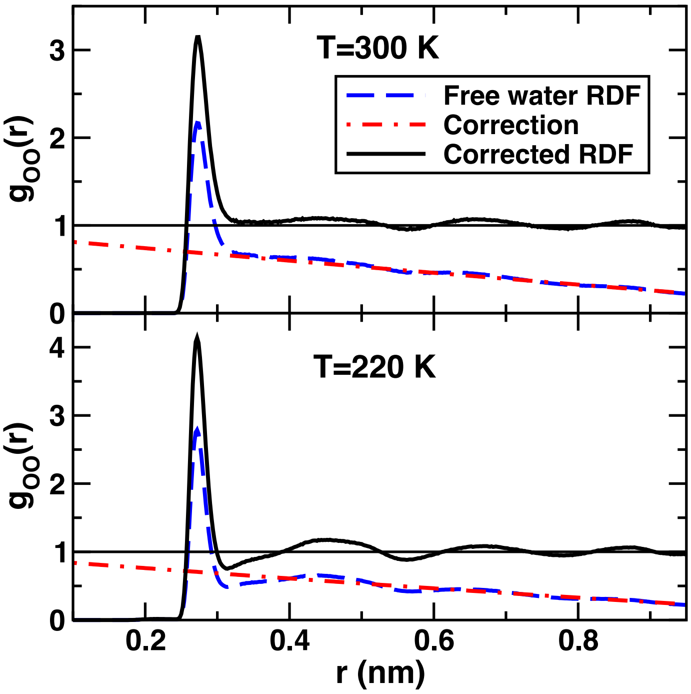

Figure 6.4: Example of oxygen-oxygen RDF of free water. The black line represents the final result after the corrections of the RDF obtained from simulation (blue long dashed line). The red point dashed curve is the function used to perform the correction, see Eq. 6.2. Upper panel $T = 300$ K, lower panel $T = 220$ K.

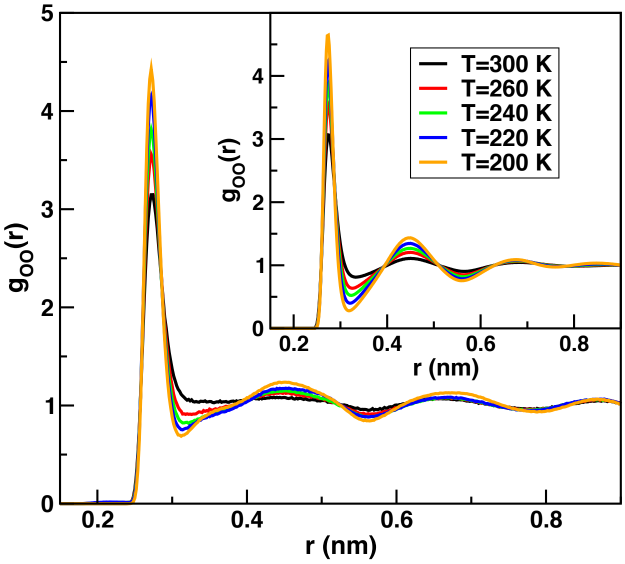

Figure 6.5: Oxygen-oxygen RDF, free water in the main panel, bulk water in the inset at the temperatures indicated in the caption.

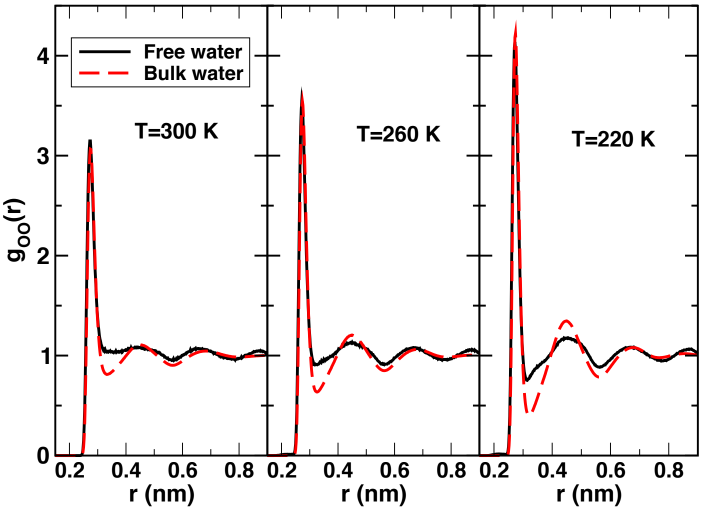

Figure 6.6: Comparison of the oxygen-oxygen RDF of free water with bulk water at decreasing temperature as indicated in the panels.

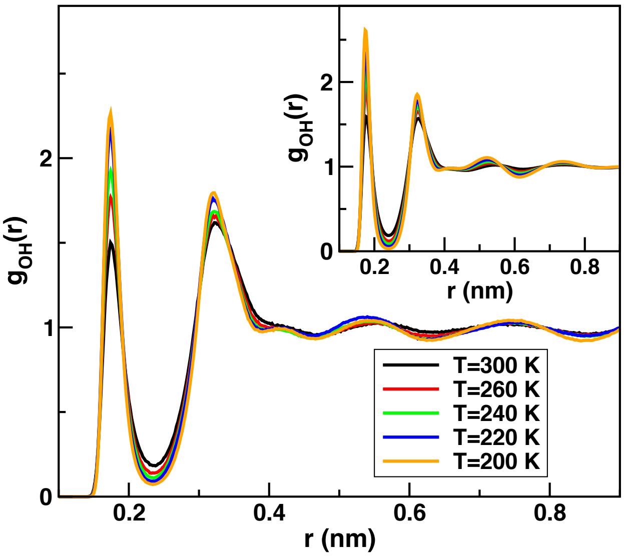

Figure 6.7: Oxygen-hydrogen RDF, free water in the main panel, bulk water in the inset at the temperatures indicated in the caption.

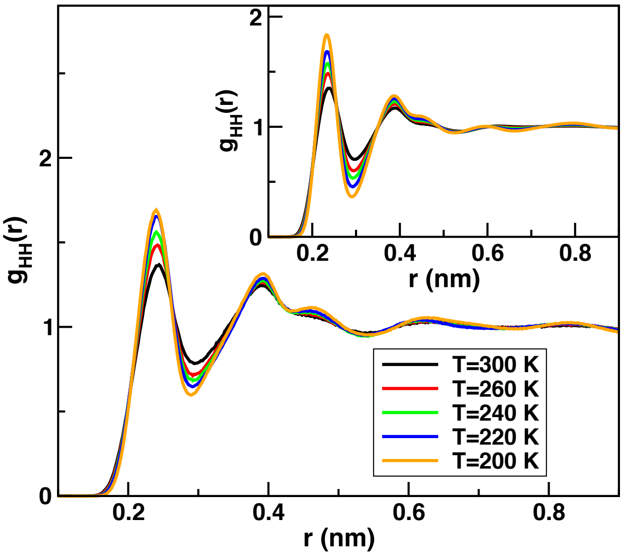

Figure 6.8: Hydrogen-hydrogen RDF, free water in the main panel, bulk water in the inset at the temperatures indicated in the caption.

By comparing the $g_{OO}(r)$ of the confined free water in Fig. 6.5 with the $g_{OO}(r)$ of the bulk, similarities and differences are found, as it is more clear from Fig. 6.6. The positions of the peaks are not modified by the confinement and the shells are approximately located around the same distance in bulk and free water. The height of the first peak for free water is sharp and high as bulk water. Nevertheless, the first minimum of the RDF of free water becomes shallower and fills in upon confinement in analogy with the case of confinement in Vycor glass [180]. The effect here however is more pronounced than for the Vycor case. The broadening of the first minimum reflects clearly a greater penetration of water molecules between the second and the first shell as a consequence of confinement. It should be noticed that the differences between the $g_{OO}(r)$ of confined free water and bulk water progressively disappear at larger distances, indicating that the impact of confinement on water structure tends to be stronger and evident in the local short range order.

The main features of $g_{OH}(r)$ and $g_{HH}(r)$, reported in Fig. 6.7 and Fig. 6.8 respectively are very similar to bulk water. The hydrophilic interaction induces a strong distortion of the layer of water close to the substrate but it perturbs less the hydrogen bond network in the middle of the pore. In fact, in Fig. 6.7 it is evident that there is practically not change in the OH structure. On contrary, the first minimum of the $g_{HH}(r)$ fills in as in the case of the $g_{OO}(r)$. This means that even if the OO and the HH distributions show slight differences in confinement, with a general filling of the space between the relative shells, the rearrangement of the oxygens and the hydrogens in confinement occurs in such a way the presence and the structure of the HB network between the water molecules is preserved.

Further information on how the local structural order of supercooled water is influenced by the confinement are provided by the calculation of the *coordination number* n_{OO} of the first shell of the $g_{OO}(r)$ defined as:

$$n_{OO} = \frac{N_O}{V} \int_0^{r_1} 4\pi r^2 g_{OO}(r) dr \qquad (6.5)$$

where N_O is the total number of the oxygen atoms in the system, V is the total volume of the pore simulated and r_1 is the radius of the first shell coinciding with the position of the first minimum. Fig. 6.9 and Fig. 6.10 show the values of the coordination number by varying temperature both in bulk and confined free water.

Both the figures display a similar behaviour. The number of oxygen atoms localized up to a distance r_1 from the center of the pore decreases upon cooling the system. This trend means that even if first peak of the oxygen radial distribution function becomes sharper and separated from the second one

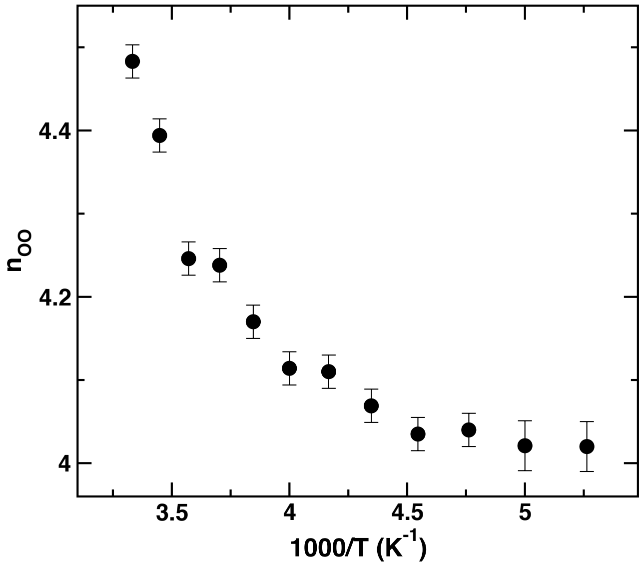

Figure 6.9: First coordination number of the oxygens as function of inverse temperature for bulk water. The error bars are due to the uncertainty in locating the first minimum.

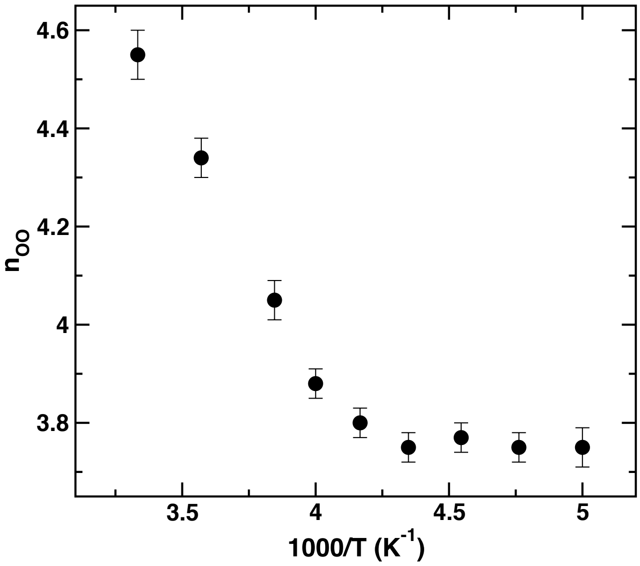

Figure 6.10: First coordination number of the oxygens as function of inverse temperature for free water in MCM-41. The error bars are due to the uncertainty in locating the first minimum.

by lowering temperature, the simultaneous decrease of the first minimum and movement of its position at shorter distances leads to an overall decrease of coordination number of the first shell. Moreover, around $T = 220$ K for bulk and free water n_{OO} seems to asymptotically saturate towards an almost constant number. This behaviour is a clear sign of the progressive crossover of the liquid structure from a high density, fluid phase where particles have more mobility towards a low density, ordered state where molecules are more localized and less free to move. Remembering the interpretation of the Fragile to Strong Crossover as a dynamical transition from a dense disordered phase to a more frozen and open state, the differences observed in the local structure of the confined free water by varying temperature are once again an important evidence of a connection between the static features and the dynamical aspects of the system, already discussed for bulk water in TIP4P/2005 in the previous Chapter. In the next Section, a possible relation between the changes in the structural properties of the bulk-like water confined in MCM-41 and the occurrence of the FSC will be investigated introducing the concept of excess entropy.

6.4 Two body entropy and the fragile to strong crossover

Gallo et al. performed Molecular Dynamics Simulations in Ref. [20, 25] on the same model studied in this work, analysing the dynamical behaviour both of the free and bound water confined in MCM-41. The results from these analysis illustrated that the dynamics of the bound water was almost completely frozen because of the multiple hydrogen bonds formed between the water molecules and the molecule of the substrate. On the contrary, through calculations of the Intermediate Scattering Functions, free water molecules revealed to behave dynamically à la Mode Coupling, with a temperature dependence of the structural relaxation time τ in the mild supercooled region perfectly in agreement with the fragile MCT power law:

$$\tau^{-1} \sim (T - T_C)^{\gamma} \tag{6.6}$$

with T_C the MCT temperature of ideal glass transition and γ power law exponent. Moreover, as discussed also for bulk TIP4P/2005 water in the previous Chapter, upon decreasing temperature towards the asymptotic temperature T_C a FSC from the power law of Eq. 6.6 to the strong Arrhenius exponential law:

$$\tau \sim e^{E_a/k_B T} \tag{6.7}$$

was observed. Values of the MCT temperature T_C and FSC temperature T_L extracted from these simulations were respectively $T_C = 195$ K and $T_L = 215$ K [20]. For comparison, from calculations of bulk SPC/E water of this work it has been found $T_C = 200$ K and a FSC at a temperature $T_L \sim 215$ K.

As already mentioned in the previous Section, dynamics and thermodynamics of supercooled water are not two separate aspects of the liquid but they are two sides extremely connected and coupled of the same system. It has been seen in previous Chapters that an important relation between thermodynamics and dynamics is established by the occurrence of the FSC at the Widom Line, proved experimentally and computationally. Therefore, provided the similarities between the MCM-41 confined free water investigated in this work and bulk water, it is reasonable to hypothesized an interdependence between the structural relaxation time and the thermodynamic functions of water in the inner layer of the pore. In particular, τ can be supposed to be connected to the available configurations in the energy landscape. According to this view, the decrease of the water diffusion coefficient upon supercooling is due to a decrease in the number of configurations accessible for the system. Since from the microscopic point of view entropy is a measure of the number of states available in the phase space, the structural relaxation of supercooled water can be written in term of its entropy, whose major contribution at low temperatures comes from the excess entropy S_{exc}. S_{exc} is defined by subtracting from the liquid entropy its ideal-gas term:

$$S_{exc} = S - S_{id} \tag{6.8}$$

Being S_{id} representative of the thermal and kinetic contribution to the total entropy, S_{exc} is determined by particle interaction and becomes the dominant term by cooling the system. Following the idea discussed for instance by Y. Rosenfeld [199], a measure of the decrease of the accessible states can be expressed in term of an exponential of the excess entropy through the empirical formula:

$$\frac{1}{\tau} = A e^{\alpha s_{exc}/k_B} \tag{6.9}$$

where $s_{exc} = S_{exc}/N$ is the excess entropy per particle. Eq. 6.9 represents a clear connection between the temporal dynamical properties of the system and its thermodynamic state. The excess entropy per particle s_{exc} can be expanded in terms of n-body terms s_n calculated by integration on the n-particle distribution functions $g^n(r_1, ..., r_n)$ [200]. Several theoretical and computational works have proved the two-body entropy s_2 to be a relevant quantity capturing the thermodynamic, dynamic and structural anomalies

of water [201–205] and to be a reasonable approximation of the excess entropy for different models of liquids [200, 206, 207].
s_2 can be derived from the radial distribution function $g(r)$ as follows:

$$s_2 = -2\pi\rho k_B \int \left\{ g_{OO}(r) ln \left[g_{OO}(r) \right] - \left[g_{OO}(r) - 1 \right] \right\} r^2 dr \qquad (6.10)$$

It should be underlined that only the contribution of the oxygen-oxygen correlation is considered since this study is centered on the translational part of the dynamics and the center of mass of the molecule can be identified with the oxygen.
Eq. 6.9 states that the temperature dependence of the structural relaxation time is directly related to the temperature variation of the numbers of configuration available to the liquid, expressed by the excess entropy. This means that the power law divergence predicted by MCT upon approaching the MCT temperature T_C and the FSC of the α relaxation time reflects into an analogous behaviour of the excess entropy. By inverting Eq. 6.9 a logarithmic divergence can be supposed for the two body entropy by getting close to T_C

$$s_2/k_B = a + b \ln \left(T - T_C \right) \qquad (6.11)$$

This relation between the TBEE and the structural relaxation time was already verified in bulk TIP4P water [208].
In order to test the validity of this hypothesis, the TBEE s_2 has been calculated from the radial distribution function for confined free water and for SPC/E bulk water at density 1.00 g/cm^3 at several temperatures.
The s_2 calculated from the bulk RDF discussed in the previous Section and the fit to the equation 6.11 are shown in Fig. 6.11. The fit is performed with the value of $T_C = 200$ K.
For confined SPC/E free water the s_2 calculated from the RDF of the previous Section is shown in Fig. 6.12 with the fit performed with $T_C = 195$ K. In both the Figures, data exhibit a good agreement with the logarithmic behaviour of Eq. 6.11 in the high temperature range, where the temperature dependence of the excess entropy is well fitted by Eq. 6.11. This confirms one again the predictions of Mode Coupling Theory in the mild supercooled regime. Moreover both bulk and confined water manifest a deviation from the fragile MCT character at temperature roughly coincidence with the FSC temperature extracted from the relaxation time, supporting the idea of a relation between dynamics and thermodynamics. It follows that the analysis of the excess entropy and the comparison between bulk and confinement lead to the conclusion that also in a cylindrical confined geometries water in the central layer of the MCM-41 pore presents bulk-like features and corroborates the hypothesis of a connection between thermodynamic and

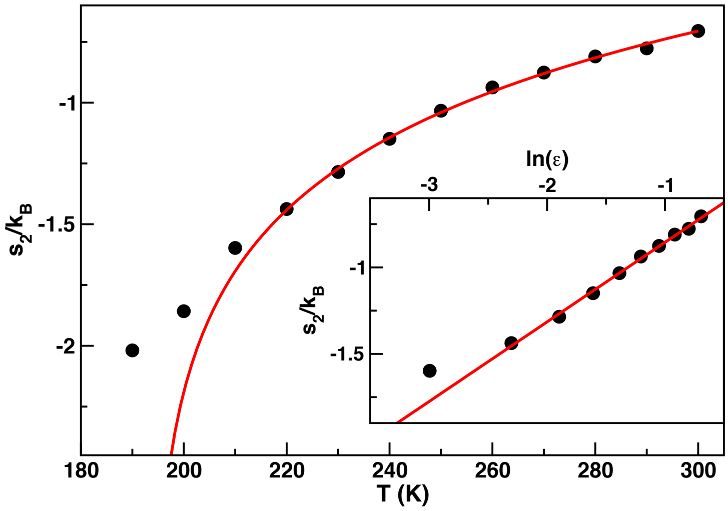

Figure 6.11: Two body entropy of bulk SPC/E water at density 1.00 g/cm^3 as function of temperature. In the inset the same function reported versus $ln\,(\epsilon)$ with $\epsilon = (T - T_C)\,/T_C$. In both panels the red curve is the fit to Eq. 6.11.

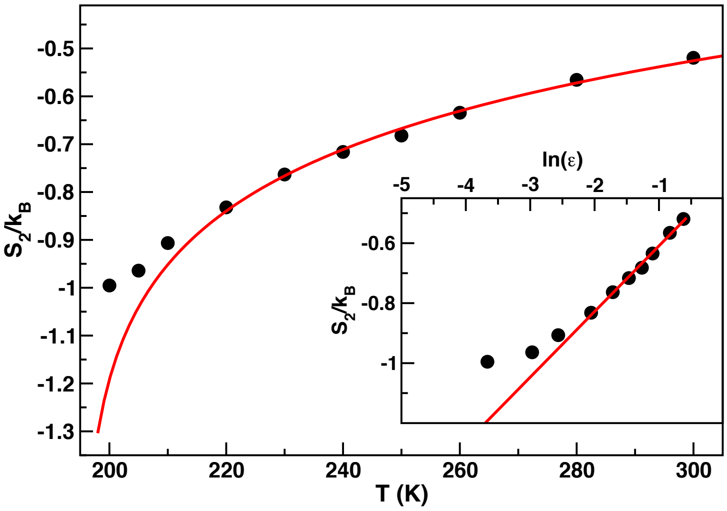

Figure 6.12: Two body entropy of confined SPC/E free water at full hydration as function of temperature. In the inset the same function reported versus $ln\left(\epsilon\right)$ with $\epsilon = \left(T - T_C\right)/T_C$. In both panels the red curve is the fit to Eq. 6.11.

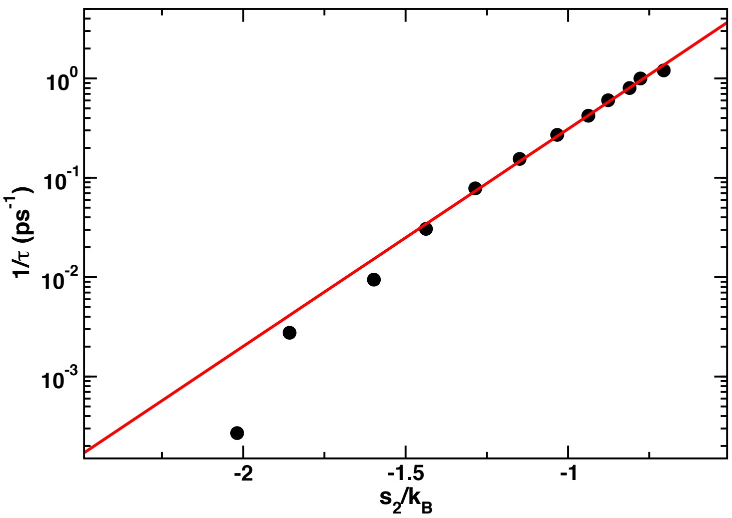

Figure 6.13: Inverse of the α relaxation time as function of the two body entropy s_2 for bulk water. The red curve is the fit to Eq. 6.9.

dynamical aspects of the supercooled phase diagram. For what concerns the coordination number discussed in the previous Section, it should be evidenced that the temperature at which n_{OO} appeared to go asymptotically towards a constant value coincides approximately with the crossover temperature of the excess entropy, validating the previous conjecture of this slow varying arrangement of the molecules with temperature as related to the dynamic transition of the system towards a low density, structured and ordered phase that occurs at the crossing of the Widom Line. To complete the test of this connection the values of τ are reported as function of s_2 at the corresponding temperature in Fig. 6.13 for bulk water and in Fig. 6.14 for water confined in MCM-41.

Data are well fitted by the exponential prediction of Eq. 6.9 and this prediction is very well satisfied in the MCT regime for both bulk and confined free water. Deviations start to show up at the FSC.

In order to estimate the importance of the total excess entropy in the thermodynamic and dynamic behaviour of supercooled water, thermodynamic calculations of s_{exc} are currently being investigated.

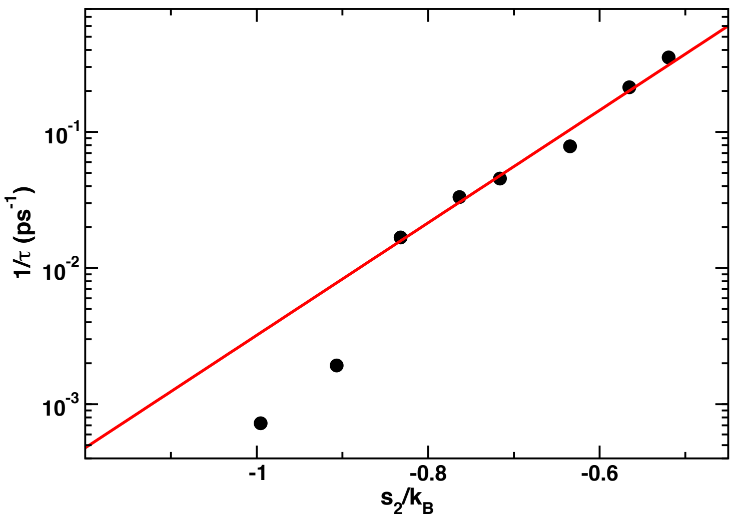

Figure 6.14: Inverse of the α relaxation time as function of the two body entropy s_2 for confined free water. The red curve is the fit to Eq. 6.9.

6.5 Confined TIP4P/2005 water: Preliminary results

In this section the results obtained from a preliminary analysis of the MD simulations performed on the same system described above but with TIP4P/2005 water potential are presented. The hydration level is lower than SPC/E, with a total number of molecules equal to 294. Fig. 6.15 exhibits the density profile for several temperatures in a range spanned from 300 K to 240 K together with the density profile of the silicon atoms. Also for TIP4P/2005 a clear separation between the external layer of water molecules bound to the substrate molecules and the so called free water can be recognized. The position of the peaks of the density profile remains approximately the same upon decreasing temperature while the local order becomes progressively more structured as evident from the increasing sharpness of the crests. A slight and unavoidable penetration of water molecule is observed. Analogously to SPC/E, the radial distribution functions for the free water layer have been calculated and corrected with the same scheme explained in the previous Section. Results from this correction on the oxygen-oxygen RDF for two temperatures T=300 K and T=240 K

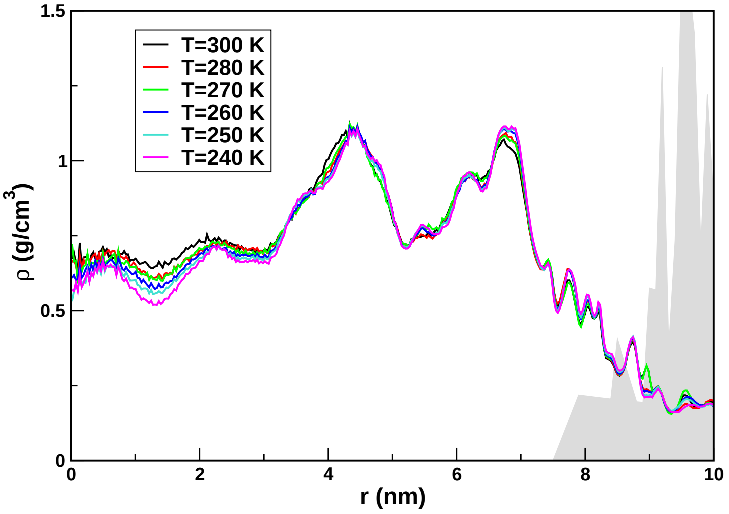

Figure 6.15: Density profile along the pore radius for several temperatures. The grey region represents the density profile of the silicon atoms of the pore.

are shown in Fig. 6.16. The evolution with temperature of the OO-RDF is also presented in Fig. 6.17. Also for TIP4P/2005 the free water confined inside the pore has smoother maxima and minima of the RDF with respect to the bulk, indicating a less ordered and regular structure and a greater infiltration of water molecules between the shells. This means that the effect of confinement of filling up the space between the shells is independent from the particular water potential used. A better view of the differences in the local arrangement between bulk and confined water is given in Fig. 6.18, where a comparison of the corrected oxygen-oxygen RDF and the correspondent bulk oxygen-oxygen RDF at density $\rho = 0.95$ g/cm^3 are displayed.

This figure shows a trend similar to the one found for SPC/E. In particular the position of the first peak remains unaltered for the three temperatures between bulk and free water. It should be noticed, finally, that in correspondence of the third peak a slight shift towards shorter distance with respect to the bulk is observed. This displacement is a sign of a decline of the tetrahedral order in the long range due to the confinement. These and other results will be examined in the future in order to determine general properties of water inside MCM-41 independently from the detailed of the

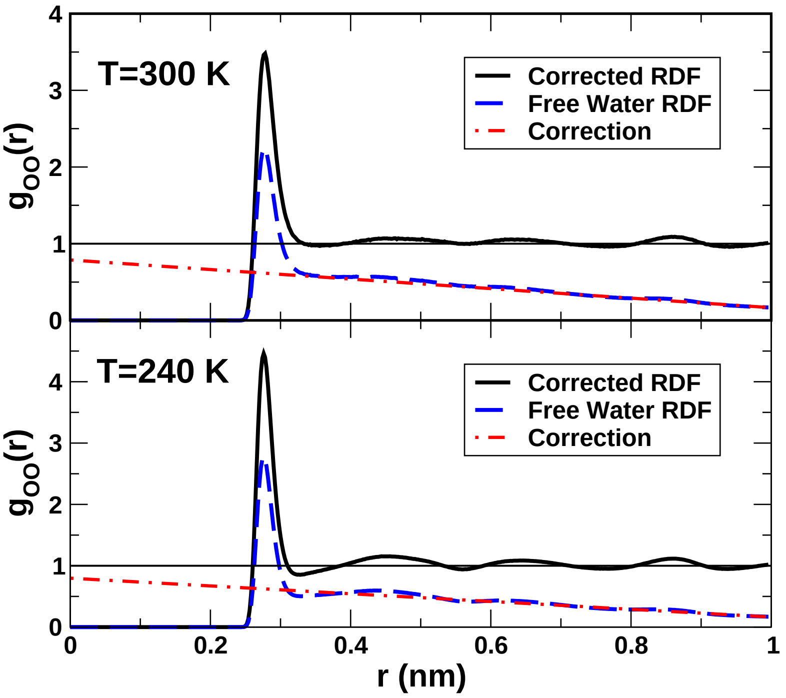

Figure 6.16: Example of oxygen-oxygen RDF of free water. The black line represents the final result after the corrections of the RDF obtained from simulation (blue long dashed line). The red point dashed curve is the function used to perform the correction, see Eq. 6.2. Upper panel $T = 300$ K, lower panel $T = 240$ K.

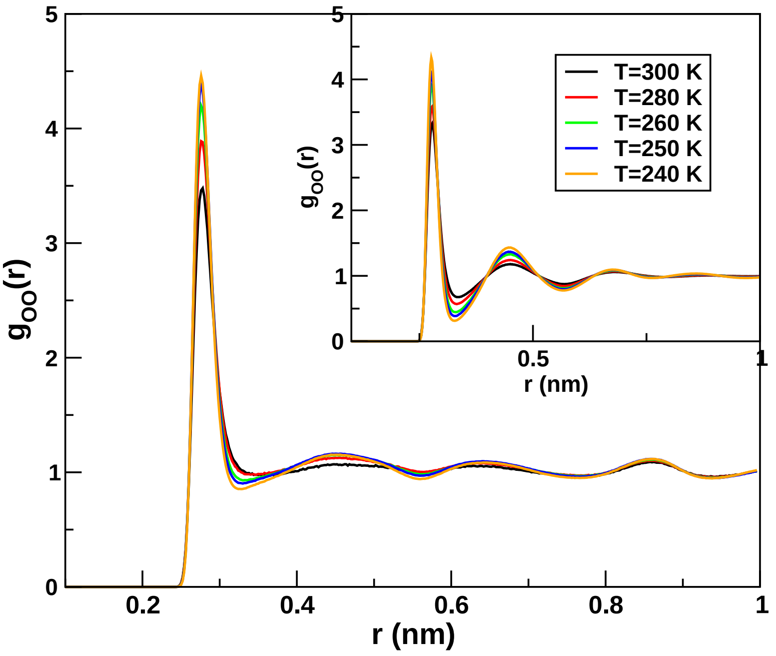

Figure 6.17: Oxygen-oxygen RDF, free water in the main panel, bulk water in the inset at the temperatures indicated in the caption.

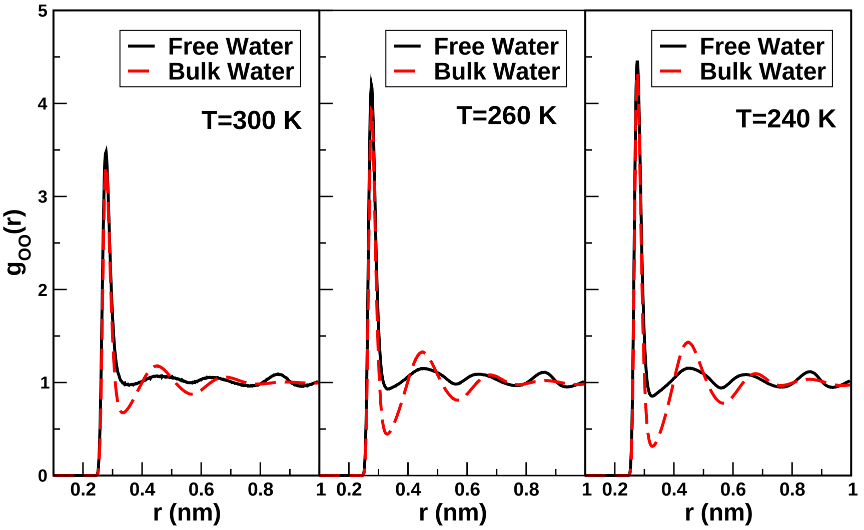

Figure 6.18: Comparison of the oxygen-oxygen RDF of free water with bulk water at decreasing temperature as indicated in the panels.

simulation.

7

Conclusions

The goal of this PhD Thesis has been the study of the dynamical properties of bulk water first of all in the mild and deep supercooled regime. Results on the Self Intermediate Scattering Functions and Van Hove Self Correlation Functions have allowed to draw an exhaustive picture of the structural relaxation mechanism in supercooled bulk water both from the macroscopic and microscopic point of view.

In particular, in the first part of this PhD Thesis the slow dynamics upon supercooling of TIP4P/2005 water and its connection with the thermodynamic properties determined by the presence of a LLCP, already found for this model [23] has been analysed. TIP4P/2005 is considered one of the best all atoms classic rigid potential for water, being able to reproduce remarkably well many experimental features of this liquid, like the TMD line, the complex ices phase diagram and the experimental temperature dependence of the diffusivity [24].

Results from MD simulations performed in the mild supercooled region show that the TIP4P/2005 water follows the MCT predictions remarkably well. Particle motion is dominated by the so-called cage effect determining a double relaxation regime with the long time decay described by a stretched exponential. Upon further supercooling hopping processes start to affect the structural relaxation, as in other glass formers and cause the deviation from the fragile (MCT) behaviour toward a strong Arrhenius behaviour of the liquid. Similar to what has been found for other potentials, this fragile to strong crossover takes place at the crossing of the Widom line individuated by the calculations of the maxima of the specific heat in the single phase region upon approaching the LLCP.

This result is a further confirmation that in water the dynamics is intimately related to thermodynamics in all its very complex phase diagram, as made evident also from the recent results on its supercritical phase [209, 210] where a dynamic crossover from a gas-like to a liquid-like phase has been found upon crossing the WL of the liquid-gas critical point.

The transition of the system from a high temperature fragile character to a low temperature Arrhenius strong character can be interpreted in term of the increase of the hopping rate by lowering temperature, that become progressively the dominant mechanism of relaxation upon approaching the Mode Coupling Temperature

Due to the clear evidence of the hopping effects in determining the activated dynamics just above the asymptotic ideal MCT transition temperature [164] MD simulations on TIP4P/2005 have been further explored more in detail, in order to verify the microscopic origin of the FSC and investigate quantitatively and qualitatively how hopping phenomena appear and modify the relaxation mechanism of bulk water at different densities. For that purpose, the dynamical behaviour of supercooled TIP4P/2005 water has been examined through the computation of Van Hove Self Correlation Functions (VHSCF) for the three different densities investigated focusing on the connections between the hopping phenomena and the Fragile to Strong Crossover. The results from this analsys show that in the mild supercooled region the dynamics of TIP4P/2005 exhibits the typical cage effect of supercooled liquids. As function of time after the initial ballistic regime, the intermediate transient cage regime takes place before the final diffusive regime. The VHSCF in the cage regime suggest a possible harmonic character of the confining potential with an elastic constant stronger and stronger at lower temperatures and densities. For all the densities investigated, at temperatures near the respective Mode Coupling temperature T_C the VHSCF deform progressively their diffusive shape and by crossing the FSC a weak hopping peak arises and becomes more evident and sharp at lower temperatures. This phenomenon is a clear evidence of the connection between the FSC and the occurrence of hopping processes as the dominant relaxation process in deep supercooled regime. At T_C the VHSCF show that structural relaxation through the cage breaking is not more possible and activated hopping processes dominate the dynamics. When this happens multiple peaks appear in correspondence of the peaks of the oxygen-oxygen radial distribution functions revealing that particle escapes from the cage and jumps consecutively from one shell to another at greater distance. Compared to the Lennard Jones Binary Mixtures [164, 211, 212], the hopping peaks in TIP4P/2005 are less clear and visible and this is probably due to the molecular character of liquid water. Moreover, an analysis in density shows that hopping is more favored at lower densities, where the system is more structurally ordered and has less mobility. To conclude all the aspects of the cage regime and hopping phenomena found in MD simulations on TIP4P/2005 bulk water confirm hopping as the cause of the FSC in water and link its raise to the crossing of the Widom line, being hopping more favored where water is less dense. These results confirm the interpretation of the LDL phase of water as a state more ordered and structured where the strong character of the liquid derives from the dominance of hopping processes in the structural relaxation mechanism. HDL side, instead, is the phase where water is more fluid and has more mobility thanks to the thermal fluctuations of the system that allow the cage to dissolve and particles to diffuse with Brownian motion. The Widom line separates therefore two regimes with different structures and dynamical relaxation processes.

The interpretation of the anomalies of supercooled water is still the matter of a vivid debate [9]. We expect that improved experimental techniques would be able to shed more light on water in approaching its glass transition and to test the theoretical approaches and hypothesis.

The presence of a connection between dynamics and thermodynamics open the doors to important questions on the deep meaning of these two aspects of the same system.

Besides the analysis of bulk water, the properties of supercooled water and the possible existence of a connection between dynamics and thermodynamics has been explore also in confinement. In particular MD simulations have been performed on SPC/E water confined in a silica pore representing the MCM-41 material, a study complement to a previous work on the dynamical properties [20].

The role and properties of confined water is a subject of major interest in many fields of research in physics and chemistry. From the point of view of understanding the anomalies of water the interest resides in the possibility of observing liquid water in a thermodynamic region that is more easily accessible in experiment when water is confined. How much the properties of water change under confinement or in contact with substrate is still matter of debate and in this respect computer simulation can give new microscopic insights. Previous works [20, 25] have shown that water in MCM-41 exhibits a layered structure that makes possible the extraction of useful information on the structure and dynamics of supercooled water. Even if the external double layer of water close to the surface of the pore appears to be strongly affected by the interactions with the substrate, the inner free water molecules show a bulk-like behaviour. Upon supercooling the dynamics of the free water can be described in terms of MCT and that a fragile to strong crossover takes place similar to the bulk phase.

The site radial distribution functions for the free water with the use of the finite volume corrections have been derived in the second part of the PhD project. By comparing the RDF of the free water upon supercooling with the RDF of bulk water at the same temperatures the structure of the free water analyzed through the calculation of the oxygens-oxygens, the hydrogen-oxygen and the hydrogen-hydrogen radial distribution functions stay nearly unaltered except an overall filling up of the space between the first shells. The trend in temperature of the RDF present, as in bulk, a progressive sharpening of the maxima and minima of the $g(r)$. Most importantly, although the slight differences between the $g_{OO}(r)$ and $g_{HH}(r)$ of the bulk and confined free water, the hydrogen bond structure results totally preserved, indicating that the general rearrangement of water molecules in the central part of the pore happens in order to preserve the hydrogen bond in spite of the perturbation of the HB network.

As already evidenced in Section 5.2.3, also confined free water presents an important connection between dynamical and thermodynamical properties, showing a relation between the structural relaxation times and the excess entropy of the system. Following the idea of an interplay between the relaxation mechanism and the number of configuration available to the system,in fact, a logarithmic asymptotic divergence to the MCT T_C of the excess entropy extracted from the RDF at several temperatures has been found. Moreover signature of a deviation from this logarithmic trend occurs in correspondence of the FSC temperature previously determined in Ref. [20] and Ref.[25]. An analogous signature of the FSC in the two body entropy appeared in bulk TIP4P [208].

These results finally show that also in confined water, similar to the bulk, thermodynamic and structural properties are strictly related and that the two body entropy, that can be calculated for the RDFs, marks with good approximation the crossover from the fragile to the strong regime. Preliminary results on TIP4P/2005 water confined in MCM-41 show similarities with SPC/E and present several interesting aspects that will be examined in the future.

To conclude, the analysis performed in this PhD thesis in bulk and confined water have drawn a comprehensive description of the dynamical behaviour of this liquid in the supercooled regime. In both the system important connections between the thermodynamics, dynamics and structure of water through the correspondence between the Widom Line and the Fragile to Strong Crossover have been found. This observation provide new insight on a better understanding of the anomalous phase diagram of supercooled water and on a possible explanation of several thermodynamical and dynamical phenomena.

8

Publications and Presentations

8.1 Publications

1. **Mode coupling theory and fragile to strong transition in supercooled TIP4P/2005 water**

   Reference: M. De Marzio, G. Camisasca, M. Rovere and P. Gallo, The Journal of Chemical Physics 144, 074503 (2016).

   Abstract: We study by molecular dynamics simulations supercooled water with the TIP4P/2005 potential. This model is able to predict many properties of water in a large range of the thermodynamic space in agreement with experiments. We explore the dynamical behavior and, in particular, the self intermediate scattering function of the oxygen atoms. We find that the structural relaxation in the range of mild supercooling is in agreement with the Mode Coupling Theory (MCT). The ideal MCT crossover takes place at decreasing temperature with increasing density. Deviations from the MCT behavior are found upon further supercooling. A crossover from the MCT, fragile, regime to a strong, Arrhenius, regime is found and it is connected to the presence of a liquid-liquid phase transition and the Widom line emanating from the liquid-liquid criticalpoint.

2. **Fragile to Strong Crossover in Supercooled Water: a comparison between TIP4P and TIP4P/2005 models**

   Reference: M. De Marzio, G. Camisasca, M. Rovere and P. Gallo, Wokshop Proceedings in Press on Il nuovo Cimento C (2016).

Abstract: We present recent simulation results on the dynamics of supercooled water with the TIP4P/2005 potential. We find that the dynamical behaviour of the translational motion of the molecules is well interpreted in terms of the Mode Coupling Theory, as it was found for supercooled TIP4P water. We compare the results of the two models and in particular we find also in TIP4P/2005 a crossover from a fragile to a strong regime. We connect this crossover to the crossing of the Widom line emanating from the liquid-liquid critical point.

3. Microscopic origin of the Fragile to Strong Crossover in Supercooled Water: the role of Activated Processes

Reference: M. De Marzio, G. Camisasca, M. Rovere and P. Gallo, Submitted to J. Chem. Phys. (2016).

Abstract: We perform an accurate analysis of the density self correlation functions of TIP4P/2005 water upon supercooling on approaching the region of the liquid-liquid critical point. In a previous work on this model we provided evidence of a fragile to strong crossover of the dynamical behaviour in the deep supercooled region. The structural relaxation follows the Mode Coupling Theory in the fragile region and then deviates Mode Coupling regime to a strong Arrhenius behaviour. To better understand the origin of this crossover we compute now the van Hove self correlation functions. In particular we aim to investigate the presence and the role of the hopping phenomena, that are the cause of the fragile to strong crossover in simple liquids. In TIP4P/2005 water we find hopping processes too and we analyse how they depend on temperature and density upon approaching the fragile to strong crossover and the Mode Coupling ideal crossover temperature. Our results show that water behaves like a simple glass former, after an initial ballistic regime the cage effect dominates the mild supercooled region, with diffusion taking place at long time. At the fragile to strong crossover we find that hopping (activated) processes start to play a role, evidenced by the appearance of peaks in the van Hove correlation functions. In the deep supercooled regime our analysis clearly indicates that activated processes dominate the dynamics. The comparison between the van Hove functions and the radial distribution functions allows to better understand the mechanism of hopping phenomena in supercooled water.

4. Structural properties and fragile to strong transition in confined water

Reference: M. De Marzio, G. Camisasca, M. Martin Conde, M. Rovere and P. Gallo, Submitted to J. Chem. Phys. (2016).

Abstract: We derive by computer simulation the radial distribution functions of water confined in a silica pore modeled to reproduce MCM-41. We perform the calculations in a range of temperature from ambient to deep supercooling for the subset of water molecules that resides in the inner shell (free water) by applying the excluded volume corrections. By comparing with bulk water we find that the first shell of the oxygen-oxygen and hydrogen-hydrogen radial distribution functions is less sharp and the first minimum fills in while the oxygen-hydrogen structure does not significantly change indicating that the free water keeps the hydrogen bond short range order. The two body excess entropy of supercooled water is calculated from the radial distribution functions. We connect the behavior of this function to the relaxation time of the same system already studied in previous simulations. We show that the two body entropy changes its behavior in coincidence with the crossover of the relaxation time from the Mode Coupling fragile to the strong Arrhenius regime. As for bulk water also in confinement the two body entropy has a strict connection with the dynamical relaxation.

8.2 Workshops, Conferences and Schools

1. *30 Nov-5 Dec 2015*: Conference **MRS Fall Meeting and Exhibit 2015**, Symposium Liquids and Glassy Soft Matter-Theoretical and Neutron Scattering Studies. Held in Boston. Poster presentation.

2. *7-12 Sept 2015*: Conference **Frontiers in Water Biophysics**. Held at Ettore Majorana Foundation and Center for Scientific Culture,

Erice. Poster presentation.

3. *10-12 Jun 2015*: Workshop **Roma Tre Workshop on Water under Extreme Conditions** held at Università degli Studi Roma Tre, Rome. Members of the Local Organizing Committee.

4. *14-15 May 2015*: Course **Parallel IO and management of large scientific data**. Held at CINECA, Rome.

5. *23-25 Feb 2015*: Course **Introduction to Parallel Computing with MPI and OpenMP**. Held at CINECA, Rome.

6. *4-6 Feb 2015*: Course **High Performance Molecular Dynamics**. Held at CINECA, Rome.

7. *17-18 Sept 2014*: Workshop **Italian Soft Days**. Held at Sapienza Università di Roma, Rome.

8. *13-21 Jul 2014*: CCP5 Summer School **Methods in Molecular Simulations**. Held at CECAM, Manchester.

9

Acronyms and abbreviations

In the following a list of the acronyms and abbreviations used throughout the thesis together with their meaning is reported. The spelling out of acronyms was given at the first occurrence in each Chapter and wherever it was deemed necessary for greater clarity.

1. **LLCP** liquid-liquid critical point
2. **LLPT** liquid-liquid phase transition
3. **WL** Widom Line
4. **LDL** low density liquid
5. **HDL** high density liquid
6. **MD** molecular dynamics
7. **TMD** temperature of maximum density
8. **LMS** limit of mechanical stability
9. **HDA** high density amorphous
10. **LDA** low density amorphous
11. **VFT** Vogel-Fulcher-Tamman
12. **KWW** Kohlrausch-Williams-Watts
13. **VSL** Von Schweidler law
14. **MCT** mode coupling theory
15. **FSC** fragile to strong crossover
16. **HB** Hydrogen Bonds
17. **RDF** radial distribution function
18. **SISF** Self Intermediate Scattering Functions
19. **VHSCF** Van Hove Self Correlation Functions

Bibliography

[1] Franks, F. *Water: a matrix of life* volume 21. Royal Society of Chemistry (2000).

[2] Ball, P. Water - an enduring mystery. *Nature* **452**, 291–292 (2008).

[3] Sakai, A., Matsumoto, T., Hirai, D., and Niino, T. Newly developed encapsulation-dehydration protocol for plantcryopreservation. *Cryo letters* **21**, 53–62 (1999).

[4] Kauzmann, W. Some factors in the interpretation of protein denaturation. *Advances in protein chemistry* **14**, 1–63 (1959).

[5] Debenedetti, P. G. Supercooled and glassy water. *Journal of Physics: Condensed Matter* **15**, R1669 (2003).

[6] Debenedetti, P. G. and Stanley, H. E. Supercooled and glassy water. *Phys. Today* **56**, 40 (2003).

[7] Debenedetti, P. G. *Metastable liquids: concepts and principles.* Princeton University Press (1996).

[8] Pauling, L. *General chemistry.* Courier Corporation (1988).

[9] Gallo, P., Amann-Winkel, K., Angell, C. A., Anisimov, M. A., Caupin, F., Chakravarty, C., Lascaris, E., Loerting, T., Panagiotopoulos, A. Z., Russo, J., Sellberg, J. A., Stanley, H. E., Tanaka, H., Vega, C., Xu, L., and Pettersson, L. G. M. Water: A tale of two liquids. *Chemical Reviews* **116**, 7463–7500 (2016).

[10] Stanley, H., Kumar, P., Xu, L., Yan, Z., Mazza, M., Buldyrev, S., Chen, S.-H., and Mallamace, F. The puzzling unsolved mysteries of liquid water: Some recent progress. *Physica A: Statistical Mechanics and its Applications* **386**, 729–743 (2007).

[11] Mishima, O. and Stanley, H. E. The relationship between liquid, supercooled and glassy water. *Nature* **396**, 329 (1998).

[12] Mishima, O. and Stanley, H. E. Decompression-induced melting of ice IV and the liquid-liquid transition in water. *Nature* **392**, 164 (1998).

[13] Poole, P. H., Sciortino, F., Essmann, U., and Stanley, H. E. Phase behaviour of metastable water. *Nature* **360**, 324 (1992).

[14] Gallo, P., Sciortino, F., Tartaglia, P., and Chen, S.-H. Slow dynamics of water molecules in supercooled states. *Phys. Rev. Lett.* **76**, 2730 (1996).

[15] Sciortino, F., Gallo, P., Tartaglia, P., and Chen, S.-H. Supercooled water and the kinetic glass transition. *Phys. Rev. E* **54**, 6331 (1996).

[16] Götze, W. *Complex Dynamics of Glass-Forming Liquids: A Mode-Coupling Theory.* Oxford University Press Oxford (2009).

[17] Torre, R., Bartolini, P., and Righini, R. Structural relaxation in supercooled water by time-resolved spectroscopy. *Nature* **428**, 296–299 (2004).

[18] Dehaoui, A., Issenmann, B., and Caupin, F. Viscosity of deeply supercooled water and its coupling to molecular diffusion. *Proc. Natl. Acad. Sci. U.S.A.* **112**, 12020 (2015).

[19] Liu, L., Chen, S.-H., Faraone, A., Yen, C.-W., and Mou, C.-Y. Pressure dependence of fragile-to-strong transition and a possible second critical point in supercooled confined water. *Phys. Rev. Lett.* **95**, 117802 (2005).

[20] Gallo, P., Rovere, M., and Chen, S.-H. Dynamic crossover in supercooled confined water: Understanding bulk properties through confinement. *J. Phys. Chem. Lett.* **1**, 729 (2010).

[21] Abascal, J. L. F. and Vega, C. A general purpose model for the condensed phases of water: TIP4P/2005. *J. Chem. Phys.* **123**, 234505 (2005).

[22] Pi, H. L., Aragones, J. L., Vega, C., Noya, E. G., Abascal, J. L. F., Gonzalez, M. A., and McBride, C. Anomalies in water as obtained from computer simulations of the TIP4P/2005 model: density maxima, and density, isothermal compressibility and heat capacity minima. *Mol. Phys.* **107**, 365 (2009).

[23] Abascal, J. L. F. and Vega, C. Widom line and the liquid-liquid critical point for the TIP4P/2005 water model. *J. Chem. Phys.* **133**, 234502 (2010).

[24] Vega, C., Abascal, J. L., Conde, M., and Aragones, J. What ice can teach us about water interactions: a critical comparison of the performance of different water models. *Faraday Discuss.* **141**, 251–276 (2009).

[25] Gallo, P., Rovere, M., and Chen, S.-H. Water confined in MCM-41: a mode coupling theory analysis. *J. Phys.: Condens. Matt.* **24**, 064109 (2012).

[26] Berendsen, H. J. C., Grigera, J. R., and Straatsma, T. P. The missing term in effective pair potentials. *J. Phys. Chem.* **91**, 6269 (1987).

[27] Hasted, J. Liquid water: Dielectric properties. In *The Physics and Physical Chemistry of Water* pages 255–309. Springer (1972).

[28] Eisenberg, D. and Kauzmann, W. *The structure and properties of water.* Oxford University Press on Demand (1969).

[29] Martin, F. and Zipse, H. Charge distribution in the water molecule - a comparison of methods. *Journal of computational chemistry* **26**, 97–105 (2005).

[30] Lovas, F. J. Microwave spectral tables ii. triatomic molecules. *Journal of Physical and Chemical Reference Data* **7**, 1445–1750 (1978).

[31] Stillinger, F. H. Water revisited. *Science* **209**, 451–457 (1980).

[32] Angell, C. and Kanno, H. Density maxima in high-pressure supercooled water and liquid silicon dioxide. *Science* **193**, 1121–1122 (1976).

[33] Fine, R. A. and Millero, F. J. The high pressure pvt properties of deuterium oxide. *The Journal of Chemical Physics* **63**, 89–95 (1975).

[34] Kanno, H. and Angell, C. Volumetric and derived thermal characteristics of liquid d2o at low temperatures and high pressures. *The Journal of chemical physics* **73**, 1940–1947 (1980).

[35] Kanno, H. and Angell, C. Water: Anomalous compressibilities to 1.9 kbar and correlation with supercooling limits. *The Journal of chemical physics* **70**, 4008–4016 (1979).

[36] Sastry, S., Debenedetti, P. G., Sciortino, F., and Stanley, H. E. Singularity-free interpretation of the thermodynamics of supercooled water. *Phys. Rev. E* **53**, 6144 (1996).

[37] Angell, C., Sichina, W., and Oguni, M. Heat capacity of water at

extremes of supercooling and superheating. *The Journal of Physical Chemistry* **86**, 998–1002 (1982).

[38] Speedy, R. J. and Angell, C. A. Isothermal compressibility of supercooled water and evidence for a thermodynamic singularity at 45 ° c. *J. Chem. Phys.* **65**, 851 (1976).

[39] Starr, F. W., Sciortino, F., and Stanley, H. E. Dynamics of simulated water under pressure. *Phys. Rev. E* **60**, 6757 (1999).

[40] Scala, A., Starr, F. W., La Nave, E., Sciortino, F., and Stanley, H. E. Configurational entropy and diffusivity of supercooled water. *Nature* **406**, 166–169 (2000).

[41] Errington, J. R. and Debenedetti, P. G. Relationship between structural order and the anomalies of liquid water. *Nature* **409**, 318 (2001).

[42] Angell, C., Finch, E., and Bach, P. Spin–echo diffusion coefficients of water to 2380 bar and -20 ° C. *J. Chem. Phys.* **65**, 3063–3066 (1976).

[43] Prielmeier, F., Lang, E., Speedy, R., and Lüdemann, H.-D. Diffusion in supercooled water to 300 Mpa. *Phys. Rev. Lett.* **59**, 1128 (1987).

[44] Sellberg, J. A., Huang, C., McQueen, T. A., Loh, N. D., Laksmono, H., Schlesinger, D., Sierra, R. G., Nordlund, D., Hampton, C. Y., Starodub, D., DePonte, D. P., Beye, M., Chen, C., Martin, A. V., Barty, A., Wikfeldt, K. T., Weiss, T. M., Caronna, C., Feldkamp, J., Skinner, L. B., Seibert, M. M., Messerschmidt, M., Williams, G. J., Boutet, S., Pettersson, L. G. M., Bogan, M. J., and Nilsson, A. Ultrafast x-ray probing of water structure below the homogeneous ice nucleation temperature. *Nature* **510**, 381 (2014).

[45] Johari, G., Hallbrucker, A., and Mayer, E. The glass–liquid transition of hyperquenched water. *Nature* **330**, 552–553 (1987).

[46] Hallbrucker, A., Mayer, E., and Johari, G. Glass-liquid transition and the enthalpy of devitrification of annealed vapor-deposited amorphous solid water: a comparison with hyperquenched glassy water. *The Journal of Physical Chemistry* **93**, 4986–4990 (1989).

[47] Velikov, V., Borick, S., and Angell, C. The glass transition of water, based on hyperquenching experiments. *Science* **294**, 2335–2338 (2001).

[48] Angell, C. Liquid fragility and the glass transition in water and aqueous solutions. *Chemical reviews* **102**, 2627–2650 (2002).

[49] Mishima, O., Calvert, L. D., and Whalley, E. An apparently first-order transition between two amorphous phases of ice induced by pressure. *Nature* **314**, 76 (1985).

[50] Winkel, K., Elsaesser, M., Mayer, E., and Loerting, T. Water polyamorphism: Reversibility and (dis)continuity. *J. Chem. Phys.* **128**, 044510 (2008).

[51] Kim, C. U., Barstow, B., Tate, M. V., and Gruner, S. M. Evidence for liquid water during the high-density to low-density amorphous ice transition. *Proc. Natl. Acad. Sci. U.S.A.* **106**, 4596 (2009).

[52] Winkel, K., Mayer, E., and Loerting, T. Equilibrated high-density amorphous ice and its first-order transition to the low-density form. *J. Phys. Chem. B* **115**, 14141 (2011).

[53] Mishima, O., Calvert, L., and Whalley, E. Melting icei at 77 k and 10 kbar: a new method of making amorphous solids. *Nature* **310**, 393–395 (1984).

[54] Finney, J., Hallbrucker, A., Kohl, I., Soper, A., and Bowron, D. Structures of high and low density amorphous ice by neutron diffraction. *Physical review letters* **88**, 225503 (2002).

[55] Koza, M., Schober, H., Fischer, H., Hansen, T., and Fujara, F. Kinetics of the high-to low-density amorphous water transition. *Journal of Physics: Condensed Matter* **15**, 321 (2003).

[56] Mishima, O. and Suzuki, Y. Propagation of the polyamorphic transition of ice and the liquid–liquid critical point. *Nature* **419**, 599–603 (2002).

[57] Mishima, O. Reversible first-order transition between two h_2o amorphs at 0.2 gpa and 135 k. *The Journal of chemical physics* **100**, 5910–5912 (1994).

[58] Hallbrucker, A. and Mayer, E. Calorimetric study of the vitrified liquid water to cubic ice phase transition. *Journal of Physical Chemistry* **91**, 503–505 (1987).

[59] Amann-Winkel, K., Boehmer, R., Fujara, F., Gainaru, C., Geil, B., and Loerting, T. Colloquium: Water's controversial glass transitions. *Rev. Mod. Phys.* **88**, 011002 (2016).

[60] Stanley, H. E. Unsolved mysteries of water in its liquid and glass states. *MRS bulletin* **24**, 22 (1999).

[61] Smith, R. S. and Kay, B. D. The existence of supercooled liquid water at 150 k. *Nature* **398**, 788–791 (1999).

[62] Speedy, R. J. Stability-limit conjecture. an interpretation of the properties of water. *J. Chem. Phys.* **86**, 982 (1982).

[63] Rebelo, R. P., Debenedetti, P. G., and Sastry, S. Singularity-free interpretation of the thermodynamics of supercooled water. ii. thermal and volumetric behavior. *J. Chem. Phys.* **109**, 626 (1998).

[64] Angell, C. A. Insights into phases of liquid water from study of its unusual glass-forming properties. *Science* **319**, 582 (2008).

[65] Debenedetti, P. G. Supercooled and glassy water. *J. Phys.: Condens. Matt.* **15**, R1669 (2003).

[66] Holten, V., Bertrand, C. E., Anisimov, M. A., and Sengers, J. V. Thermodynamics of supercooled water. *J. Chem. Phys.* **136**, 094507 (2012).

[67] Xu, L., Kumar, P., Buldyrev, S. V., Chen, S. H., Poole, P. H., Sciortino, F., and Stanley, H. E. Relation between the Widom line and the dynamic crossover in systems with a liquid-liquid phase transition. *Proc. Natl. Acad. Sci. U.S.A.* **102**, 16558 (2005).

[68] Franzese, G. and Stanley, H. E. The widom line of supercooled water. *J. Phys.: Condens. Matt.* **19**, 205126 (2007).

[69] Anisimov, M. A., Sengers, J., and Levelt Sengers, J. Near-critical behavior of aqueous systems. *Aqueous Systems at Elevated Temperatures and Pressures: Physical Chemistry in Water, Steam and Hydrothermal Solutions* **1** (2004).

[70] Xu, L., Buldyrev, S. V., Angell, C. A., and Stanley, H. E. Thermodynamics and dynamics of the two-scale spherically symmetric jagla ramp model of anomalous liquids. *Physical Review E* **74**, 031108 (2006).

[71] Kumar, P., Franzese, G., and Stanley, H. E. Predictions of dynamic behavior under pressure for two scenarios to explain water anomalies. *Phys. Rev. Lett.* **100**, 105701 (2008).

[72] Stokely, K., Mazza, M. G., Stanley, H. E., and Franzese, G. Effect of hydrogen bond cooperativity on the behavior of water. *Proceedings of the National Academy of Sciences* **107**, 1301–1306 (2010).

[73] Yan, Z., Buldyrev, S. V., Kumar, P., Giovambattista, N., and Stanley, H. E. Correspondence between phase diagrams of the tip5p water model and a spherically symmetric repulsive ramp potential with two characteristic length scales. *Physical Review E* **77**, 042201 (2008).

[74] Poole, P. H., Sciortino, F., Essmann, U., and Stanley, H. E. Spinodal of liquid water. *Phys. Rev. E* **48**, 3799 (1993).

[75] Poole, P. H., Sciortino, F., Grande, T., Stanley, H. E., and Angell, C. A. Effect of hydrogen bonds on the thermodynamic behavior of liquid water. *Physical review letters* **73**, 1632 (1994).

[76] Poole, P. H., Saika-Voivod, I., and Sciortino, F. Density minimum and liquid-liquid phase transition. *J. Phys.: Condens. Matt.* **17**, L431 (2005).

[77] Kumar, P., Buldyrev, S. V., Starr, F. W., Giovambattista, N., and Stanley, H. E. Thermodynamics, structure, and dynamics of water confined between hydrophobic plates. *Physical Review E* **72**, 051503 (2005).

[78] Paschek, D. How the liquid-liquid transition affects hydrophobic hydration in deeply supercooled water. *Physical review letters* **94**, 217802 (2005).

[79] Paschek, D., Ruüppert, A., and Geiger, A. Thermodynamic and structural characterization of the transformation from a metastable low-density to a very high-density form of supercooled tip4p-ew model water. *Chem. Phys. Chem.* **9**, 2737 (2008).

[80] Sciortino, F., Poole, P. H., Essmann, U., and Stanley, H. Line of compressibility maxima in the phase diagram of supercooled water. *Physical Review E* **55**, 727 (1997).

[81] Liu, Y., Panagiotopoulos, A. Z., and Debenedetti, P. G. Low-temperature fluid-phase behavior of st2 water. *J. Chem. Phys.* **131**, 104508 (2009).

[82] Yamada, M., Mossa, S., Stanley, H., and Sciortino, F. Interplay between time-temperature transformation and the liquid-liquid phase transition in water. *Phys. Rev. Lett.* **88**, 195701 (2002).

[83] Jedlovszky, P. and Vallauri, R. iquid-vapor and liquid-liquid phase equilibria of the brodholt-sampoli-vallauri polarizable water model. *J. Chem. Phys.* **122**, 081101 (2005).

[84] Tanaka, H. Phase behaviors of supercooled water: reconciling a critical point of amorphous ices with spinodal instability. *The Journal of chemical physics* **105**, 5099–5111 (1996).

[85] Harrington, S., Poole, P. H., Sciortino, F., and Stanley, H. E. Equation of state of supercooled water simulated using the extended simple point charge intermolecular potential. *J. Chem. Phys.* **107**, 7443–7450 (1997).

[86] Corradini, D., Rovere, M., and Gallo, P. A route to explain water anomalies from results on an aqueous solution of salt. *J. Chem. Phys.* **132**, 134508 (2010).

[87] Truskett, T. M., Debenedetti, P. G., Sastry, S., and Torquato, S. A single-bond approach to orientation-dependent interactions and its implications for liquid water. *The Journal of chemical physics* **111**, 2647–2656 (1999).

[88] Zhang, Y., Faraone, A., Kamitakahara, W. A., Liu, K.-H., Mou, C.-Y., Leão, J. B., Chang, S., and Chen, S.-H. Density hysteresis of heavy water confined in a nanoporous silica matrix. *Proceedings of the National Academy of Sciences* **108**, 12206–12211 (2011).

[89] Liu, D., Zhang, Y., Chen, C.-C., Mou, C.-Y., Poole, P. H., and Chen, S.-H. Observation of the density minimum in deeply supercooled confined water. *Proceedings of the National Academy of Sciences* **104**, 9570–9574 (2007).

[90] Liu, L., Chen, S.-H., Faraone, A., Yen, C.-W., Mou, C.-Y., Kolesnikov, A. I., Mamontov, E., and Leao, J. Quasielastic and inelastic neutron scattering investigation of fragile-to-strong crossover in deeply supercooled water confined in nanoporous silica matrices. *Journal of Physics: Condensed Matter* **18**, S2261 (2006).

[91] Banerjee, D., Bhat, S., Bhat, S., and Leporini, D. Esr evidence for 2 coexisting liquid phases in deeply supercooled bulk water. *Proceedings of the National Academy of Sciences* **106**, 11448–11453 (2009).

[92] Mahoney, M. W. and Jorgensen, W. L. A five-site model for liquid water and the reproduction of the density anomaly by rigid, nonpolarizable potential functions. *The Journal of Chemical Physics* **112**, 8910–8922 (2000).

[93] Harrington, S., Zhang, R., Poole, P. H., Sciortino, F., and Stanley,

H. E. Liquid-liquid phase transition: Evidence from simulations. *Physical Review Letters* **78**, 2409 (1997).

[94] Yamada, M., Stanley, H. E., and Sciortino, F. Equation of state of supercooled water from the sedimentation profile. *Physical Review E* **67**, 010202 (2003).

[95] Palmer, J., Martelli, F., Liu, Y., Car, R., Panagiotopoulos, A. Z., and Debenedetti, P. G. Metastable liquid-liquid transition in a molecular model of water. *Nature* **510**, 385 (2014).

[96] Smallenburg, F., Poole, P., and Sciortino, F. Phase diagram of the st2 model of water. *Mol. Phys.* **113**, 2791 (2015).

[97] Smallenburg, F., Filion, L., and Sciortino, F. Erasing no-man's land by thermodynamically stabilizing the liquid-liquid transition in tetrahedral particles. *Nature Phys.* **10**, 653 (2014).

[98] Poole, P. H., Bowles, R. K., Saika-Voivod, I., and Sciortino, F. Free energy surface of st2 water near the liquid-liquid phase transition. *J. Chem. Phys.* **138**, 034505 (2013).

[99] Palmer, J., Car, R., and Debenedetti, P. The liquid-liquid transition in supercooled st2 water: a comparison between umbrella sampling and well-tempered metadynamics. *Faraday Discuss.* **167**, 77 (2013).

[100] Kesselring, T. A., Franzese, G., Buldyrev, S. V., Herrmann, H. J., and Stanley, H. E. Nanoscale dynamics of phase flipping in water near its hypothesized liquid-liquid critical point. *Sci. Rep.* **2**, 474 (2012).

[101] Liu, Y., Palmer, J. C., Panagiotopoulos, A. Z., and Debenedetti, P. G. Liquid-liquid transition in st2 water. *J. Chem. Phys.* **137**, 214505 (2012).

[102] Sciortino, F., Saika-Voivod, I., and Poole, P. H. Study of the st2 model of water close to the liquid-liquid critical point. *Phys. Chem. Chem. Phys.* **13**, 19759 (2011).

[103] Poole, P. H., Becker, S. R., Sciortino, F., and Starr, F. W. Dynamical behavior near a liquid-liquid phase transition in simulations of supercooled water. *J. Phys. Chem. B* **115**, 14176 (2011).

[104] Buhariwalla, C., Bowles, R., Saika-Voivod, I., Sciortino, F., and Poole, P. Free energy of formation of small ice nuclei near the widom line in simulations of supercooled water. *Eur. Phys. J. E* **38**, 39 (2015).

[105] Tanaka, H. A self-consistent phase diagram for supercooled water. *Nature* **380**, 328–330 (1996).

[106] Scala, A., Starr, F. W., La Nave, E., Stanley, H., and Sciortino, F. Free energy surface of supercooled water. *Physical Review E* **62**, 8016 (2000).

[107] Buldyrev, S. V., Kumar, P., Debenedetti, P. G., Rossky, P. J., and Stanley, H. E. Water-like solvation thermodynamics in a spherically symmetric solvent model with two characteristic lengths. *Proceedings of the National Academy of Sciences* **104**, 20177–20182 (2007).

[108] Xu, L., Buldyrev, S. V., Giovambattista, N., Angell, C. A., and Stanley, H. E. A monatomic system with a liquid-liquid critical point and two distinct glassy states. *The Journal of chemical physics* **130**, 054505 (2009).

[109] Yan, Z., Buldyrev, S. V., Giovambattista, N., and Stanley, H. E. Structural order for one-scale and two-scale potentials. *Physical review letters* **95**, 130604 (2005).

[110] Yan, Z., Buldyrev, S. V., Giovambattista, N., Debenedetti, P. G., and Stanley, H. E. Family of tunable spherically symmetric potentials that span the range from hard spheres to waterlike behavior. *Physical Review E* **73**, 051204 (2006).

[111] Yan, Z., Buldyrev, S. V., Kumar, P., Giovambattista, N., Debenedetti, P. G., and Stanley, H. E. Structure of the first-and second-neighbor shells of simulated water: Quantitative relation to translational and orientational order. *Physical Review E* **76**, 051201 (2007).

[112] Xu, L., Ehrenberg, I., Buldyrev, S. V., and Stanley, H. E. Relationship between the liquid–liquid phase transition and dynamic behaviour in the jagla model. *Journal of Physics: Condensed Matter* **18**, S2239 (2006).

[113] Kumar, P., Buldyrev, S. V., Sciortino, F., Zaccarelli, E., and Stanley, H. E. Static and dynamic anomalies in a repulsive spherical ramp liquid: theory and simulation. *Physical Review E* **72**, 021501 (2005).

[114] Gallo, P. and Sciortino, F. Ising universality class for the liquid-liquid critical point of a one component fluid: A finite-size scaling test. *Phys. Rev. Lett.* **109**, 177801 (2012).

[115] Wang, Z., Ito, K., Leão, J. B., Harriger, L., Liu, Y., and Chen, S.-H. Liquid–liquid phase transition and its phase diagram in deeply-cooled

heavy water confined in a nanoporous silica matrix. *The journal of physical chemistry letters* **6**, 2009–2014 (2015).

[116] Taschin, A., Bartolini, P., Eramo, R., Righini, R., and Torre, R. Evidence of two distinct local structures of water from ambient to supercooled conditions. *Nat. Commun.* **4**, 2401 (2013).

[117] Kumar, P., Franzese, G., and Stanley, H. E. Dynamics and thermodynamics of water. *Journal of Physics: Condensed Matter* **20**, 244114 (2008).

[118] Jeffery, C. and Austin, P. A new analytic equation of state for liquid water. *The Journal of chemical physics* **110**, 484–496 (1999).

[119] Franzese, G. and Stanley, H. E. Liquid-liquid critical point in a hamiltonian model for water: analytic solution. *Journal of Physics: Condensed Matter* **14**, 2201 (2002).

[120] Holten, V. and Anisimov, M. Entropy-driven liquid-liquid separation in supercooled water. *Sci. Rep.* **2**, 713 (2012).

[121] Holten, V., Palmer, J. C., Poole, P. H., Debenedetti, P. G., and Anisimov, M. A. Two-state thermodynamics of the st2 model for supercooled water. *J. Chem. Phys.* **140**, 104502 (2014).

[122] Bengtzelius, U., Gotze, W., and Sjolander, A. Dynamics of supercooled liquids and the glass transition. *Journal of Physics C: solid state Physics* **17**, 5915 (1984).

[123] Gotze, W. and Sjogren, L. Scaling properties in supercooled liquids near the glass transition. *Journal of Physics C: Solid State Physics* **21**, 3407 (1988).

[124] Frick, B., Farago, B., and Richter, D. Temperature dependence of the nonergodicity parameter in polybutadiene in the neighborhood of the glass transition. *Physical review letters* **64**, 2921 (1990).

[125] Sokolov, A., Hurst, J., and Quitmann, D. Dynamics of supercooled water: mode-coupling theory approach. *Physical Review B* **51**, 12865 (1995).

[126] Gallo, P. and Rovere, M. Mode coupling and fragile to strong transition in supercooled TIP4P water. *J. Chem. Phys.* **137**, 164503 (2012).

[127] Gallo, P., Corradini, D., and Rovere, M. Fragile to strong crossover at the Widom line in supercooled aqueous solutions of NaCl. *J. Chem. Phys.* **139**, 204503 (2013).

[128] Gallo, P., Rovere, M., and Spohr, E. Supercooled confined water and the mode coupling crossover temperature. *Phys. Rev. Lett.* **85**, 4317 (2000).

[129] Gallo, P., Rovere, M., and Spohr, E. Glass transition and layering effects in confined water: A computer simulation study. *J. Chem. Phys.* **113**, 11324 (2000).

[130] Kob, W. and Andersen, H. C. Testing mode-coupling theory for a supercooled binary lennard-jones mixture i: The van hove correlation function. *Physical Review E* **51**, 4626 (1995).

[131] Van Megen, W. and Underwood, S. Glass transition in colloidal hard spheres: Measurement and mode-coupling-theory analysis of the coherent intermediate scattering function. *Physical Review E* **49**, 4206 (1994).

[132] Li, a., Du, W., Chen, X., Cummins, H., and Tao, N. Testing mode-coupling predictions for α and β relaxation in ca 0.4 k 0.6 (no 3) 1.4 near the liquid-glass transition by light scattering. *Physical Review A* **45**, 3867 (1992).

[133] Götze, W. Recent tests of the mode-coupling theory for glassy dynamics. *Journal of Physics: condensed matter* **11**, A1 (1999).

[134] Kob, W. and Andersen, H. C. Testing mode-coupling theory for a supercooled binary lennard-jones mixture. ii. intermediate scattering function and dynamic susceptibility. *Physical Review E* **52**, 4134 (1995).

[135] Kob, W. and Andersen, H. C. Scaling behavior in the β-relaxation regime of a supercooled lennard-jones mixture. *Physical review letters* **73**, 1376 (1994).

[136] Angell, C. Perspective on the glass transition. *Journal of Physics and Chemistry of Solids* **49**, 863–871 (1988).

[137] Kob, W. Computer simulations of supercooled liquids and glasses. *Journal of Physics: Condensed Matter* **11**, R85 (1999).

[138] Coslovich, D. and Pastore, G. Understanding fragility in supercooled lennard-jones mixtures. i. locally preferred structures. *The Journal of chemical physics* **127**, 124504 (2007).

[139] Coslovich, D. and Pastore, G. Understanding fragility in supercooled

lennard-jones mixtures. ii. potential energy surface. *The Journal of chemical physics* **127**, 124505 (2007).

[140] Coslovich, D. and Pastore, G. Dynamics and energy landscape in a tetrahedral network glass-former: direct comparison with models of fragile liquids. *Journal of Physics: Condensed Matter* **21**, 285107 (2009).

[141] Hansen, J.-P. and McDonald, I. R. *Theory of simple liquids.* Elsevier (1990).

[142] Starr, F. W., Sciortino, F., and Stanley, H. E. Dynamics of simulated water under pressure. *Phys. Rev. E* **60**, 6757 (1999).

[143] Corradini, D., Gallo, P., Buldyrev, S. V., and Stanley, H. Fragile-to-strong crossover coupled to the liquid-liquid transition in hydrophobic solutions. *Phys. Rev. E* **85**, 051503 (2012).

[144] Corradini, D., Buldyrev, S. V., Gallo, P., and Stanley, H. E. Effect of hydrophobic solutes on the liquid-liquid critical point. *Phys. Rev. E* **81**, 061504 (2010).

[145] Mallamace, F., Broccio, M., Corsaro, C., Faraone, A., Wanderlingh, U., Liu, L., Mou, C., and Chen, S.-H. The fragile-to-strong dynamic crossover transition in confined water: nuclear magnetic resonance results. *J. Chem. Phys.* **124**, 161102 (2006).

[146] Faraone, A., Liu, L., Mou, C.-Y., Yen, C.-W., and Chen, S.-H. Fragile-to- strong liquid transition in deeply supercooled confined water. *J. Chem. Phys.* **121**, 10843 (2004).

[147] Zhang, Y., Lagi, M., Fratini, E., Baglioni, P., Mamontov, E., and Chen, S.-H. Dynamic susceptibility of supercooled water and its relation to the dynamic crossover phenomenon. *Phys. Rev. E* **79**, 040201 (2009).

[148] Wang, Z., Le, P., Ito, K., Leão, J. B., Tyagi, M., and Chen, S.-H. Dynamic crossover in deeply cooled water confined in mcm-41 at 4 kbar and its relation to the liquid-liquid transition hypothesis. *The Journal of chemical physics* **143**, 114508 (2015).

[149] Gallo, P., Rovere, M., and Chen, S.-H. Anomalous dynamics of water confined in MCM-41 at different hydrations. *J. Phys.: Condens. Matt.* **22**, 284102 (2010).

[150] Zanotti, J.-M., Bellissent-Funel, M.-C., and Chen, S.-H. Relaxational

dynamics of supercooled water in porous glass. *Physical Review E* **59** , 3084 (1999).

[151] Metropolis, N., Rosenbluth, A. W., Rosenbluth, M. N., Teller, A. H., and Teller, E. Equation of state calculations by fast computing machines. *The journal of chemical physics* **21**, 1087–1092 (1953).

[152] Alder, B. and Wainwright, T. Phase transition for a hard sphere system. *The Journal of chemical physics* **27**, 1208 (1957).

[153] Rahman, A. Correlations in the motion of atoms in liquid argon. *Physical Review* **136**, A405 (1964).

[154] Allen, M. P. and Tildesley, D. J. *Computer simulation of liquids.* Oxford university press (1989).

[155] Hoover, W. G. Canonical dynamics: equilibrium phase-space distributions. *Physical review A* **31**, 1695 (1985).

[156] Berendsen, H. J., Postma, J. v., van Gunsteren, W. F., DiNola, A., and Haak, J. Molecular dynamics with coupling to an external bath. *The Journal of chemical physics* **81**, 3684–3690 (1984).

[157] Evans, D. J. and Morriss, O. Non-newtonian molecular dynamics. *Computer Physics Reports* **1**, 297–343 (1984).

[158] Melchionna, S., Ciccotti, G., and Lee Holian, B. Hoover npt dynamics for systems varying in shape and size. *Molecular Physics* **78**, 533–544 (1993).

[159] De Marzio, M., Camisasca, G., Rovere, M., and Gallo, P. Mode coupling theory and fragile to strong transition in supercooled TIP4P/2005 water. *J. Chem. Phys.* **144**, 074503 (2016).

[160] De Marzio, M., Camisasca, G., Rovere, M., and Gallo, P. Microscopic origin of the fragile to strong crossover in supercooled water: the role of activated processes. *Submitted to J. Chem. Phys* (2016).

[161] Grossman, J. C., Schwegler, E., Draeger, E. W., Gygi, F., and Galli, G. Towards an assessment of the accuracy of density functional theory for first principles simulations of water. *The Journal of chemical physics* **120**, 300–311 (2004).

[162] De Marzio, M., Camisasca, G., Rovere, M., and Gallo, P. Fragile-to-strong crossover in supercooled water: A comparison between tip4p and tip4p/2005 models. *In press on Il nuovo Cimento C* (2016).

[163] Gallo, P., Pellarin, R., and Rovere, M. Mode coupling relaxation scenario in a confined glass former. *Europhys. Lett.* **57**, 212 (2002).

[164] Gallo, P., Attili, A., and Rovere, M. Mode-coupling behavior of a Lennard-Jones binary mixture upon increasing confinement. *Phys. Rev. E* **80**, 061502 (2009).

[165] Kumar, P., Buldyrev, S. V., Becker, S. R., Poole, P. H., Starr, F. W., and Stanley, H. E. Relation between the widom line and the breakdown of the Stokes-Einstein relation in supercooled water. *Proc. Natl. Acad. Sci. U.S.A.* **104**, 9575 (2007).

[166] Rasaiah, J. C., Garde, S., and Hummer, G. Water in nonpolar confinement: From nanotubes to proteins and beyond*. *Annu. Rev. Phys. Chem.* **59**, 713–740 (2008).

[167] Ball, P. Water as an active constituent in cell biology. *Chemical reviews* **108**, 74–108 (2008).

[168] De Marzio, M., Camisasca, G., Conde Martin, M., Rovere, M., and Gallo, P. Structural properties and fragile to strong transition in confined water. *Submitted to J. Chem. Phys* (2016).

[169] Cerveny, S., Mallamace, F., Swenson, J., Vogel, M., and Xu, L. Confined water as model of supercooled water. *Chemical reviews* (2016).

[170] Bergman, R. and Swenson, J. Dynamics of supercooled water in confined geometry. *Nature* **403**, 283–286 (2000).

[171] Mamontov, E., Burnham, C., Chen, S.-H., Moravsky, A., Loong, C.-K., De Souza, N., and Kolesnikov, A. Dynamics of water confined in single-and double-wall carbon nanotubes. *The Journal of chemical physics* **124**, 194703 (2006).

[172] Giovambattista, N., Debenedetti, P. G., and Rossky, P. J. Effect of surface polarity on water contact angle and interfacial hydration structure. *The Journal of Physical Chemistry B* **111**, 9581–9587 (2007).

[173] Giovambattista, N., Rossky, P. J., and Debenedetti, P. G. Effect of temperature on the structure and phase behavior of water confined by hydrophobic, hydrophilic, and heterogeneous surfaces. *The Journal of Physical Chemistry B* **113**, 13723–13734 (2009).

[174] Kumar, P., Han, S., and Stanley, H. E. Anomalies of water and hydrogen bond dynamics in hydrophobic nanoconfinement. *Journal of Physics: Condensed Matter* **21**, 504108 (2009).

[175] Kumar, P., Starr, F. W., Buldyrev, S. V., and Stanley, H. E. Effect of water-wall interaction potential on the properties of nanoconfined water. *Physical Review E* **75**, 011202 (2007).

[176] Alothman, Z. A. A review: Fundamental aspects of silicate mesoporous materials. *Materials* **5**, 2874–2902 (2012).

[177] Faraone, A., Liu, K.-H., Mou, C.-Y., Zhang, Y., and Chen, S.-H. Single particle dynamics of water confined in a hydrophobically modified mcm-41-s nanoporous matrix. *J. Chem. Phys.* **130**, 134512 (2009).

[178] Liu, L., Faraone, A., Mou, C., Yen, C., and Chen, S. Slow dynamics of supercooled water confined in nanoporous silica materials. *Journal of Physics: Condensed Matter* **16**, S5403 (2004).

[179] Spohr, E., Hartnig, C., Gallo, P., and Rovere, M. Water in porous glasses. a computer simulation study. *Journal of Molecular Liquids* **80**, 165–178 (1999).

[180] Gallo, P., Ricci, M., and Rovere, M. Layer analysis of the structure of water confined in vycor glass. *The Journal of chemical physics* **116**, 342–346 (2002).

[181] Gallo, P., Rovere, M., Ricci, M., Hartnig, C., and Spohr, E. Evidence of glassy behaviour of water molecules in confined states. *Philosophical Magazine B* **79**, 1923–1930 (1999).

[182] Cucini, R., Taschin, A., Bartolini, P., and Torre, R. Acoustic, thermal and flow processes in a water filled nanoporous glass by time-resolved optical spectroscopy. *Journal of the Mechanics and Physics of Solids* **58**, 1302–1317 (2010).

[183] Cucini, R., Taschin, A., Bartolini, P., and Torre, R. Acoustic phenomena and hydrodynamic flow in a water filled nano-porous glass studied by transient grating spectroscopy. *Journal of Physics: Conference Series* **214**, 012032 (2010).

[184] Taschin, A., Bartolini, P., Marcelli, A., Righini, R., and Torre, R. A comparative study on bulk and nanoconfined water by time-resolved optical kerr effect spectroscopy. *Faraday discussions* **167**, 293–308 (2013).

[185] Taschin, A., Bartolini, P., Eramo, R., Righini, R., and Torre, R. Optical kerr effect of liquid and supercooled water: The experimental and data analysis perspective. *The Journal of chemical physics* **141**, 084507 (2014).

[186] Taschin, A., Bartolini, P., Marcelli, A., Righini, R., and Torre, R. Supercooling and freezing processes in nanoconfined water by time-resolved optical kerr effect spectroscopy. *Journal of Physics: Condensed Matter* **27**, 194107 (2015).

[187] Vessal, B., Amini, M., and Catlow, C. Computer simulation of the structure of silica glass. *Journal of non-crystalline solids* **159**, 184–186 (1993).

[188] Bryk, T. and Haymet, A. The ice/water interface: Density–temperature phase diagram for the spc/e model of liquid water. *Molecular Simulation* **30**, 131–135 (2004).

[189] Vega, C. and Abascal, J. Relation between the melting temperature and the temperature of maximum density for the most common models of water. *The Journal of chemical physics* **123**, 144504 (2005).

[190] Starr, F. W., Harrington, S., Sciortino, F., and Stanley, H. E. Slow dynamics of water under pressure. *Phys. Rev. Lett.* **82**, 3629 (1999).

[191] Guissani, Y. and Guillot, B. A computer simulation study of the liquid–vapor coexistence curve of water. *The Journal of chemical physics* **98**, 8221–8235 (1993).

[192] Smith, P. E. and van Gunsteren, W. F. The viscosity of spc and spc/e water at 277 and 300 k. *Chemical physics letters* **215**, 315–318 (1993).

[193] Baez, L. A. and Clancy, P. Existence of a density maximum in extended simple point charge water. *The Journal of chemical physics* **101**, 9837–9840 (1994).

[194] Brodka, A. and Zerda, T. Properties of liquid acetone in silica pores: Molecular dynamics simulation. *The Journal of chemical physics* **104** , 6319–6326 (1996).

[195] Hess, B., Kutzner, C., der Spoel, D. V., and Lindahl, E. Gromacs 4: algorithms for highly efficient, load-balanced, and scalable molecular simulation. *J. Chem. Theory Comp.* **4**, 435 (2008).

[196] Mahadevan, T. S. and Garofalini, S. H. Dissociative chemisorption of water onto silica surfaces and formation of hydronium ions. *Journal of Physical Chemistry C* **112**, 1507–1515 (2008).

[197] Skinner, L. B., Huang, C., Schlesinger, D., Pettersson, L. G., Nilsson, A., and Benmore, C. J. Benchmark oxygen-oxygen pair-distribution

function of ambient water from x-ray diffraction measurements with a wide q-range. *The Journal of chemical physics* **138**, 074506 (2013).

[198] Skinner, L., Benmore, C., Neuefeind, J., and Parise, J. The structure of water around the compressibility minimum. *The Journal of chemical physics* **141**, 214507 (2014).

[199] Rosenfeld, Y. A quasi-universal scaling law for atomic transport in simple fluids. *Journal of Physics: Condensed Matter* **11**, 5415 (1999).

[200] Baranyai, A. and Evans, D. J. Direct entropy calculation from computer simulation of liquids. *Physical Review A* **40**, 3817 (1989).

[201] Krekelberg, W. P., Mittal, J., Ganesan, V., and Truskett, T. M. How short-range attractions impact the structural order, self-diffusivity, and viscosity of a fluid. *The Journal of chemical physics* **127**, 044502 (2007).

[202] Saija, F., Saitta, A. M., and Giaquinta, P. V. Statistical entropy and density maximum anomaly in liquid water. *The Journal of chemical physics* **119**, 3587–3589 (2003).

[203] Yan, Z., Buldyrev, S. V., and Stanley, H. E. Relation of water anomalies to the excess entropy. *Physical Review E* **78**, 051201 (2008).

[204] Agarwal, M., Singh, M., Sharma, R., Parvez Alam, M., and Chakravarty, C. Relationship between structure, entropy, and diffusivity in water and water-like liquids. *The Journal of Physical Chemistry B* **114**, 6995–7001 (2010).

[205] Allegrini, P., Douglas, J. F., and Glotzer, S. C. Dynamic entropy as a measure of caging and persistent particle motion in supercooled liquids. *Physical Review E* **60**, 5714 (1999).

[206] Bretonnet, J.-L. Self-diffusion coefficient of dense fluids from the pair correlation function. *The Journal of chemical physics* **117**, 9370–9373 (2002).

[207] Yokoyama, I. On dzugutov's scaling law for atomic diffusion in condensed matter. *Physica B: Condensed Matter* **269**, 244–248 (1999).

[208] Gallo, P. and Rovere, M. Relation between the two-body entropy and the relaxation time in supercooled water. *Physical Review E* **91**, 012107 (2015).

[209] Gallo, P., Corradini, D., and Rovere, M. Widom line and dynamical

crossovers as routes to understand supercritical water. *Nat. Commun.* **5**, 5806 (2014).

[210] Corradini, D., Rovere, M., and Gallo, P. The widom line and dynamical crossover in supercritical water: Popular water models versus experiments. *J. Chem. Phys.* **143**, 114502 (2015).

[211] Gallo, P., Pellarin, R., and Rovere, M. Slow dynamics of a confined supercooled binary mixture: Direct space analysis. *Phys. Rev. E* **67**, 041202 (2003).

[212] Attili, A., Gallo, P., and Rovere, M. Mode coupling behavior of a lennard-jones binary mixture: A comparison between bulk and confined phases. *J. Chem. Phys.* **123**, 174510 (2005).